energies

MDPI

Article

A Smart PDIPM–GSF Framework for Congestion-Aware Optimal Power Flow and Electricity Pricing in Wind-Integrated Power Systems: Applications to the Algerian Electricity Market

Riyadh Bouddou [1], Abdallah Belabbes [2], Nasreddine Bouchikhi [3], Benali Alouache [4], Farid Benhamida [5], Emad Abd-Elrady [6,*] and Mohamed I. Mosaad [7]

[1] Department of Electrical Engineering, Faculty of Technology, University of Naama, Naama 45000, Algeria; bouddou@cuniv-naama.dz
[2] Institute of Industrial Maintenance and Safety, University of Oran 2 Mohammed Ben Ahmed, Oran 31000, Algeria; abdallah.belabbes@gmail.com
[3] Department of Electrical Engineering, Mechatronics Laboratory (LMETR), University of Setif 1, Setif 19000, Algeria; bouchikhi.nasreddine@univ-setif.dz
[4] Electrical Engineering and Renewable Energies Laboratory (LGEER), Electrical Engineering Department, Hassiba Benbouali University, Chlef 02180, Algeria; b.alouache@univ-chlef.dz
[5] IRECOM Laboratory, Department of Electrical and Electronic Engineering, Djillali Liabes University, Sidi Bel Abbes 22000, Algeria; farid.benhamida@yahoo.fr
[6] Faculty of Engineering Technology & Science, Higher Colleges of Technology, Abu Dhabi 25026, United Arab Emirates
[7] Yanbu Industrial College (YIC), Alnahdah, Yanbu Al Sinaiyah, Yanbu 46452, Saudi Arabia; m_i_mosaad@hotmail.com
* Correspondence: emad.abdelrady@hct.ac.ae

Abstract

This study presents a new improved primal–dual interior point method associated with a generation scaling factor (PDIPM–GSF) for congestion-aware optimal power flow (OPF) in power systems with renewable integration in a deregulated electricity market. The proposed framework combines the robustness of the primal–dual interior point method with an adaptive generation scaling strategy that adjusts generator outputs according to transmission line flow sensitivities, enabling early congestion mitigation, improved power flow feasibility, and accurate determination of locational marginal prices (LMPs). The proposed approach is evaluated on the IEEE 30-bus test system and a real 114-bus Algerian power network. The results demonstrate that the proposed framework can reduce generation costs and improve social profit under both single-sided and double-sided market operation through enhanced coordination between generation, demand, and congestion management. The impact of integrating wind energy is analyzed under different levels of wind energy penetration in the first IEEE 30-bus test system, showing that the integration of wind energy can not only improve social welfare and save generation costs but also lower transmission losses. Additionally, the results show that the placement of wind farms can improve the performance of the proposed PDIPM–GSF framework in terms of congestion management and reduction in LMPs at important nodes. For the 114-bus Algerian transmission network, renewable energy integration further demonstrates the capability of the proposed framework to reduce transmission losses and generation costs while improving overall market performance. These results demonstrate that the proposed PDIPM–GSF framework provides an effective smart optimization approach for renewable-integrated power systems by improving congestion management, facilitating large-scale WE integration, enhancing market efficiency, and ensuring reliable LMP computation. The proposed method, therefore, represents a practical and efficient solution for supporting

Check for updates

Academic Editor: Lars Johanning

Received: 24 July 2026
Revised: 4 September 2026
Accepted: 6 September 2026
Published: 8 September 2026

Copyright: © 2026 by the authors. Licensee MDPI, Basel, Switzerland. This article is an open access article distributed under the terms and conditions of the Creative Commons Attribution (CC BY) license.

future renewable energy transition and competitive electricity market operation in Algeria and other renewable-rich power systems.

Keywords: electricity market; optimal power flow; primal–dual interior point method; generation scaling factor; locational marginal pricing; wind energy integration; renewable energy; smart optimization; Algeria

1. Introduction

Electricity market deregulation is a reconfiguration of the power system regulations and market incentives related to the power sector economy that the government puts in place for governing and controlling the electricity sector [1,2]. The traditional structure of the electricity sector, which is monopolistic, is modified after deregulation is implemented by introducing competition between the supply and demand sides to maximize social benefits and profits and enhance the power system's efficiency, where power consumers and generating companies (GENCOs) participate in the electricity market [3,4]. Today, the electricity markets' operations include renewable generation participation, such as wind generators, through various policy incentives [5]. The independent system operator (ISO) faces a significant challenge related to the intermittent and unpredictable nature of wind energy (WE) [6,7]. Therefore, the electricity markets operated by ISOs have seen substantial growth in WE share turbines in terms of capacity purchases from the generation portfolio. The California ISO (CAISO), the Electric Reliability Council of Texas (ERCOT), and the Midcontinent ISO (MISO) are the three leading ISO markets operated with the largest WE penetration in the United States of America and all over the world [8]. The LMP technique is a clearing mechanism in the electricity market, which is a leading method that determines the optimal dispatching of generation and power prices in specified areas and zones. This technique was implemented in a variety of ISOs' electricity markets, including New York ISO (NYSO), CAISO, and MISO [9–11]. In the context of perfect competition in the LMP market, the price of energy is transformed into a factor that is not controllable by the participants. Perfect competition in the market is based on the hypothesis that all participants are genuine regarding their marginal cost. However, the participants are generally efficient and seek maximum profits [12,13]. Thus, they can submit power quantity and price bids to the market operator that differ from their real marginal cost to allocate market price to increase their profit. These strategic bids can affect the market's efficiency by affecting the economic dispatch (ED) or the optimal power flow (OPF) for market-clearing [14,15]. These economic operations in the electricity markets lead to a lower cost of production in power generation systems, which leads to maximum profit. Thermal generation units that are not identical due to different aspects such as distance, location, and efficiency cause different and higher operating costs and LMPs than wind generation units. The OPF schedule is important for deciding on each unit's capacity, which is critically important for meeting demand at minimum cost during power trading [16,17]. Over the last few years, increasing RESs, mainly solar and wind production, have dramatically changed the operating and economic perspectives of deregulated electricity markets. Unlike conventional thermal generators, renewable units have close-to-zero marginal fuel costs, limited dispatchability, and high dependency on environmental conditions, which directly impact the market-clearing outcome, LMPs, and transmission congestion patterns [18]. In this context, it becomes essential that electricity markets are redesigned considering renewable participation, maintaining system reliability, economic efficiency, and fairness among the market participants [19]. With inherent stochasticity and substantial variability over short

intervals, WE integration has therefore received considerable attention in the domain of electricity market research [20,21]. Such traits create a need for probabilistic modeling approaches, reserve allocation mechanisms, and penalty schemes to manage forecast deviations and preserve system balance. Participating in market auctions, wind generators may have some impact on LMP formation, congestion distribution, and social welfare, particularly in the context of high penetration levels [22]. Therefore, there is an increasing need for more precise wind modeling in OPF-based market-clearing frameworks for both ISOs and GENCOs [23]. Simultaneously, solar photovoltaic (PV) generation has seen a paradigm shift as a major renewable driver in today's power markets because of advances in technology with decreasing costs of installed capacity [24]. Besides its intermittent characteristics similar to wind generation, solar PV's generation pattern varies relatively slowly with smooth day profiles. Therefore, solar PV generation can be modeled in a deterministic fashion in day-ahead power markets according to forecasted irradiations [25]. When appropriately assimilated into OPF-based LMP markets, solar PVs can play a positive role in shaping market outcomes for alleviating network congestion with peaked generation costs to some extent. With the joint participation of solar and wind energy in competitive electricity markets, certain operating issues arise, such as congestion redistribution, price fluctuations, and alterations in the scheduling of generation, which become complex, particularly in networks where there is less scope for transmission expansion and where the concentration of renewables is higher in certain buses [26]. Hence, there arises the need for the use of advanced OPF and robust optimization methods to deal with convergence and the calculation of the LMP in the mentioned conditions. In addition to traditional renewable generators, there has been growing interest in recent years in the coordination of the participation of flexible resources, virtual power plants, and multi-energy systems in electricity markets. Using a VPP framework allows for the aggregation and joint scheduling of resources located in different geographical locations, such as renewable energy generators, energy storage, flexible loads, and other controllable resources, and hence provides flexibility in participating in the electricity market. Multi-energy systems, on the other hand, have used optimization frameworks to operate multiple energy carriers at once using the flexibility of buildings and distributed resources. Such approaches demonstrate the importance of coordinated resource scheduling for improving renewable utilization, flexibility, and market efficiency. However, their main focus is generally on resource aggregation, multi-energy coordination, or flexibility-market scheduling rather than on transmission-level congestion management and LMP formation through adaptive generation-flow sensitivity within an AC-OPF framework. Therefore, these developments further motivate the need for market-clearing approaches capable of linking flexible renewable participation with network congestion and nodal price formation [27,28]. The power sector in Algeria is still largely vertically integrated and controlled by the Algerian public company SONELGAZ in the fields of production, transport, distribution, and the sale of electric power and natural gas. SONELGAZ'S monopoly has so far hindered the entry of new competing companies and the establishment of the principles of competitive markets in the sector, despite the efforts of the SONELGAZ sector's restructuring law of 2002 that envisioned the unbundling of SONELGAZ'S business and the private sector's entry into the electricity sector production and possibly the electric energy supply sector; in any event, sectorial full opening has still been hindered by political choices in the Algerian country that support the current sector's structure by way of subsidies in the pricing sector [29,30]. The energy transition plan that is currently being adopted at the state level takes into account an increased need for modernizing the energy sector to raise the integration of renewable energy sources (RES). Algeria has shown significant ambition to increase the expansion of renewable energy, including solar energy as well as wind farms,

which would increase the country's production of clean energy significantly by the year 2030 [31,32]. SONELGAZ itself has undergone restructuring to meet future challenges, like renewable energy development. Even in the face of the dominance of fossil fuel-based power generation, mainly gas, there are indications of a gradual development of the power sector in Algeria [33]. This is evident through investments being made in the power grid of the country, as well as in the development of other energy resources, which highlight an overall trend of improving the power sector's reliability and making it favorable for overall market entrants. Today, there is an increasing trend of exporting power to other nearby nations [34,35]. Several previous works have studied the impact of wind energy integration on the electricity markets' auction for supply and demand bidding to maximize profit and minimize the generation cost using various approaches. The researchers have developed a multi-objective optimization method that solves the problem of security-constrained optimal power flow (SCOPF) to reduce generation costs and increase wind penetration level under uncertain variable load and wind power [36]. The stochastic programming (SP)-based method is presented for optimizing the bidding of wind and thermal GENCOs with air energy storage for profit maximization in a double-sided bidding electricity market [37]. To study the impact of price making by a GENCO in the electricity market, a GENCO pricing model, including wind generators, was presented and discussed in [38]. The economic effects of the electrical system, with losses in transmission lines and voltage at buses, are examined after integrating wind generators instead of one generator. The optimum bidding procedure of a wind energy company for social profit maximization and generation cost minimization in a deregulated electricity market was investigated [39]. A novel dynamic cost factor has been implemented for maximizing the profit of wind farms and GENCOs, considering wind speed uncertainty and demand variation [40]. An OPF problem, including unified power flow controller (UPFC) integration, is solved in a deregulated electricity market using a hybrid algorithm [41]. In [42], a market modeling approach has been proposed for WE integration effects with different pricing techniques in the electricity market. An OPF problem based on electricity pricing with WE penetration in a double-sided market auction is solved in [43] using a sequential quadratic programming (SQP) algorithm. The IPM algorithm is among the most effective methods for solving optimization problems in the power system. However, because of the operating processes involved, it has a fast processing speed. In this work, two power systems were employed to comprehensively evaluate the proposed PDIPM–GSF framework under different market structures and operational objectives. The IEEE 30-bus test system was first used to analyze electricity market bidding strategies and pricing mechanisms under both single- and double-sided auction models. In the single-sided auction, only generators submit bids while demand is considered inelastic, whereas in the double-sided auction, both generators and consumers participate strategically in the market. The suggested technique exhibited better convergence characteristics, lower generation cost, higher social welfare, and better congestion control using LMP-based market clearing. After the bidding simulation, the effect of the RES on the IEEE 30-bus system was considered at various penetrations of wind energy. It was found that higher wind energy penetration decreases generation cost, transmission losses, and nodal power prices and increases social welfare. The optimal location of the wind generator was also determined to further enhance system performance. To assess the applicability of the proposed method to a larger practical network, the framework was subsequently tested on the 114-bus Algerian power system, which was represented as a virtual deregulated electricity market. Unlike the IEEE 30-bus system, the Algerian case study focused on the impact of RES integration without considering alternative bidding strategies. Comparative OPF results for cases with and without RES integration demonstrated improvements in both network and market performance, in-

cluding reduced transmission losses and production costs, increased market profit, and lower LMPs at several load buses. Although the inclusion of RES slightly increased the convergence time because of the additional modeling complexity, stable convergence was maintained. Overall, the results demonstrate that the proposed PDIPM–GSF framework can effectively model market bids, manage congestion, determine LMPs, and support RES integration in both benchmark and practical power-system environments. This paper is structured as follows: In the Section 2, the related works are presented and explained. The renewable energy transition and power system deregulation in Algeria are presented in Section 3. The OPF optimization problem is formulated in Section 4. The PDIPM–GSF approach to solving the OPF problem and the implementation procedure are described and discussed in Section 5. The findings and results discussion of the test system and the Algerian 114-bus power system market are presented and discussed in Section 6. Finally, the Section 7 presents the conclusions, perspectives, and future directions.

2. Related Works

Several researchers have proposed optimal power flow (OPF)-based and locational marginal pricing (LMP)-based approaches to address transmission congestion and improve the economic performance of deregulated power systems. Researchers proposed a hybrid genetic algorithm–generation scaling factor (GA–GSF) approach for simultaneously solving the OPF problem, managing transmission congestion, and calculating LMPs and generator profits. The method was evaluated on IEEE 14-, 30-, and 57-bus systems and demonstrated improvements in generation dispatch and congestion management; however, the approach relies on a population-based metaheuristic optimization process, which may involve higher computational effort and does not exploit the structured primal–dual optimization mechanism available in interior-point methods [1]. Hemamalini proposed an LMP-based bi-level congestion management strategy in which LMP differences were used to identify congestion zones and Monarch Butterfly Optimization was employed to determine the optimal placement of distributed generation, while the OPF solution was obtained using linear programming. The algorithm was examined both under the conditions of supply bidding and demand bidding using IEEE 30-bus and 118-bus test networks; however, the alleviation of congestion mainly depends on the proper allocation of distributed generation without considering any kind of adaptive generation rescaling scheme in the nonlinear optimal power flow model [2]. In addition, there exists an LMP-based congestion management technique for the allocation of distributed generation in which LMP variation along the transmission lines determines the congestion-prone zones, and then suitable positions for distributed generation are selected. Although it is a good economic tool for assessing congestion, it mainly concentrates on the identification of congestion zones and DG placement [3]. In a subsequent study, researchers proposed a multi-objective congestion management strategy based on optimal distributed-generation sizing and hybrid swarm optimization, considering congestion reduction, power-loss minimization, voltage-profile improvement, and investment costs. Although the proposed approach demonstrated improved results compared with conventional PSO on IEEE 30- and 57-bus systems, it depends on metaheuristic optimization and focuses mainly on DG allocation and sizing rather than directly integrating line-flow sensitivity information into a primal–dual OPF framework for simultaneous dispatch and LMP calculation [4]. Habibi and Zangeneh proposed a congestion management and generation-cost reduction approach based on optimal transmission switching and linearized AC-OPF, solved through mixed-integer linear programming. Their approach effectively determines transmission-line switching decisions and reduces both congestion and generation costs; however, it requires network topology modifications and focuses on transmission switching rather

than adaptive generation rescheduling based on generation-flow sensitivities within an AC-OPF market-clearing process [5]. Stochastic optimal power flow with reconfiguration was suggested for the management of congestion and integration of renewable energy in an uncertain environment. It proved successful in demonstrating how network reconfiguration is helpful in mitigating congestion costs and renewable energy curtailment, especially during post-contingency situations; the main emphasis of the approach is on stochastic integration of renewable energy and network reconfiguration rather than LMP-based electricity prices and sensitivity analysis for generation scheduling [6]. In another approach, Researchers introduced congestion management through OPF for a deregulated electricity market with calculation of LMP during both normal and congestion situations and also determination of the best placement of TCSC and DG through sensitivity analysis. The OPF problem was solved by using primal linear programming and genetic algorithms; however, the approach depends on network devices and their placement and lacks an integrated iterative algorithm for generation rescaling and a primal–dual interior-point OPF solver [7]. Researchers further extended the GA–GSF concept to reduce LMPs and relieve transmission congestion through the optimal placement and sizing of distributed generation. This approach has succeeded in detecting the congested transmission lines and assigning the optimal DG placement and capacity, but the whole study is focused more on DG planning, and the GA-GSF method is validated only on the IEEE 14-bus test case [8], without being formulated for an integrated AC-OPF and market clearing model. Researchers developed an intelligent LMP control strategy for congestion management using genetic and hybrid optimization techniques combined with distributed solar PV generation and fuzzy logic control. The results demonstrated reductions in LMP differences and improvements in the technical performance of the DG system; however, the approach focuses on intelligent DG control and converter operation and does not directly address the integration of generation-flow sensitivity information into an iterative OPF-based dispatch and pricing procedure [9]. Finally, researchers proposed a simplified LMP formulation based on lossless DC-OPF to provide transparent nodal price signals under congested operating conditions. Although the approach offers a straightforward representation of energy and congestion price components, the adopted DC approximation neglects transmission losses and reactive-power and voltage constraints, thereby limiting its ability to represent the complete nonlinear characteristics of practical AC power systems [10]. Despite these significant contributions, existing studies generally apply congestion indicators, sensitivity analysis, GSF, metaheuristic optimization, DG placement, network reconfiguration, or OPF-based LMP calculation as separate mechanisms. The remaining gap is the lack of an integrated framework in which generation-flow sensitivity adaptively modifies generator outputs within the primal–dual interior-point iterations while simultaneously addressing AC-OPF, congestion, LMP formation, renewable integration, and electricity-market operation. However, based on the reviewed literature, limited attention has been given to directly integrating generation-flow sensitivity information into a primal–dual interior-point optimization procedure to guide generator adjustments during the iterative AC-OPF solution while simultaneously considering transmission congestion, LMP formation, wind-power integration, and electricity-market performance. To address this limitation, the present study proposes a smart primal–dual interior-point method integrated with a generation scaling factor (PDIPM–GSF) for congestion-aware AC optimal power flow and LMP calculation. Unlike approaches in which the sensitivity analysis or congestion management strategy is applied as a separate planning, placement, or post-processing procedure, the proposed framework incorporates the generation scaling factor into the iterative optimization process, allowing line-flow sensitivity information to influence generation adjustments and the resulting economically optimal dispatch. The proposed framework is further evaluated under

single-sided and double-sided electricity market mechanisms, different wind penetration levels, and optimal wind-farm locations on the IEEE 30-bus system, followed by validation on a real 114-bus Algerian power network. Therefore, the main contribution of this work lies in the unified integration of primal–dual optimization, generation-flow sensitivity analysis, congestion-aware dispatch, LMP calculation, renewable-energy integration, and electricity-market assessment within a single AC-OPF framework.

Table 1 presents a comparison of related studies with the proposed PDIPM–GSF framework.

Table 1. Comparison of related studies with the proposed PDIPM–GSF framework.

Ref.	Method	OPF	Congestion Management	GSF/Sensitivity	LMP Calculation	Renewable/DG Integration	Electricity Market Analysis
[1]	GA–GSF	✓	✓	✓	✓	✗	✓
[2]	MBO + LP	✓	✓	✓	✓	✓	✓
[3]	LMP-based zonal approach	✗	✓	✓	✓	✓	✓
[4]	PSO/Hybrid Swarm Optimization	✓	✓	✓	✓	✓	✗
[5]	Linearized AC-OPF+ MILP	✓	✓	✗	✗	✗	✗
[6]	Stochastic OPF+ Network Reconfiguration	✓	✓	✗	✗	✓	✗
[7]	PLP/GA+ Sensitivity Indices	✓	✓	✓	✓	✓	✓
[8]	GA–GSF	✓	✓	✓	✓	✓	✗
[9]	GA + Hybrid Control + FLC	✗	✓	✓	✓	✓	✓
[10]	DC-OPF	✓	✓	✗	✓	✗	✓
This study	PDIPM–GSF	✓	✓	✓	✓	✓	✓

3. Renewable Energy Transition and Power System Deregulation in Algeria

Renewable Energy Sector in Algeria

Algeria has a very strong renewable energy potential, especially solar and WE, given its location in the solar belt and the extent of its desert territory. Regarding solar energy, the Algerian territory benefits from among the world's highest levels of solar radiation. The Saharan regions can receive an average of between 2000 and 3500 h of sunshine per year, with global horizontal irradiation (GHI) typically ranging between 2100 and 2650 kWh/m^2/year depending on the area, making it a particularly favorable resource for PV installations and concentrated solar power systems. Algeria also has a significant WE resource. Its approximately 1300 km Mediterranean coastline and inland desert areas provide wind speeds that are suitable for electricity generation. Studies assessing wind potential show that certain regions in the south and the Highlands have average annual wind speeds exceeding 5–6 m/s, which is compatible with energy production from commercial wind turbines. The combination of these two resources can be advantageous. In several areas of Algeria, analysis of the complementary nature of solar and WE in terms of space and time resources shows that they can contribute to smoothing total renewable energy production, which is an important aspect for integration into the electricity grid and for planning future hybrid farms. Despite this high potential, the actual integration of RES into the electricity mix remains modest, with current production relying mainly on fossil fuels. One of the challenges of Algeria's energy transition is therefore to boost the usage of its RES to satisfy growing electricity demand and reduce dependence on hydrocarbons, while

adapting the electricity market infrastructure to a more competitive and decentralized model. Figure 1 presents the spatial distribution of global horizontal irradiation in Algeria (in kWh/m^2/year). Figure 2 presents a map of wind speeds across Algeria [44,45].

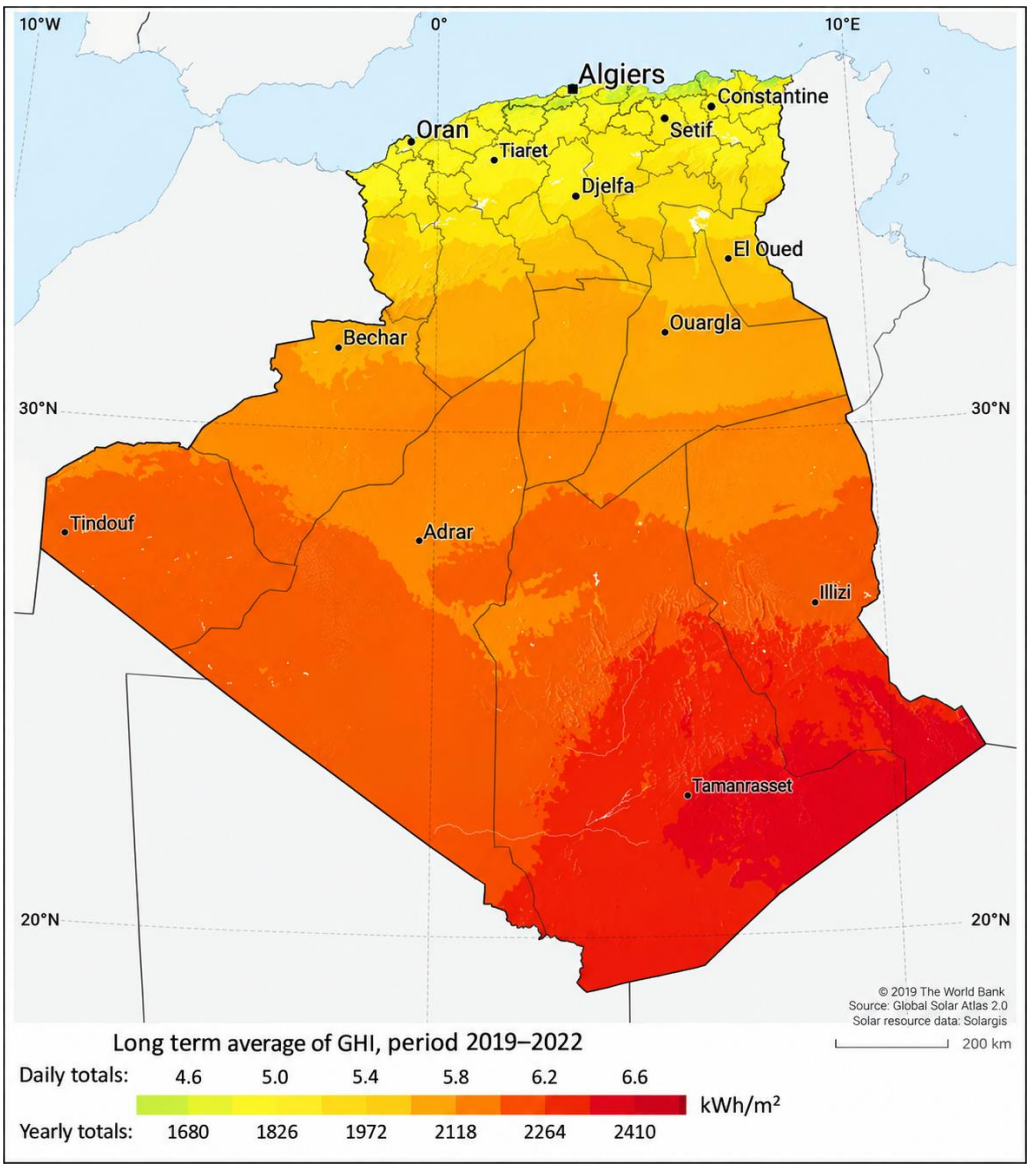


Figure 1. Spatial distribution of global horizontal irradiation in Algeria (in kWh/m^2/year).

The Algerian Government launched the Algerian program for renewable energy and energy efficiency in 2011. The primary objective of the national program was to develop the use of renewable energy and increase the country's RES. It has the objective of achieving a 27% share of RES in the country's total energy generation by 2030. The renewable energy production goals are set to be accomplished in two phases (between 2015 and 2020, and between 2021 and 2030), encouraging investment in all RES. Table 2 presents the major renewable energy objectives for electricity production during these two periods. By 2030, a total of 22 GW is expected to be produced from RES, of which 12 GW will be for the domestic market and 10 GW for export. Producing this amount of RE will save more than 300 billion m^3 of natural gas (eight times the national consumption in 2014) [46]. In addition, it will reduce CO_2 emissions by 348 Mt [47]. Figure 3 shows the total share of energy sources (2015–2030).

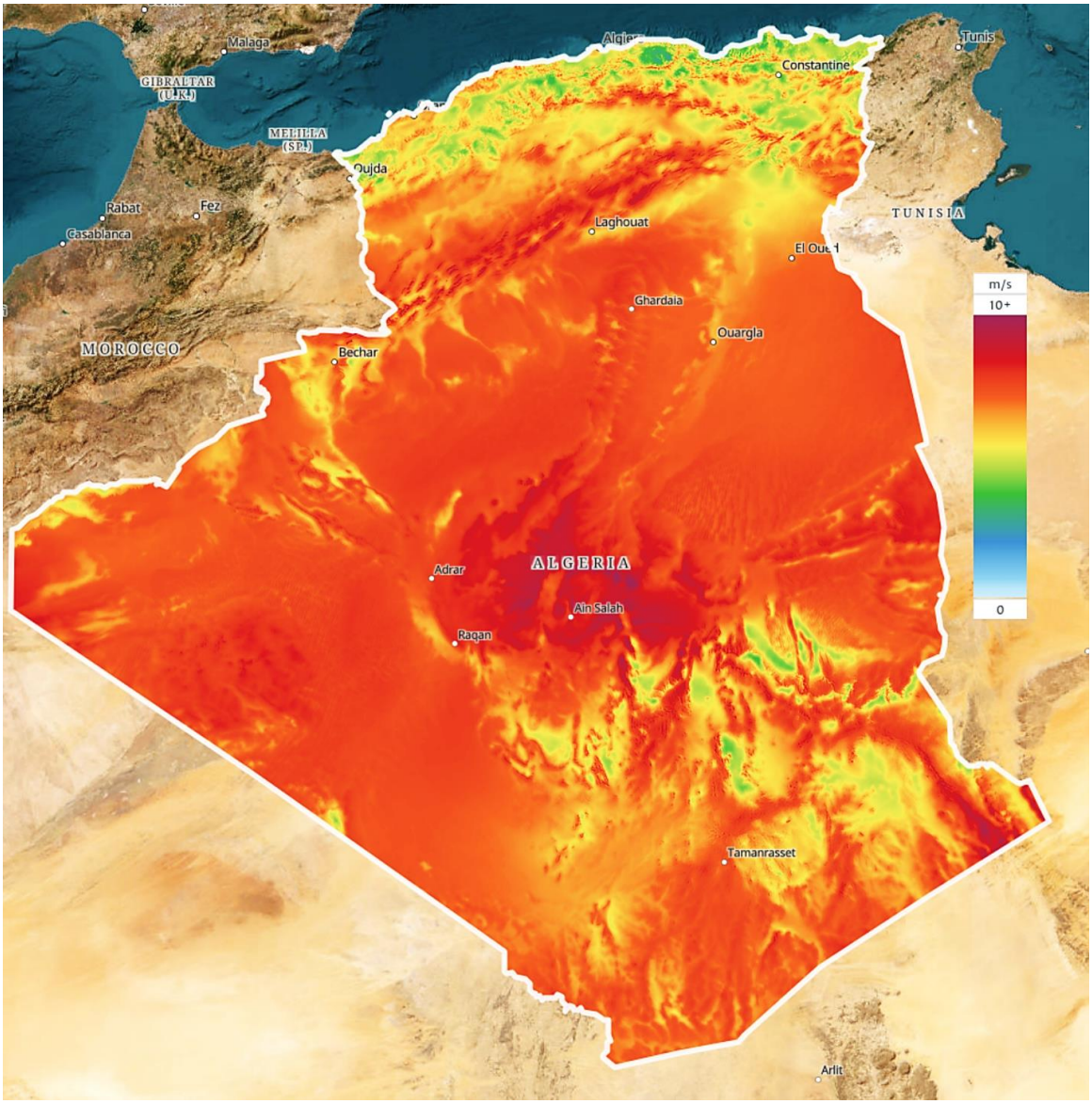


Figure 2. Wind speed potential map in Algeria.

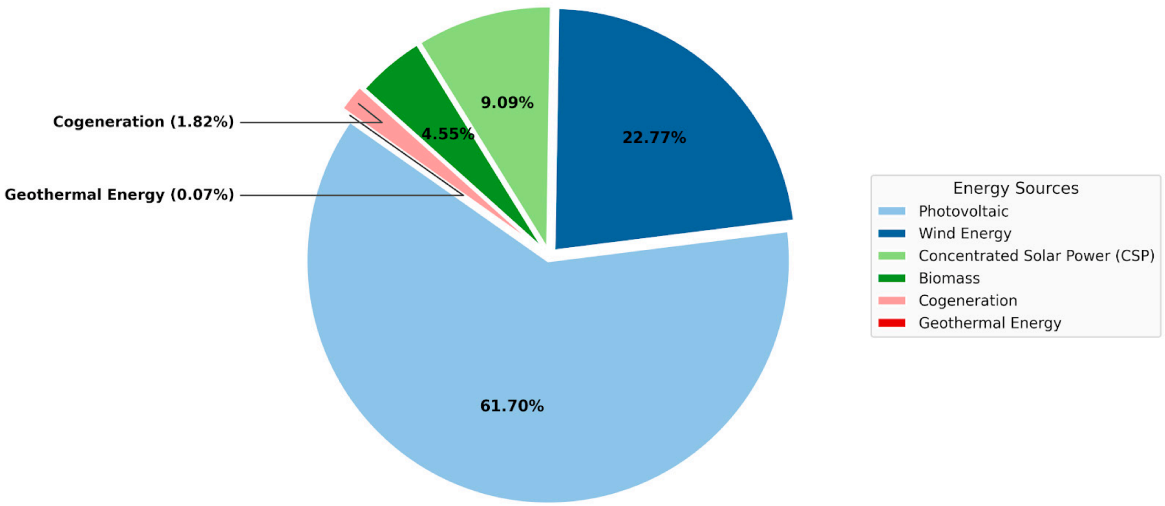


Figure 3. The total renewable energy share targets for electricity generation during the two periods in the Algerian renewable energy program (2015–2030).

In Algeria, the deployment of RES is part of an ambitious national strategy led by Sonelgaz, aimed at gradually incorporating solar and wind energies into the electricity grid. To date, several PV projects have been commissioned across the country, with a total installed capacity of around 501 MWp, spread across numerous wilayas, particularly in the Highlands and south of Algeria. Furthermore, a 10.2 MW wind farm has been constructed in the state of Adrar (Kabertene), which represents the first industrial wind power project in Algeria. In addition, Sonelgaz has launched a vast program to build 3200 MWp of PV power plants, currently in the implementation phase, as part of the overall objective of 15,000 MW of renewable capacity by 2035, in order to strengthen energy security and reduce dependence on fossil fuels. Figure 4 shows the geographical distribution of RES projects implemented and under construction in Algeria, including PV power plants already in operation, the Kabertène wind farm (Adrar), and sites selected as part of the national program for 3200 MWp of solar PV power plants led by Sonelgaz [48–50].

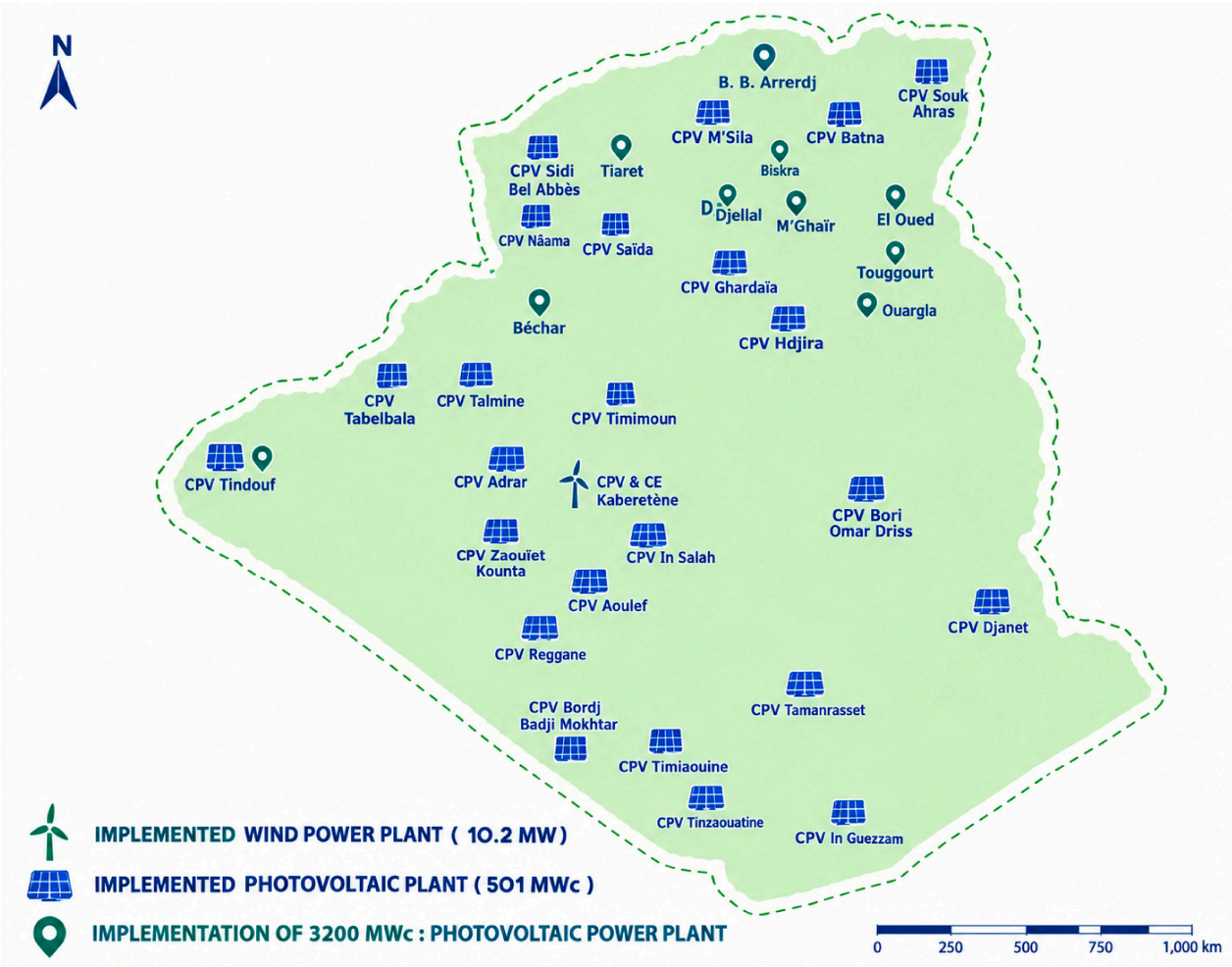


Figure 4. Geographical distribution of renewable energy projects implemented and under construction in Algeria.

Table 2. RES targets for electricity production during the Algerian renewable energy transition period.

Periodic Phases	First Period (2015–2020)	Second Period (2021–2030)	Total Periods
PV (MW)	3000	10,575	13,575
WE (MW)	1010	4000	5010
CSP (MW)	–	2000	2000

Table 2. *Cont.*

Periodic Phases	First Period (2015–2020)	Second Period (2021–2030)	Total Periods
Biomass (MW)	360	640	1000
Cogeneration (MW)	150	250	400
Geothermal Energy (MW)	5	10	15
Total (MW)	4525	17,475	22,000

4. Problem Formulation

The objective of the OPF-based electricity market is to find the optimal scheduling of power plants with the minimized production cost and the LMPs in the market. The mathematical model is then formulated based on the supply and demand bids received from GENCOs and customers. In Figure 5, there are several zones in the electricity system model, and energy flows between them. Here, energy trading on the electricity market is managed by the ISO [51]. The ISO determines the optimal supply from GENCOs in a real-time market by balancing generators to meet customer demand. LMP prices are set based on the intersection of supply and demand curves. In this model, WE units can participate in the electricity market alongside thermal generators. The extra electricity produced by wind sources can minimize generation cost and reduce LMPs, which allows GENCOs to make a profit [52].

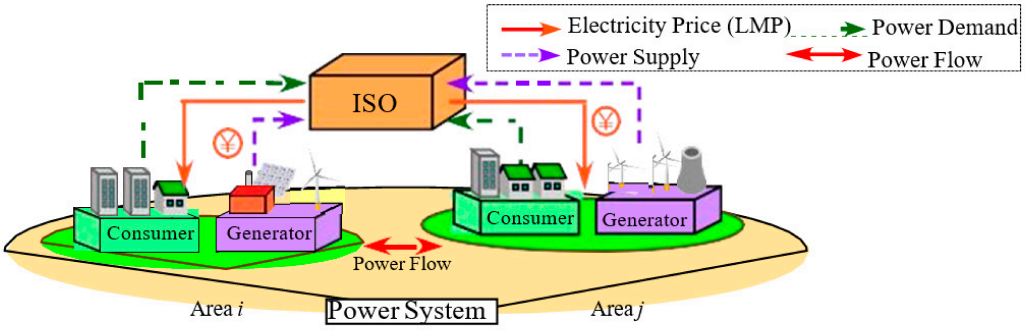


Figure 5. Power system model for the electricity market under LMP pricing.

4.1. Objective Function of the Electricity Market

The LMP clearing mechanism maximizes efficiency based on the presumption that market participants are price-takers, which means that they have no market power. For this purpose, the market is cleared based on actual supply and demand-side bids. The OPF-based LMP pricing is a typical nonlinear clearing problem modeled for the objective of profit maximization of generators in the electricity market [53,54]. The objective function is formulated with two sub-functions. It is mathematically formulated as follows:

$$Max(PF) = TRV - TC \tag{1}$$

$$MaxPF = \left[\sum_{j=1}^{N_{gn}} LMP_j \cdot P_{g,j} - \left(\sum_{i=1}^{N_{gn}} C_{g,i}(P_{g,i})\right)\right] \tag{2}$$

4.2. Objective Function of the OPF Problem

The main objective in formulating the OPF is to minimize the total power generation cost. The energy cost function of every unit varies depending on the power generated and is represented by a second-order polynomial curve. The objective function of the complete power system is calculated by adding the energy cost functions of every power unit [55,56].

$$C_{g,i}(P_{g,i}) = aP_{(g,i)}{}^2 + bP_{(g,i)} + c \tag{3}$$

$$C_{w,j}(P_{w,j}) = d_{w,j}P_{w,j} \tag{4}$$

4.3. Equality Constraint

When minimizing the objective function, the power generation should be equal to the demand for electricity and transmission line losses. Consequently, the power flow equations are treated as constraints and must be satisfied to obtain an OPF [57,58]. They are given by the following expressions:

$$\begin{pmatrix} \Delta P_i \\ \Delta Q_i \end{pmatrix} = \begin{bmatrix} \Delta P_i(V,\theta) - (P_{g,i} - P_{D,i}) \\ \Delta Q_i(V,\theta) - (Q_{g,i} - Q_{D,i}) \end{bmatrix} = 0 \tag{5}$$

Injected active and reactive power in bus i is defined as follows:

$$P_i(V,\theta) = \sum_{j=1}^{Ng} V_i V_j \left(G_{i,j}\cos\theta_{i,j} + B_{i,j}\sin\theta_{i,j}\right) \tag{6}$$

$$Q_i(V,\theta) = \sum_{j=1}^{Ng} V_i V_j \left(G_{i,j}\sin\theta_{i,j} + B_{i,j}\cos\theta_{i,j}\right) \tag{7}$$

The loss of power in the grid, reducing the power from power production to consumption, is one of the important factors in OPF. Consequently, the energy generated by the power units is equivalent to the power consumption and grid energy losses [59].

$$\sum_{i=1}^{N} P_i P_D + P_{Los} \tag{8}$$

$$P_{Loss} = \sum_{i=1}^{Nbus}\sum_{j=1}^{Nbus} \left|V_i\right| V_j Y_{busi,j} cos(\theta_{busi,j} - \delta_i + \delta_j) \tag{9}$$

4.4. Inequality Constraint

The inequality constraints of the OPF represent the physical limits of the electrical system's components, as well as the restrictions imposed for system stability. The typical types of unbalanced constraints are high-voltage restrictions on the buses linked to the power generation units and low-voltage constraints on the buses connected to the power units. Production limits comprise the maximal and minimal active power generated by generators, the maximal transmission line capacity, and the tap-change and phase-change limitations of the on-load tap-changer (TCUL) transformer. The unbalanced constraints of the problem include the upper and lower bands of active power generated in buses that have generators. Generators are operated within specified minimum and maximum active-power limits to satisfy operational and security requirements. This is also known as a security constraint, which is stated by the following formula [60,61].

$$P_{g,i\min} \le P_{g,i} \le P_{g,i\max} \tag{10}$$

Upper and lower limits of reactive power produced in the buses equipped with generators and reactive power injected into the buses equipped with a VAR compensator are expressed as follows:

$$Q_{g,i\min} \le Q_{g,i} \le Q_{g,i\max} \tag{11}$$

$$Q_{c,i\min} \le Q_{c,i} \le Q_{c,i\max} \tag{12}$$

High and low bands of voltage magnitude in all buses are expressed as follows:

$$V_{g,i\min} \le V_{g,i} \le V_{g,i\max} \tag{13}$$

$$V_{L,i\min} \le V_{L,i} \le V_{L,i\max} \tag{14}$$

High and low bands in the phase angle of bus voltage are expressed as follows:

$$\theta_{g,i\min} \le \theta_{g,i} \le \theta_{g,i\max} \tag{15}$$

The maximum apparent-power flow limit of each transmission line is expressed in MVA and is determined according to the thermal and stability limits of the transmission system, expressed as follows [62,63].

$$\left|P_{i,j}\right| \le P_{i,j}^{\max} \tag{16}$$

4.5. Calculating the Market Price of Electricity

The LMP function in the electricity market model is formulated with a more detailed description provided in the subsections as follows:

$$LMP_i = LMP^{ref} + LMP_i^{cong} + LMP_i^{loss} \tag{17}$$

$$LMP^{ref} = \lambda \tag{18}$$

$$LMP^{loss} = LMP^{ref} \cdot (DF_i - 1) \tag{19}$$

$$LMP^{Congestion} = -\sum_{k=1}^{M} GSF_{k-i} \cdot \mu_k \tag{20}$$

Like the line constraint, the binding constraint occurs at the limit of the line's power flow. Its value is the incremental shifting of the generators' total generation cost divided by the limit of the constraint's incremental shifting [64].

$$\mu_k = \frac{\text{shifting in total cost}}{\text{shifting in flow constraints}} \tag{21}$$

The GSF represents the sensitivity of the power flow on transmission line k to an incremental change in active-power injection at bus i [65,66].

$$GSF_{k-i} = \frac{(B_{(a,i)}^{-1} - B_{(b,i)}^{-1})}{x_k} \tag{22}$$

Mathematical Implementation of the Generation Scaling Factor

The generation scaling factor (GSF) is introduced to quantify the sensitivity of transmission-line power flows to changes in generator active-power outputs. For a transmission line and a generator connected at a bus, the GSF is defined as the partial derivative of the active power flow of the line with respect to the active power injection at the generator bus:

$$\mathrm{GSF_{k,i}} = \frac{\partial F_k}{\partial P_{Gi}} \tag{23}$$

where denotes the active power flow through the transmission line, and represents the active power output of the generator. The GSF therefore indicates both the direction and magnitude of the influence of a generator on a particular transmission-line flow.

For a small variation in generator output, the corresponding variation in the line flow can be approximated using the first-order sensitivity relationship:

$$\Delta F_{\mathrm{k}} = \mathrm{GSF}_{\mathrm{k,i}} \Delta P_{Gi} \tag{24}$$

When several generators are simultaneously rescheduled, the change in the flow of the line can be expressed as

$$\Delta F_{\mathrm{k}} = \sum_{\mathrm{i}\in \mathrm{G}} \mathrm{GSF}_{\mathrm{k,i}} \Delta P_{Gi} \tag{25}$$

where G denotes the set of online generators and is the change in the active-power output of generator. In matrix form, Equation (25) can be written as

$$\Delta F = \mathrm{GSF} \Delta P_G \tag{26}$$

where ΔF is the vector of transmission-line flow changes, and ΔP_G is the vector of generator-output adjustments.

The physical interpretation of the GSF is directly related to the direction of power-flow changes. A positive value of $GSF_{k,i}$ means that increasing the output of generator i tends to increase the power flow through line k. Conversely, a negative value indicates that increasing the output of generator i tends to reduce the flow through the considered line. Therefore, when a transmission line becomes congested, the GSF information can be used to identify generators that are most effective for relieving the congestion.

For a congested transmission line, the required flow correction is defined as

$$\Delta F_k^{reg} = F_k^{lim} - F_k \tag{27}$$

where F_k^{lim} is the allowable flow limit of line k, and F_k is its flow obtained from the current OPF iteration. The generation rescheduling is then determined as

$$\sum_{\mathrm{i}\in \mathrm{G}} \mathrm{GSF}_{\mathrm{k,i}} \Delta P_{Gi} = \Delta F_k^{reg} \tag{28}$$

Thus, for an overloaded line, the generation output of units with positive GSF values can be reduced, while the output of units with negative GSF values can be increased, subject to the generator operating limits and the power-balance constraint. The generator outputs must satisfy as follows:

$$P_{Gi}^{min} \le P_{Gi} + \Delta P_{Gi} \le P_{Gi}^{max} \tag{29}$$

The resulting generation adjustment is incorporated into the primal–dual interior-point optimization process. Accordingly, the updated generator output can be represented as

$$P_{Gi}^{(t+1)} = P_{Gi}^{(t)} + \alpha GSF \, \Delta P_{Gi}^{GSF} + \alpha p \, \Delta P_{Gi}^{IPM} \tag{30}$$

where $P_{Gi}^{(t)}$ is the generator output at iteration t, ΔP_{Gi}^{GSF} is the sensitivity-based generation adjustment, ΔP_{Gi}^{IPM} is the generation correction obtained from the primal–dual Newton step, αGSF is the GSF scaling coefficient, and αp is the primal step size.

The GSF is recalculated at each relevant OPF iteration because the transmission-flow sensitivity depends on the current operating point of the nonlinear AC power system. Consequently, the proposed PDIPM–GSF method establishes an iterative feedback mechanism in which the OPF solution is first used to determine the current line flows, congested lines are then identified, the corresponding GSF values are calculated, and the generator outputs are rescheduled according to their congestion sensitivities. The modified generation schedule is subsequently introduced into the primal–dual KKT system and the OPF problem is solved again. This procedure is repeated until the power-flow constraints, generator

limits, transmission-line limits, and primal–dual convergence criteria are simultaneously satisfied. From an electricity-market perspective, this sensitivity-guided rescheduling directly affects the congestion component of the LMP. When a transmission constraint becomes binding, its associated shadow price contributes to the nodal congestion price. By redistributing generation toward units that reduce the flow on the congested corridor, the proposed GSF mechanism mitigates the binding constraint and consequently reduces or redistributes its marginal congestion contribution to the LMP. Therefore, GSF does not represent an additional generation source; rather, it provides a sensitivity-based mechanism for determining how existing generators should be rescheduled to obtain a feasible and economically efficient congestion-aware OPF solution.

To formally assess the optimality of the proposed PDIPM–GSF procedure, the GSF-based generation adjustment is incorporated into the primal–dual KKT conditions rather than being treated solely as a heuristic rescheduling operation. For the constrained OPF problem, the KKT residual vector can be expressed as

$$RKKT\ (x, \lambda, s) = \begin{bmatrix} \nabla x\ L(x, \lambda, s) \\ g(x) \\ h(x) \\ SZe - \mu e \end{bmatrix} = 0 \tag{31}$$

where x denotes the primal OPF variables; λ represents the equality-constraint multipliers; s and z denote the inequality slacks and their associated dual variables, respectively; $g(x)$ represents the power-balance equations; $h(x)$ represents the inequality constraints; and μ is the primal–dual barrier parameter. The GSF correction is accepted only when the resulting generation schedule remains within the feasible operating region and the subsequent PDIPM iteration reduces the KKT residual while maintaining the power-balance and transmission constraints. Accordingly, the convergence quality of the proposed method is evaluated through the normalized KKT residual:

$$\varepsilon KKT\ = \| RKKT\ \| \infty\ = imax\ \mid RKKT, i\ \mid, \varepsilon KKT\ \to 0 \tag{32}$$

Hence, the role of the GSF is not merely to modify the convergence trajectory of the OPF algorithm. By directing generation adjustments according to the sensitivity of congested transmission flows, GSF provides a feasible search direction that is subsequently corrected by the primal–dual Newton step. The final solution is considered optimal only when the KKT residual approaches zero, all generator and transmission constraints are satisfied, and the nodal power-balance equations are simultaneously fulfilled. In this sense, the PDIPM–GSF framework preserves the KKT-based optimality conditions of the underlying OPF problem while improving the ability of the solver to reach a congestion-feasible market-clearing solution. For the electricity-market interpretation, satisfaction of the power-balance equations together with the transmission constraints ensures that the resulting generation schedule and associated LMPs correspond to a feasible market-clearing state rather than merely an intermediate sensitivity-based rescheduling.

4.6. Wind Power Integration in the Electricity Market

Wind power has been one of the most widely used RES in the world over the last decade. It has many advantages, such as low operating costs and zero pollution. Today, electricity market operations include the participation of renewable generation, such as wind generators, thanks to various policy interventions. System operators face a significant problem related to the intermittency and unpredictability of wind power. As a result, electricity markets operated by ISOs have seen considerable growth in the percentage of

wind turbine integration in terms of capacity purchases from the generation portfolio [67]. The CAISO, the MISO, and the ERCOT are the three main ISO-operated markets with the highest penetration of wind power in the United States of America and worldwide. Global WE Council (GWEC) data stated that 117 GW of new capacity was installed globally in 2024, bringing the total capacity to over 1136 GW. Due to the reliability and low production cost of wind power, many private companies and businesses continue to turn to this type of energy source. In addition, many large investors have been attracted by its stable revenues and profits [68].

4.6.1. WE Estimation

However, WE varies with location, availability, and wind speed, resulting in a large uncertainty in the power produced. The wind speed has been calculated for the desired height using the power law equation.

$$\frac{Ws_h}{Ws_{10}} = \left(\frac{h}{10}\right)^N \tag{33}$$

The WE system in the electricity market includes the optimized design of the wind turbine and its characteristics, and the optimization of WE production at nominal wind speed, which is stated below.

$$P_W = \frac{1}{2} C_p \cdot \rho \cdot \pi \cdot R_P^2 \cdot V_W^3 \tag{34}$$

The wind speed is a variable value in this equation. By neglecting minor non-linearities, the function between a particular wind speed and energy generation can be represented in Figure 6.

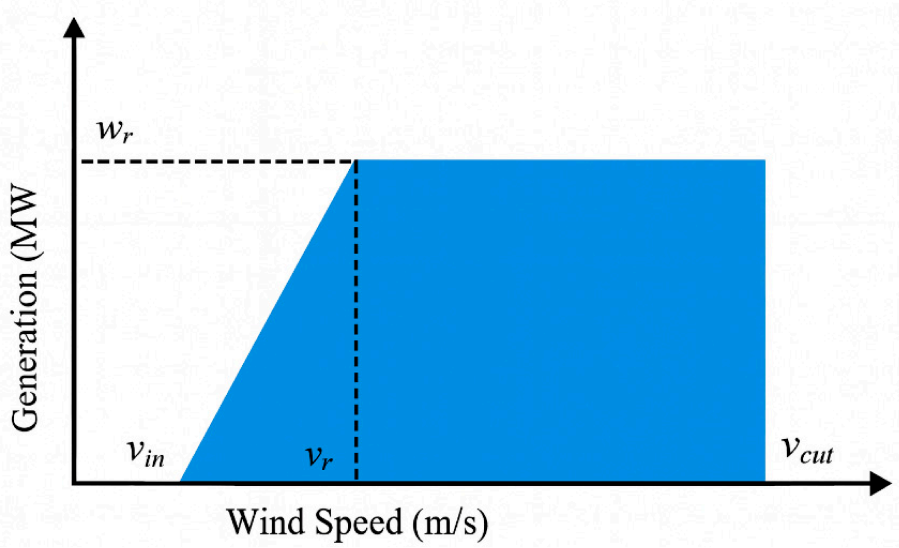


Figure 6. Global power curve for a wind generator.

The figure above shows that no power is produced at wind speeds lower than v_{in} or higher than v_{out}. The power produced at wind speeds between v_r and v_{out} is equivalent to the rated output of the wind turbine. For wind speeds from *vin* to *vr*, the power produced is a linear function. Therefore, wind generator power can be expressed by the following expression:

$$\begin{cases} W = 0, & V < v_{in} \text{ or } V > v_{out} \\ W = aV + b, & v_{in} \le V \le v_r \\ W = w_r, & v_r \le V \le v_{out} \end{cases}, \; a = \frac{w_r}{v_r - v_{in}}, \; b = -\frac{v_{in} w_r}{v_r - v_{in}} \tag{35}$$

The Weibull probability density function (PDF) is used to simulate the wind speed (v in m/s), and it can be defined as follows:

$$f(v) = \left(\frac{\partial}{\varnothing}\right)\left(\frac{v}{\varnothing}\right)^{(\partial-1)} e^{-(-v/\varnothing)} \tag{36}$$

A wind turbine's output power is discontinuous at specific wind speeds, as shown by Equation (4), which calculates the probability of wind power in discrete zones [69–71]:

$$f_w(P_{wind})\{P_{wind} = 0\} = 1 - exp\left[-\left(\frac{v_{in}}{\varnothing}\right)^{(\partial)}\right] + exp\left[-\left(\frac{v_{out}}{\varnothing}\right)^{(\partial)}\right] \tag{37}$$

4.6.2. WE Cost Estimation

The objective function for optimization when the wind generator participates in the electricity market is to maximize the market participant's social profit by reducing the generation cost. The integration of wind generators into the market depends on its dynamics, governmental policy, and various factors that are difficult to model, like wind speed variations, sensitivity to the power system, and the variation in the power injected into the system. It may be written as a co-optimization problem. The first term is the revenue cost. The second is the generation cost function of thermal and wind units [72].

$$\overbrace{\text{Max PF}}^{PF} = \overbrace{\left(\sum_{j=1}^{N_{gn}} LMP_j \cdot P_{g,j}\right)}^{RV} - \overbrace{\left(\sum_{i=1}^{N_{gn}} C_{g,i}(P_{g,i}) + \sum_{\omega}^{W} C_{\omega,j}(P_{\omega,j})\right)}^{TC} \tag{38}$$

A wind power plant is typically owned by a private GENCO, which supplies an agreed amount of power to the ISO grid operator. Therefore, if the ISO owns a wind power plant, it may not incur any direct costs except for the initial setup, i.e., the initial configuration. This could be considered a maintenance cost. However, if the wind power plant is owned by a private GENCO, the ISO will pay a fixed tariff agreed upon by the ISO and the wind power plant owner based on the expected amount of electricity. As a result, the direct costs of wind power can be expressed as follows:

$$C_{w,j}(P_{w,j}) = d_{w,j}P_{w,j} \tag{39}$$

Given the nature of wind power, the active power generated by wind power plants is subject to variation [73,74]. The actual generated output can be less than expected. When the potential of WE is overestimated, the ISO needs to keep a reserve to meet demand. The cost of keeping this reserve is classified as reserve expenditure. In contrast to overestimation, it is possible that the electricity production of wind farms may be measured as higher than the power planned in accordance with legal agreements. If the power cannot be utilized by reducing the output of thermal generators, it is wasted. The ISO is charged a penalty for surplus energy [70].

4.6.3. Wind Power Uncertainty and Reserve Requirement

The Weibull probability distribution adopted in this study provides a practical representation of the statistical variability of wind speed and, consequently, the probabilistic availability of wind generation. However, it does not explicitly capture short-term wind-power forecasting errors or temporal correlations between successive operating periods. Therefore, the adopted model is intended to represent the probabilistic variability of wind generation within the proposed OPF framework rather than detailed real-time forecasting dynamics. Under uncertain wind generation, the reserve requirement is associated

with the potential shortfall between the scheduled or expected wind generation and the actual available wind power. When the available wind generation is lower than its expected value, additional reserve is required to compensate for the resulting generation deficit and maintain system balance. In the proposed formulation, this uncertainty is reflected through the reserve requirement and the corresponding reserve cost associated with wind-power deviations.

The required upward reserve is determined from the wind-power shortfall between the scheduled and actual available generation. For each wind power unit i, the required reserve capacity is defined as

$$R_i^{up} = max\left(0, P_i^{sch} - P_i^{act}\right) \tag{40}$$

where P_i^{sch} is the scheduled (or expected) wind power and P_i^{act} is the actual available wind power. Thus, when $P_i^{act} < P_i^{sch}$, the difference $P_i^{sch} - P_i^{act}$ represents the upward reserve required to compensate for the wind-power deficit. If $P_i^{act} \geq P_i^{sch}$, no upward reserve is required from this shortfall criterion. The total upward reserve requirement is therefore obtained as

$$R_{tot}^{up} = \sum_i R_i^{up} \tag{41}$$

This rule provides an explicit and reproducible representation of the reserve requirement while remaining consistent with the probabilistic wind-generation framework adopted in this study.

4.7. Solar PV Power Integration in the Electricity Market

Increasingly, PV electricity production is included in competitive electricity markets, particularly in consideration of the environmental advantage and low marginal cost of operation. Unlike wind power, which exhibits high stochastic variability and is therefore modeled probabilistically, solar PV generation is assumed to be deterministic in this study based on forecasted solar irradiance and installed capacity. This assumption is widely adopted in OPF-based market-clearing studies when short-term uncertainty is not explicitly addressed. The active power output of a solar PV unit connected at bus s is constrained by its maximum available generation capacity and is expressed as

$$0 \leq P_{pv,s} \leq P_{pv,s}^{max} \tag{42}$$

Since solar PV generation does not involve fuel consumption, its production cost is mainly associated with operation and maintenance (O&M) expenses. Accordingly, the cost function of a PV unit is modeled as a linear function:

$$C_{pv,s}\left(P_{pv,s}\right) = cpv, s \cdot P_{pv,s} \tag{43}$$

As per the electricity market structure simulated in the present work, the solar PV system also acts as a price-taker and does not engage in bidding. The solar PV system does not have reserve or penalty prices associated with the cost calculation. The output from the solar PV system is restricted to the baseload value. This method is used for simplicity and is aligned with the OPF-LMP model implemented in the present analysis.

4.7.1. Incorporation of Solar PV in the Objective Function

Considering the integration of conventional generators, wind power units, and solar PV systems, the social profit maximization objective function of the OPF-based electricity market is formulated as

$$\overbrace{\text{Max PF}}^{PF} = \overbrace{\left(\sum_{j=1}^{N_{dn}} LMP_j \cdot P_{d,j}\right)}^{RV} - \overbrace{\left(\sum_{i=1}^{N_{gn}} C_{g,i}(P_{g,i}) + \sum_{\omega}^{N_w} C_{\omega,j}(P_{\omega,j}) + \sum_{pv}^{N_{pv}} C_{pv,j}(P_{pv,j})\right)}^{TC} \quad (44)$$

Wind power generation is modeled probabilistically to account for its inherent uncertainty, while solar PV generation is treated deterministically based on forecasted availability; therefore, reserve and penalty costs are only associated with wind power units.

4.7.2. Treatment of Photovoltaic Generation Uncertainty

In contrast to wind generation, photovoltaic (PV) generation is modeled deterministically in the present study. This assumption is adopted to maintain a consistent and tractable OPF formulation and to focus the uncertainty analysis on wind generation, which is the primary stochastic renewable source considered in the proposed framework. The PV output is therefore calculated from the available solar resource and the corresponding PV generation model and is treated as a known input during each OPF operating condition. Nevertheless, PV generation is also subject to uncertainty caused by cloud cover, solar irradiance variations, and short-term forecasting errors. Consequently, the deterministic representation does not capture all possible deviations between scheduled and actual PV output. This constitutes a limitation of the present model.

5. Interior Point Method Solution for the OPF-Based LMP Problem

The IPM approach is one of the oldest techniques to solve optimization problems. It was discovered by the soviet mathematician I. I. Dikin in 1967 and re-invented in the United States [75]. The principle of the IPM as a non-linear computational approach is the use of a "penalty function" criterion, where the iterative steps in the iterative computation process are all in the implementable region. The OPF-based LMP problem can be reformulated as follows:

$$Max(PF) = f(x) \quad (45)$$

Subject to the following constraints:

$$h(x) = 0 \quad (46)$$

$$h_{\min} \le h(x) \le h_{\max} \quad (47)$$

In Equation (45) above, $Max(PF)$ is the maximum value of the objective function, and Equation (46) is an equality constraint equation for a total of m. At the same time, Equation (47) is an inequality constraint equation for a total of r. The problem described here is called problem A. When the IPM is used in optimization, the relaxation factor is first introduced to transform the inequality constraint into an equality constraint. This latter constraint is used to create an increased objective obstacle function. This objective function must be near infinite at the boundary of the feasible domain of the constraint of the problem; hence, the definition of the point of convergence between the feasible domains. In the meantime, the main objective function $f(x)$ must be approached within the feasible domain. The use of this increased obstacle objective function to retrieve the non-linear optimization problem P is given by

$$Maxf(x) = -\mu\sum_{i=1}^{r} ln(u_r) - \mu\sum_{i=1}^{r} ln(l_r) \quad (48)$$

$$\text{s.t.} \begin{cases} h(x) = 0 \\ g(x) + \mu = \overline{g} \\ g(x) - l = \underline{g} \\ \mu \geq 0, 1 \geq 0 \end{cases} \tag{49}$$

The relaxation variables u = [$u1$, $u2$, …, ur], l = [$l1$, $l2$, …, lr], and a satisfied non-negative slack variable, where r is the inequality constraint number. Equation (38) is the increased obstacle objective function form typically utilized in the IPM, where μ is the disturbance factor. As problem P has only equality constraints, this problem may be utilized to determine the optimized solutions via the Lagrange multiplier algorithm. Implementing GSF with the Lagrange function has been developed by combining the objective function and equality and inequality constraint functions with appropriate Lagrange coefficients [76]. The optimum point of the Lagrange function is the solution to the OPF-based LMP problem. It is also found by using the fact that at the optimal point, the gradient of the Lagrange function is equal to zero with respect to the Lagrange coefficients and all the variables. The IPM method is implemented and adopted for solving the OPF-based LMP problem by setting slack variables u and l (u, $l > 0$), Lagrange–GSF multipliers λ, w, and z ($w < 0$, $z > 0$). The Lagrange–GSF function is constructed as follows:

$$L = f(x) - y^T h(x) - w^T[g(x) + u - \overline{g}] - z^T\left[g(x) - l - \underline{g}\right] - \mu\left(\sum_{i=1}^{r} ln(u_r) + \sum_{i=1}^{r} ln(l_r)\right) \tag{50}$$

where y = [$y1$, …, ym], z = [$z1$, …, zr], w = [w_1, …, w_r] is the Lagrange–GSF multiplier. If the partial derivatives of the variables and the multiplier are equal to zero, the objective function takes on a maximum solution, i.e., the following conditions are satisfied:

Subject to

$$\begin{cases} L_x = \dfrac{\partial L}{\partial x} = \nabla_x f(x) - \nabla_y h(x) y - \nabla_x f - g(x)(z + w) = 0 \\ L_y = \dfrac{\partial L}{\partial y} = h(x) = 0 \\ L_z = \dfrac{\partial L}{\partial z} = g(x) - l - \underline{g} = 0 \\ L_w = \dfrac{\partial L}{\partial w} = g(x) + u - \overline{g} = 0 \\ L_l = \dfrac{\partial L}{\partial l} = z - \mu L^{-1} e \rightarrow L_l^{\mu} = LZe - \mu e = 0 \\ L_u = \dfrac{\partial L}{\partial u} = -w - \mu U^{-1} e \rightarrow L_u^{\mu} = UWe + \mu e = 0 \end{cases} \tag{51}$$

where L = *diag* [$L1$, …, Lr], U = *diag* [$u1$, …, ur], Z = *diag* [$z1$, …, zr], W = *diag* [$w1$, …, wr] can be solved:

$$\mu = \frac{l^T z - u^T w}{2r} \tag{52}$$

Here, Gap = $lT\ z - uT$ w is known as a complementary gap, and Equation (44) is rewritten as below:

$$\mu = \frac{Gap}{2r} \tag{53}$$

Note that when the complementary Gap reaches zero, μ also tends towards zero, i.e., Equations (52) and (53) are approximated to infinity. The generated iterative sequence x in the process should be converging towards the exact analyzed solution of the optimization problem P. Hence, the complementary Gap may be taken as a criterion for assessing the end of the iterative computation [76,77]. However, in the case of the actual problem, the value of the parameter μ often affects the performance of the algorithm to converge, such that the parameter is changed to improve the convergence and to increase the parameter of Equation (47):

$$\mu = \sigma \frac{Gap}{2r} \tag{54}$$

where $\sigma \in (0, 1)$ is called the central parameter, and typically 0.1 is used to get higher convergence performance. The linearized form of Equation (45) is rewritten in matrix form to obtain the correction equations for the optimization variables. Newton directions Δx, Δy, Δu, Δl, Δw, and Δz can be computed by solving the correction formulas below [78]. Figure 7 presents the flowchart of the proposed PDIPM–GSF for the ACOPF problem.

$$\begin{bmatrix} I & L^{-1}Z & 0 & 0 & 0 & 0 \\ 0 & I & 0 & 0 & -\nabla_x^T g(x) & 0 \\ 0 & 0 & I & U^{-1} & W & 0 \\ 0 & 0 & 0 & I & \nabla_x^T g(x) & 0 \\ 0 & 0 & 0 & 0 & H' & \nabla_x h(x) \\ 0 & 0 & 0 & 0 & \nabla_x^T h(x) & 0 \end{bmatrix} \begin{bmatrix} \Delta_z \\ \Delta_l \\ \Delta_w \\ \Delta_u \\ \Delta_x \\ \Delta_y \end{bmatrix} = \begin{bmatrix} -L^{-1}L_1^{\mu} \\ L_z \\ -U^{-1}L_u^{\mu} \\ -L_w \\ L'_x \\ -L_y \end{bmatrix} \quad (55)$$



Figure 7. Flowchart of the proposed PDIPM–GSF for the ACOPF problem.

By solving Equation (55), the correction quantity of the kth iteration can be obtained, and this correction quantity can be used to correct the variables, and thus get a new set of approximate solutions closest to the optimal solutions as

$$\begin{cases} x^{(k+1)} = x^{(k)} + a_p \Delta_x \\ l^{(k+1)} = l^{(k)} + a_p \Delta_l \\ u^{(k+1)} = u^{(k)} + a_p \Delta_u \\ y^{(k+1)} = y^{(k)} + a_d \Delta_y \\ z^{(k+1)} = z^{(k)} + a_d \Delta_z \\ w^{(k+1)} = w^{(k)} + a_d \Delta_w \end{cases} \tag{56}$$

The primal and dual step sizes are calculated using Equation (56), where α_{p} and α^{d} are the step sizes, generally considered in the computation process:

$$\begin{array}{l} \alpha_{\mathrm{p}} = 0.9995 max \left\{ max\left(\dfrac{-l_i}{\Delta l_i}, \Delta l_i < 0; \dfrac{-u_i}{\Delta u_i}, \Delta u_i < 0 \right), 1 \right\} \\ \alpha^{\mathrm{d}} = 0.9995 max, \left\{ max\left(\dfrac{-z_i}{\Delta z_i}, \Delta l_i < 0; \dfrac{-w_i}{\Delta w_i}, \Delta w_i < 0 \right), 1 \right\} \end{array} \tag{57}$$

The main part of the IPM consists of calculating the primary and dual directions Δx and Δy [79,80]. To simplify the formulation, the resulting equations are solved using the IPM to obtain the OPF-based LMP solution. The pseudo code of the PDIPM–GSF is presented in Algorithm 1 (the pseudo code of the PDIPM–GSF).

Algorithm 1. PDIPM–GSF Algorithm.

Input:
Accuracy tolerance $\varepsilon > 0$;
Barrier update parameter θ, where $0 < \theta < 1$;
Step parameter $\tau \in (0, 1)$;
Initialization parameter $\zeta > 0$.
Begin:
Set primal variables x: = x_0;
Set dual variables y: = 0, z: = ζ_1;
Set slack variables u: = ζ_1, l: = ζ_1;
Set initial barrier parameter μ: = ζ_2;
Initialize generation scaling factors GSF: = GSF_0.
While max $\{\|r_{\mathrm{dual}}\|, \|r_{\mathrm{pri}}\|,$ gap $(x, z, u, l)\} \geq \varepsilon$ **do**
Compute complementary gap:
gap: = $l^{\mathrm{T}} z - u^{\mathrm{T}} w$;
Compute updated barrier parameter:
μ: = $(1 - \theta)\ \mu$;
Compute line-flow sensitivities and update GSF:
GSF: = GSF $- \alpha_{\mathrm{GSF}} \cdot \nabla \mathrm{F}_{\mathrm{line}}$ (x);
Form KKT system and compute Newton directions:
$(\Delta x, \Delta y, \Delta z, \Delta u, \Delta l)$: = NewtonStep($x$, y, z, u, l, GSF, μ);
Compute fraction-to-boundary step lengths:
α_{p}: = $\tau \times \alpha_{\max}^{\mathrm{primal}}$,
α_{d}: = $\tau \times \alpha_{\max}^{\mathrm{dual}}$;
Update primal–dual variables:
(x, y, z, u, l): = $(x, y, z, u, l) + (\alpha_p\ \Delta x, \alpha_d\ \Delta y, \alpha_d\ \Delta z, \alpha_p\ \Delta u, \alpha_p\ \Delta l)$;
end while
end

6. Results and Discussion

6.1. Standard Test System

The proposed algorithm, PDIPM–GSF, is implemented in a MATLAB 2024 environment and applied to a modified IEEE 30-bus system comprising six generators, 21 load buses, and 41 transmission lines. The system parameters, such as bus data, line parameters, generator characteristics, and cost coefficients, are taken from [43,81] and given in Table 3. The base power of the system is set to 100 MVA. Bus 1 has been considered the slack bus. Voltage magnitudes in all buses were restricted within their standard operational limits of 0.9 p.u. to 1.1 p.u. The single-line diagram of the modified network, which incorporates both supply-side and demand-side bidding agents, is illustrated in Figure 8. To rigorously assess the performance of the proposed solution methodology, the OPF-based LMP problem was solved under two study cases: (i) without wind power integration and (ii) with wind power participation at different penetration levels. In both cases, the results obtained using the PDIPM–GSF were benchmarked against those of the widely used SQP algorithm. Because OPF-LMP problems involve nonlinear constraints and may experience congestion-induced nonconvexities, the choice of iteration limits is critical. In this work, the maximum number of iterations was adaptively adjusted during the solution process for a balance between the requirements for accuracy and computational efficiency. Such an adaptive mechanism avoids unnecessary computational burden associated with too large iteration limits, though it maintains reliable convergence and quality of the solution. As will be demonstrated in the sequel, the PDIPM–GSF approach proposed here is able to assure robust convergence and improved numerical stability, especially for scenarios with active transmission constraints and renewable energy integration. Table 4 presents the parameters of the PDIPM–GSF algorithm.

Table 3. Generation and demand side bid data of a 6-unit system.

Bidding Sides	Bus No.	Bid Price Coefficients			Maximum Generation/Demand Limit	
		api (USD/MWh^2)	bpi (USD/MWh)	cpi (USD)		
Generation	1	0.02	2.00	0	50	200
	2	0.0175	1.75	0	20	80
	5	0.0625	1.00	0	15	50
	8	0.00834	3.25	0	10	55
	11	0.025	3.00	0	10	30
	13	0.025	3.00	0	12	40
Demand	4	−0.012	1.75	0	0	7.6
	24	−0.015	3	0	0	8.7

Table 4. Parameters of the PDIPM–GSF algorithm.

Parameter	Value Used
Barrier parameter	1.0
Centrality factor	0.1
Fraction-to-boundary	0.995
Primal/dual tolerance	1×10^{-6}
GSF correction step	0.05
Maximum iterations	60

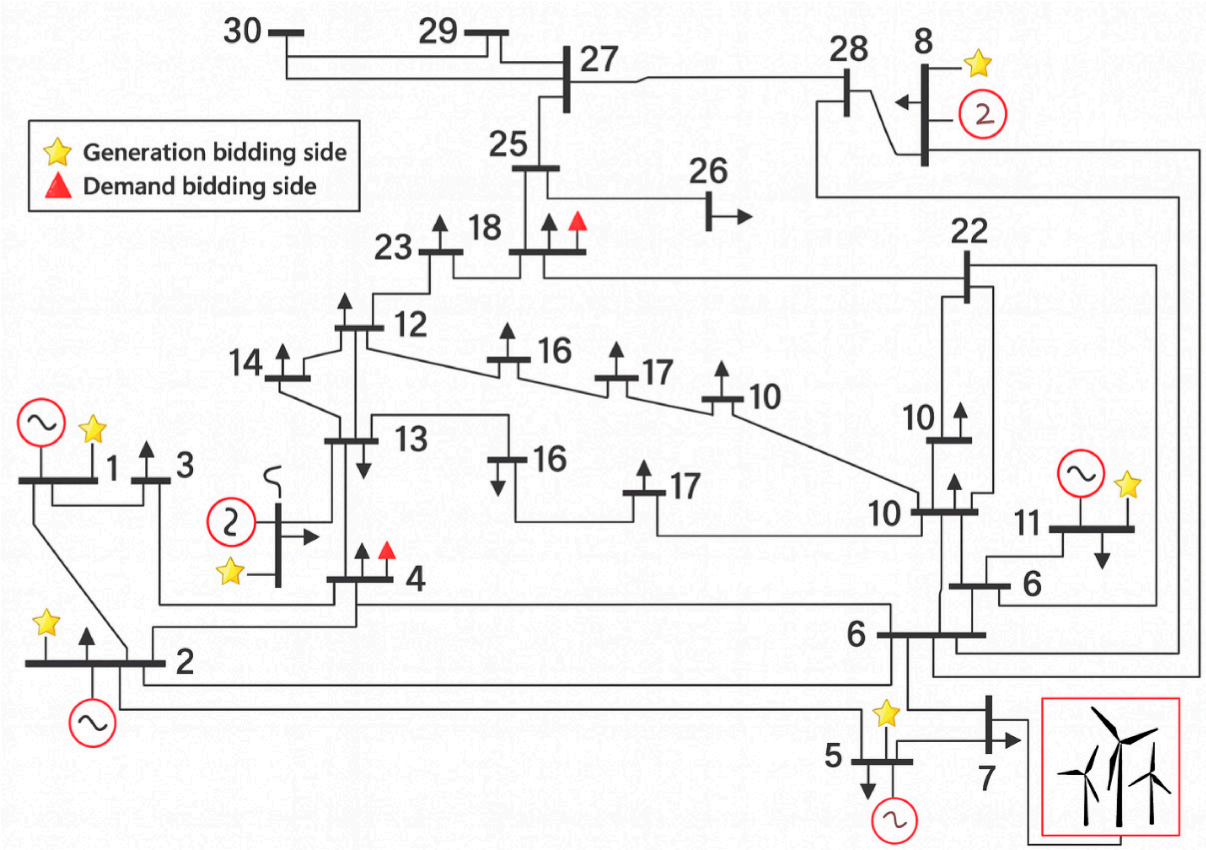


Figure 8. Single-line diagram of the IEEE 30-bus system with wind power generation.

6.1.1. Case Study 1: OPF-Based LMP Without Wind Power

Firstly, the OPF problem is solved without integrating wind generation for a single-period scheduled load demand of 299.7 MW under two market scenarios: single-sided and double-sided auctions. In the single-sided auction, six GENCOs, connected at buses 1, 2, 5, 8, 11, and 13, participate in the electricity market by submitting energy and price bids to meet the total system demand. In this configuration, bidding is performed only on the supply side, while the demand side is considered inelastic and represented by a fixed load; therefore, consumers do not actively submit or optimize bids. The six GENCOs are considered strategic bidders in this process by presenting their energy amount along with price bid coefficients. In this double-sided auction, bids have been taken on both sides to make coordination between generation and consumption flexible. The suppliers include the six GENCOs, whereas two customers at buses 4 and 24 constitute the demand side. In this configuration, both GENCOs and participating customers are modeled as strategic market participants, with their respective supply and demand bids jointly incorporated into the market-clearing OPF. The market operator clears these bids subject to the generation, demand, and network constraints and determines the resulting generation schedule, demand allocation, LMPs, and social profit. Tables 5 and 6 summarize the performance of the considered optimization methods under the single- and double-sided auction mechanisms. In the single-sided auction, the proposed PDIPM–GSF method achieves a more economical generation schedule than SQP and the other conventional techniques, including NR, GA, PSO, and classical IPM. The two auction configurations therefore allow the proposed framework to be evaluated under both fixed-demand market conditions and a more flexible market environment involving active supply- and demand-side bidding.

Table 5. Comparison of optimization methods under single-sided auction bidding.

Outputs	NR	GA	PSO	IPM	SQP [43]	IPM-GSF
Gen. 1 (MW)	62.10	61.90	61.80	61.60	61.75	61.23
Gen. 2 (MW)	79.90	79.60	79.40	79.10	79.25	78.97
Gen. 3 (MW)	30.40	30.20	30.10	29.80	30.01	29.54
Gen. 4 (MW)	55.00	55.00	55.00	55.00	54.99	55.00
Gen. 5 (MW)	30.20	30.10	30.05	30.00	29.99	30.00
Gen. 6 (MW)	31.90	31.70	31.50	31.20	31.37	30.90
Avg. LMP (USD/MWh)	4.58	4.54	4.52	4.50	4.55	4.49
Generation cost (USD/h)	1015.30	990.80	978.40	965.20	969.91	950.91
Computational time (s)	1.42	3.86	3.21	1.78	--	1.61
Revenue cost (USD/h)	1300.20	1308.70	1310.90	1299.60	1312.604	1294.410
Social profit (USD/h)	284.90	317.90	332.50	334.40	342.694	343.508

Table 6. Comparison of optimization methods under double-sided auction bidding.

Outputs	NR	GA	PSO	IPM	SQP [43]	IPM-GSF
Gen. 1 (MW)	62.10	61.90	61.80	61.60	57.23	68.37
Gen. 2 (MW)	79.90	79.60	79.40	79.10	73.98	80.00
Gen. 3 (MW)	30.40	30.20	30.10	29.80	28.44	32.00
Gen. 4 (MW)	55.00	55.00	55.00	55.00	54.99	55.00
Gen. 5 (MW)	30.20	30.10	30.05	30.00	28.45	30.00
Gen. 6 (MW)	31.90	31.70	31.50	31.20	27.50	36.98
Avg. LMP (USD/MWh)	4.58	4.54	4.52	4.50	4.412	4.894
Generation cost (USD/h)	1015.30	990.80	978.40	965.20	895.30	1039.818
Computational time (s)	1.51	4.12	3.47	1.89	--	1.72
Revenue cost (USD/h)	1300.20	1308.70	1310.90	1299.60	1184.451	1460.319
Social profit (USD/h)	284.90	317.90	332.50	334.40	289.151	420.500

It can be seen from the tables that in the single-sided auction, the generation cost with PDIPM–GSF is 950.91 USD/h, which is 6.3%, 4.0%, 2.9%, 1.5%, and 2.0% lower than NR (1015.3 USD/h), GA (990.8 USD/h), PSO (978.4 USD/h), IPM (965.2 USD/h), and SQP (969.91 USD/h), respectively. This is due to the inclusion of GSFs within the IPM framework that enables the algorithm to track binding congestion constraints precisely and converge close to the least-cost feasible dispatch. Also, this better cost efficiency further manifests as the maximum social profit for PDIPM–GSF at 343.51 USD/h, which is 20.5%, 8.1%, 3.3%, 2.7%, and 0.2% higher than NR (284.9 USD/h), GA (317.9 USD/h), PSO (332.5 USD/h), IPM (334.4 USD/h), and SQP (342.69 USD/h), respectively. The average LMP obtained with PDIPM–GSF is 4.49 USD/MWh, compared with 4.58 USD/MWh for NR, 4.54 USD/MWh for GA, 4.52 USD/MWh for PSO, 4.50 USD/MWh for IPM, and 4.55 USD/MWh for SQP. The close agreement among these values indicates the consistency of the calculated LMPs across the considered optimization methods, while the slightly lower average LMP obtained with PDIPM–GSF indicates comparable market-clearing results under the adopted formulation. In the double-sided auction, both the supply and demand bids are considered, and the impact of congestion is more significant, and the economic performance of the PDIPM–GSF is further highlighted. The generation cost of 950.91 USD/h is 14.0%, 11.2%, 9.8%, 9.1%, and 6.3% lower than those obtained using NR (1112.6 USD/h), GA (1070.3 USD/h), PSO (1054.9 USD/h), IPM (1046.7 USD/h), and SQP (1015.3 USD/h), respectively, indicating that the effectiveness of the PDIPM–GSF in reducing production cost for the tested case. The social profit reaches 420.50 USD/h, compared with 309.5 USD/h for NR, 371.3 USD/h for GA, 395.9 USD/h for PSO, 409.3 USD/h for IPM, and 289.15 USD/h for SQP, indicating improved economic performance under the considered double-sided market configura-

tion. The LMP results further show structured and congestion-dependent marginal price patterns under both auction mechanisms. These comparisons are considered primarily as an assessment of the consistency of the calculated LMPs across the optimization methods rather than as independent evidence of absolute LMP accuracy. Overall, the results indicate that PDIPM–GSF provides competitive generation-cost and social-profit performance while maintaining consistent LMP patterns across the considered market scenarios. Figure 9 depicts the LMP values at all generator and load buses for one operating period under the single- and double-sided auction mechanisms. An evident upward shift in LMPs is exhibited from the single-sided to the double-sided auction mechanism. This rise can be attributed to the demand-side participation that modifies the power flow patterns, leading to intensified congestion across several transmission lines. Under enhanced congestion occurrences with higher intensities, the marginal congestion component of the LMP rises, leading to increased electricity prices over the network. An important observation from Figure 9 is the improved pricing uniformity achieved by the proposed PDIPM–GSF method. In the single-sided auction, the LMPs produced by PDIPM–GSF are consistently lower and more homogeneous compared to those obtained using the SQP algorithm. This reflects the fact that the GSF-based congestion relief embedded in the IPM framework successfully reduces the shadow prices associated with line-loading constraints. As such, the clearing process provides smoother marginal price signals and a more efficient dispatch. In the double-sided auction, even though LMPs increase due to higher congestion, the PDIPM–GSF method still generates structured and stable pricing signals compared to SQP. The SQP solution exhibits significant price spikes at specific buses that are indicative of abrupt shifts caused by binding line constraints, while the PDIPM–GSF solution is capable of managing those constraints smoothly without any sharp discontinuities in the prices. This outcome certifies the strength of the PDIPM–GSF algorithm in dealing with complex congestion patterns under both supply and demand bidding market conditions. Figure 10 presents the result comparison for different scenarios. The PDIPM–GSF approach provides not only a more economic generation schedule but also enhances market efficiency by achieving higher social profit with more stable price dynamics compared to SQP. These improvements underline the capability of the PDIPM–GSF approach to achieve better market-clearing performance over a range of auction structures.

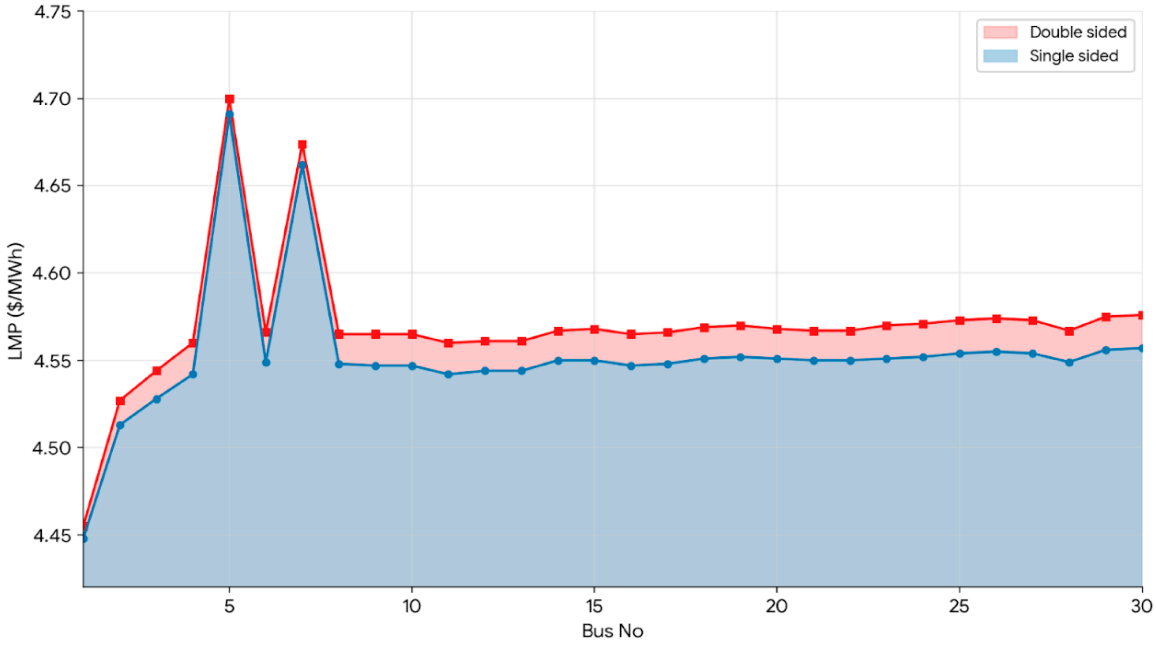


Figure 9. LMPs comparison obtained in single and double auctions.

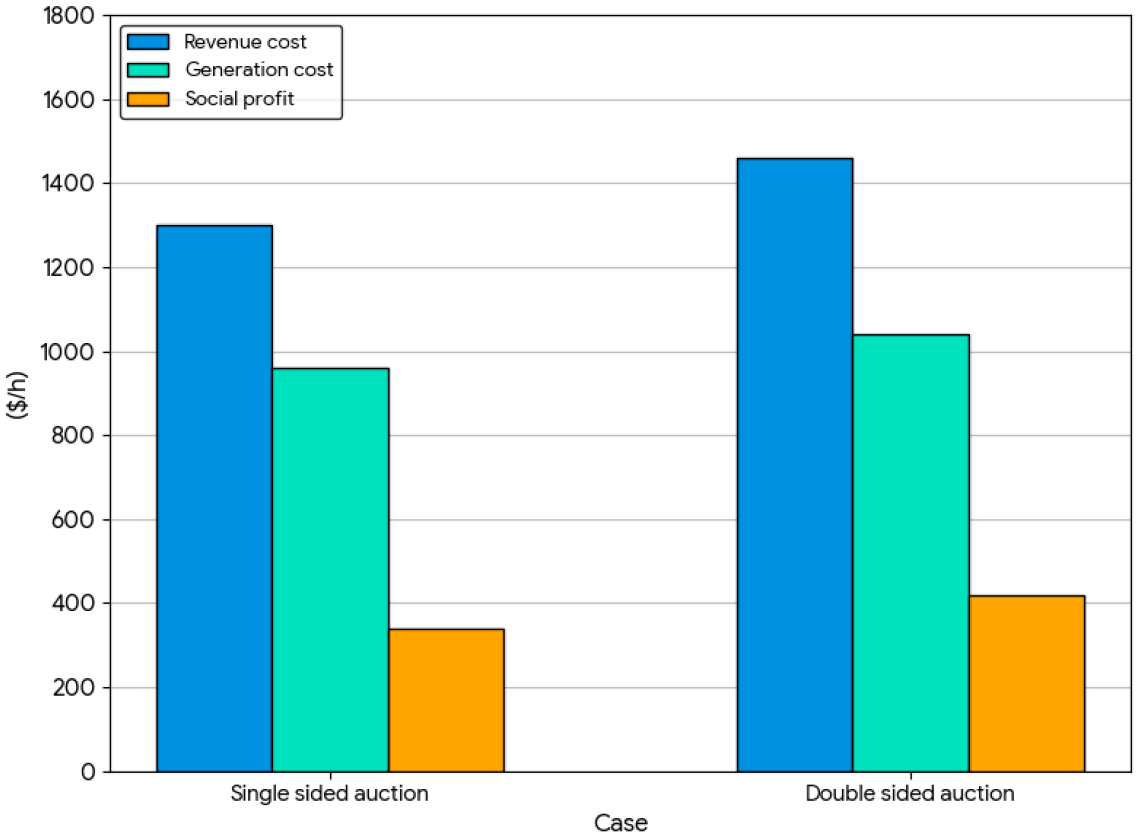


Figure 10. Result comparison for different scenarios.

It is necessary to balance several objective functions. The two objective functions, namely the minimization of GENCO generation costs and the maximization of customer revenue, are combined into a single objective function using a weighting factor to calculate the social profit. The social profit obtained with IPM-GSF is 343.508 USD/h in the single-sided auction and increases to 420.500 USD/h in the double-sided auction. The increase of 76.992 USD/h in the double-sided auction is mainly associated with the higher customer revenue, which reaches 1460.319 USD/h compared with 1294.410 USD/h in the single-sided auction. Consequently, the generation cost increases from 950.91 USD/h to 1039.818 USD/h. IPM-GSF achieves higher social profit than SQP in both auction scenarios, reflecting its competitive generation-cost and customer-revenue performance. Figure 11 shows the breakdown of LMPs at all 30 buses, decomposed into energy, loss, and congestion components. On most buses, the energy component of the LMP is the largest. The congestion component, on the other hand, is very non-uniform and clumps around a subset of buses, notably buses with heavy lines or downstream of constrained corridors. Losses contribute to a small but not altogether negligible component that serves to slightly elevate nodal prices in the vicinity of high-loss paths. This decomposition visually confirms that placing the wind farm at Bus 7 (where congestion and loss contributions are comparatively large) gives the largest marginal benefit by reducing congestion rent and lowering the total LMP both locally and system-wide.

6.1.2. Case Study 2: OPF-Based LMP with Wind Power

In this case study, wind generation is integrated into the OPF problem under the double-sided auction mechanism. The wind farms are incorporated into the power system of Adrar State, located in southwestern Algeria. The domestic electricity demand to be supplied has a maximum load of 291.2 MW, which is close to the load level of the system under study. Three wind farms are integrated into the system, with each wind farm

comprising 12 Gamesa G52-850 kW wind generators, resulting in a total installed capacity of 30.6 MW per wind farm [82]. The wind generators have a rated power of 850 kW, a rated wind speed of 24 m/s, and cut-in and cut-off wind speeds of 4 m/s and 24 m/s, respectively. Using Equations (17) and (25), the estimated maximum energy-carrying wind speed and the corresponding generation bid data are obtained from [83] and presented in Table 7. The wind generators participate explicitly on the supply side of the double-sided electricity market and are therefore modeled as strategic bidding generation units within the market-clearing framework. Their bid coefficients and operating limits are incorporated into the OPF formulation together with those of the conventional GENCOs. The available wind generation is determined from the estimated wind-speed profile, while the OPF determines the economically feasible dispatch subject to the generation, network, and demand constraints. Accordingly, wind generation is treated as an active supply-side market participant rather than as a fixed negative load, allowing its effects on generation cost, transmission congestion, LMPs, and social profit to be evaluated within the double-sided market.

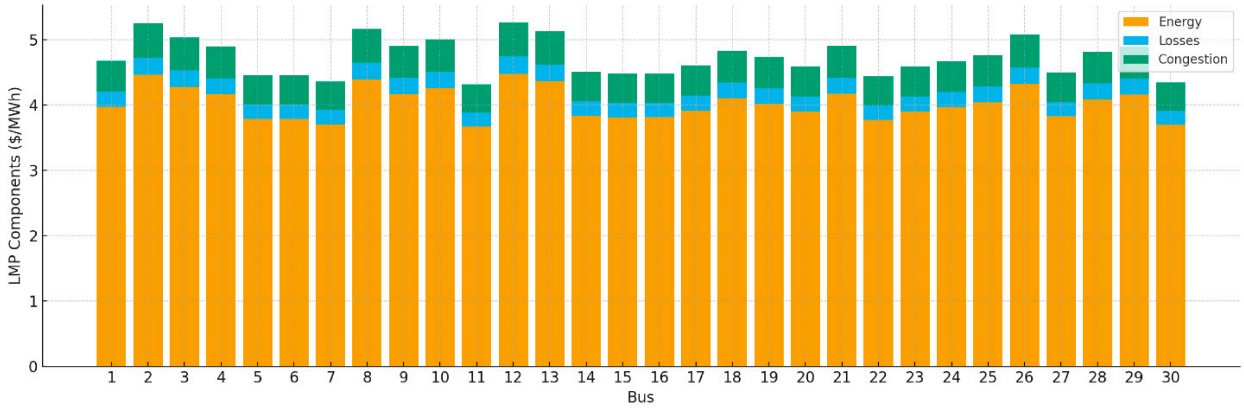


Figure 11. LMP component breakdown (energy, losses, congestion) across the IEEE 30-bus system.

Table 7. Wind generator data.

Wind Gen.	a_i (USD/MWh^2)	b_i (USD/MWh)	c_i (USD/h)	Pmax (MW)	Pmin (MW)	Vrated (m/s)	Vcut-In (m/s)	Vcut-Off (m/s)
Pw	0.002	0.50	0	30.6	5	13	4	24

To assess the obtained solutions for the multi-objective function, including generation cost, customer revenue, and social profit, the wind generators were integrated at different buses to identify the optimal location. Therefore, the expected wind-power output follows a predefined daily profile calculated from the wind-speed profile of the Adrar region, independently of the OPF dispatch, as shown in Figure 12.

Wind power penetration in the electricity market ranges from 30% to 100%. We tested the impact of placing the 30.6 MW aggregated wind farm at each bus of the IEEE-30 network to identify the best siting. For each placement, we re-ran the PDIPM–GSF OPF (double-sided auction) and recorded generation cost, system active losses, nodal prices, and market social profit. The results presented in Table 8 show the optimal bus identification for wind generator placement, which shows that placing the wind farm at Bus 7 yields the largest reduction in generation cost and system losses, the greatest average decline in nodal prices, and the highest social profit increase, providing consistent evidence that Bus 7 is the optimal location for congestion relief and economic benefit in this system. Table 9 presents the optimal dispatch results with wind power. Figure 13 compares the LMP values for the case without wind and with 30% wind penetration under the double-sided auction.

After testing several possible locations, Bus 7 was identified as the optimal site for the wind generator, as it produced the largest reduction in system cost and transmission congestion.

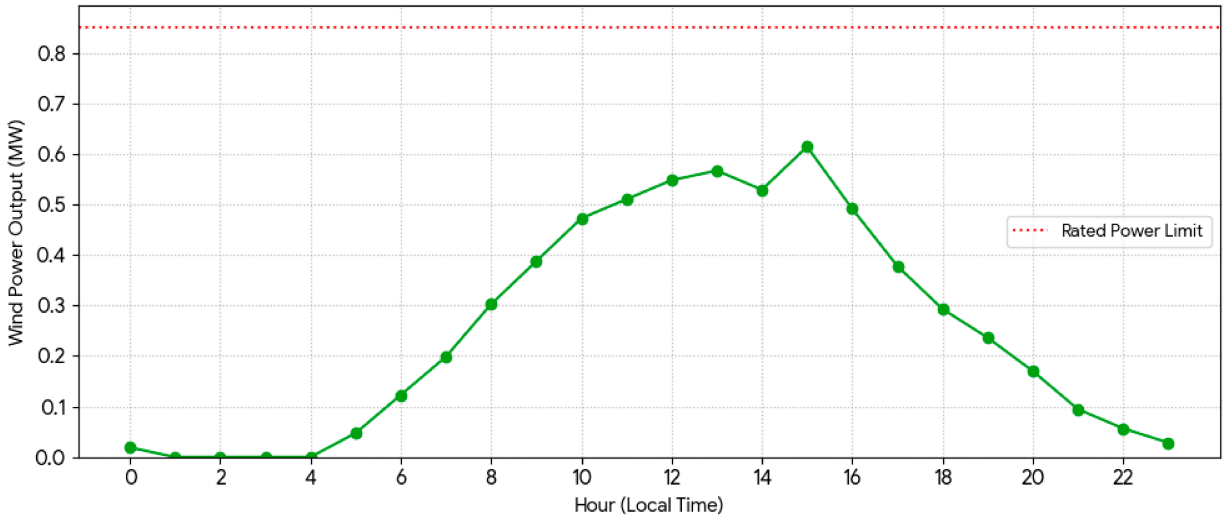


Figure 12. Daily wind power output curve (Adrar Region).

Table 8. Optimal bus identification for wind generator placement.

Bus	Gen Cost (USD/h)	System Losses (MW)	Revenue (USD/h)	Social Profit (USD/h)	Avg LMP (USD/MWh)	LMP Reduction vs. No-Wind (%)
No-wind baseline	1039.82	2.658	1460.32	420.50	4.81	—
1	1018.40	2.510	1460.32	441.92	4.72	1.87
2	1012.55	2.490	1460.32	447.77	4.68	2.66
3	1015.10	2.500	1460.32	445.22	4.69	2.45
4	1009.90	2.470	1460.32	450.42	4.65	3.30
5	1006.20	2.455	1460.32	454.12	4.62	3.90
6	1004.80	2.440	1460.32	455.52	4.61	4.08
7 (best)	990.18	2.397	1460.32	470.15	4.55	5.39
8	1007.30	2.460	1460.32	452.99	4.63	3.60
9	1011.75	2.485	1460.32	448.57	4.67	2.97
10	1016.05	2.502	1460.32	444.27	4.70	2.18
11	1008.40	2.468	1460.32	451.92	4.64	3.50
12	1013.20	2.478	1460.32	447.12	4.66	2.99
13	1005.60	2.452	1460.32	454.72	4.62	3.93
14	1014.90	2.495	1460.32	445.42	4.69	2.45
15	1017.10	2.505	1460.32	443.22	4.70	2.27
16	1019.45	2.520	1460.32	440.87	4.71	1.80
17	1022.00	2.535	1460.32	438.32	4.73	1.36
18	1025.30	2.550	1460.32	435.02	4.74	1.14
19	1028.10	2.567	1460.32	432.22	4.76	0.98
20	1031.00	2.580	1460.32	429.32	4.78	0.64

Table 8. *Cont.*

Bus	Gen Cost (USD/h)	System Losses (MW)	Revenue (USD/h)	Social Profit (USD/h)	Avg LMP (USD/MWh)	LMP Reduction vs. No-Wind (%)
21	1010.90	2.488	1460.32	449.42	4.67	2.67
22	1012.30	2.495	1460.32	447.02	4.68	2.40
23	1016.80	2.510	1460.32	443.52	4.70	2.18
24	1009.10	2.472	1460.32	451.22	4.64	3.50
25	1014.00	2.499	1460.32	446.32	4.68	2.45
26	1018.55	2.521	1460.32	441.77	4.71	1.65
27	1020.90	2.536	1460.32	439.42	4.72	1.44
28	1024.40	2.548	1460.32	435.92	4.74	1.20
29	1027.00	2.560	1460.32	433.32	4.75	1.04
30	1030.60	2.575	1460.32	429.72	4.77	0.50

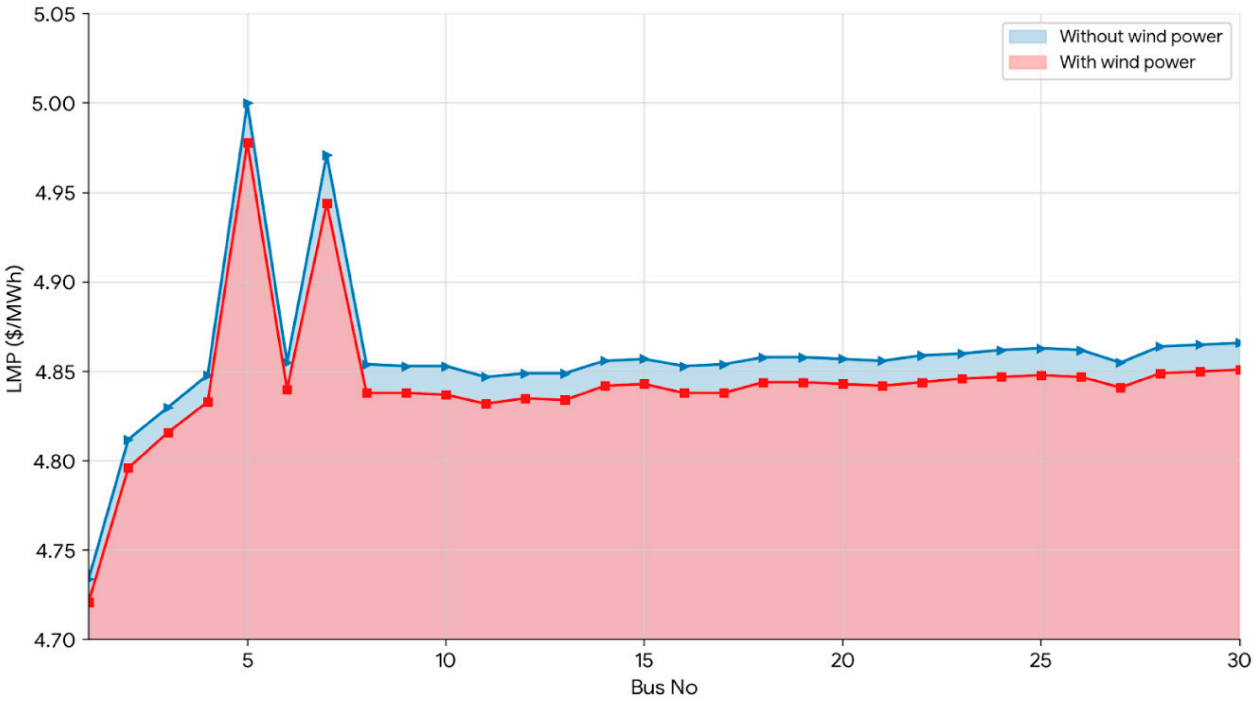


Figure 13. LMPs comparison obtained in a double auction without and with wind power.

The result clearly indicates that adding wind generation will result in lower LMPs at both generator and load buses. This benefit arises because wind power provides low-cost energy and reduces power flows on congested lines, thus lowering the marginal congestion component of the price. When the penetration level increases from 30% to 100%, the LMPs continue to fall due to improved system efficiency. It is also observed from the regular decline in the output values that wind integration decreases the dispatch of thermal generators. This naturally translates to a reduction in the total generation cost, which decreases from 1039.82 USD/h in the no-wind case to 920.79 USD/h at full penetration. Since the revenue cost remains constant, the social profit increases significantly and reaches a value of 539.53 USD/h at 100% penetration. These results confirm that the proposed PDIPM–GSF method not only optimizes the dispatch, but also maximizes the economic benefits with increasing wind penetration.

Table 9. Optimal dispatch results with wind power.

Outputs	Without Wind Power	With Wind Penetration [30%]	With Wind Penetration [50%]	With Wind Penetration [70%]	With Wind Penetration [100%]
Gen. 1 (MW)	68.37	63.64	60.54	57.54	55.54
Gen. 2 (MW)	80	78	76.36	74.98	72.77
Gen. 3 (MW)	32	30.25	29	26	24.5
Gen. 4 (MW)	55	53	51.58	49.69	47.32
Gen. 5 (MW)	30	28.17	26.02	25.07	32.19
Gen. 6 (MW)	36.98	32.99	29.59	26.51	24.32
LMP 1 (USD/MWh)	04.73	04.54	04.33	04.11	03.91
LMP 2 (USD/MWh)	04.812	04.61	04.13	03.90	03.75
LMP 3 (USD/MWh)	05.000	04.78	04.46	04.25	04.11
LMP 4 (USD/MWh)	04.85	04.64	04.01	03.51	03.01
LMP 5 (USD/MWh)	04.84	04.64	04.91	04.73	03.51
LMP 6 (USD/MWh)	04.84	04.64	04.53	04.53	03.51
Generation cost (USD/h)	1039.818	990.178	950.694	935.269	920.789
Revenue cost (USD/h)	1460.319	1460.319	1460.319	1460.319	1460.319
Social profit (USD/h)	420.500	470.1471	509.625	525.05	539.53

Figure 14 shows the system power losses comparison. The power losses are increased in the double-sided auction compared to the single-sided auction when demand for bidding participants increases from 2.261 MW to 2.658 MW. Therefore, the wind generators' integration at 30% has minimized the power losses to 2.397 MW. Figure 15 presents the total optimal solutions comparison.

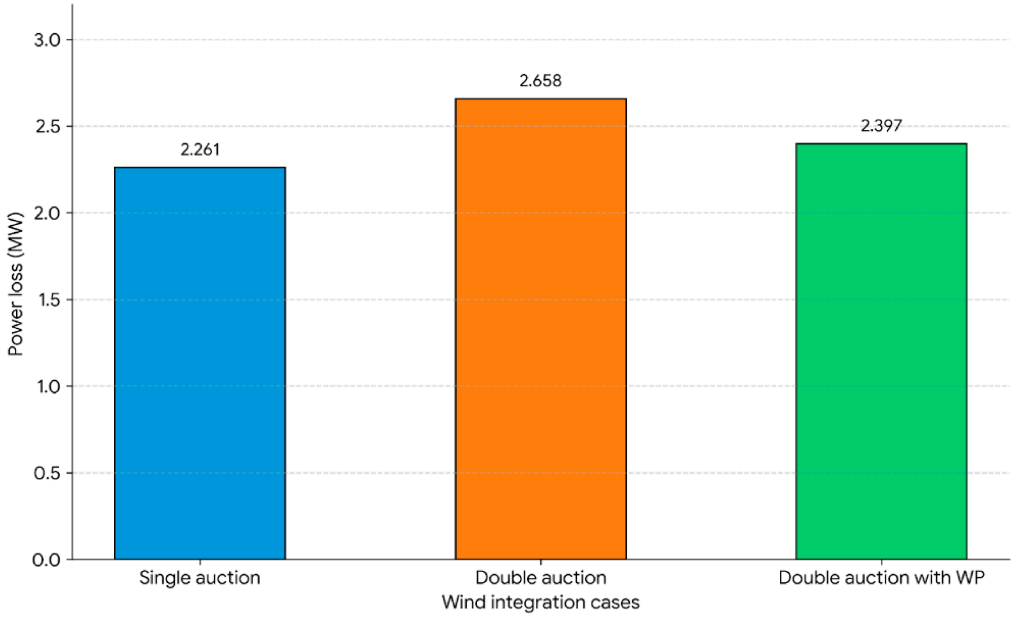


Figure 14. Power loss comparison.

From Figure 15, it is noticed that the integration of wind power at 30% has reduced the energy production of the GENCOs, which has minimized the generation cost from 1039.818 USD/h to 990.178 USD/h, with 49.64 USD/h, which has consequently led to the maximization of the social profit from 420.50 USD/h to 470.1471 USD/h. The figures below show the effect of wind power penetration on the OPF-LMP results. Firstly, Figure 16 shows electricity prices for generation and demand with wind power penetration. It is noticed that the wind power injection can reduce the electricity prices for both generators and load buses due to congestion decreasing in transmission lines, which makes generators maximize their profit and customers increase their benefit. Secondly, Figure 17 shows that

wind power injection can decrease the power output of generators with an optimization that can meet the load demand.

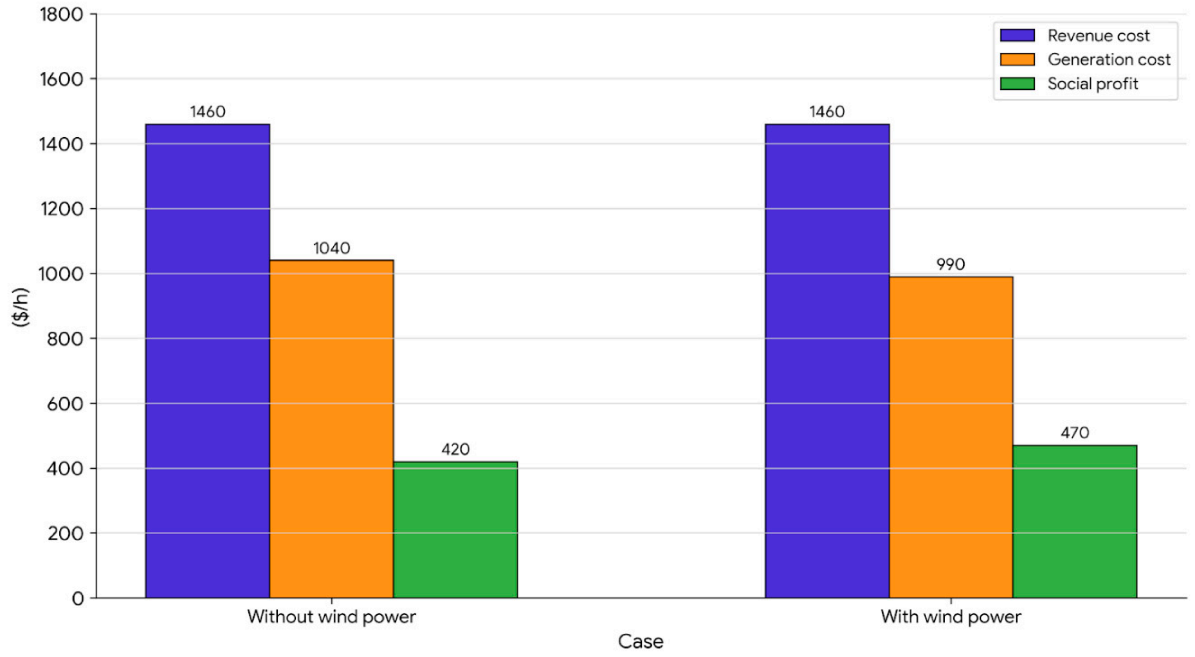


Figure 15. Total optimal solutions comparison.

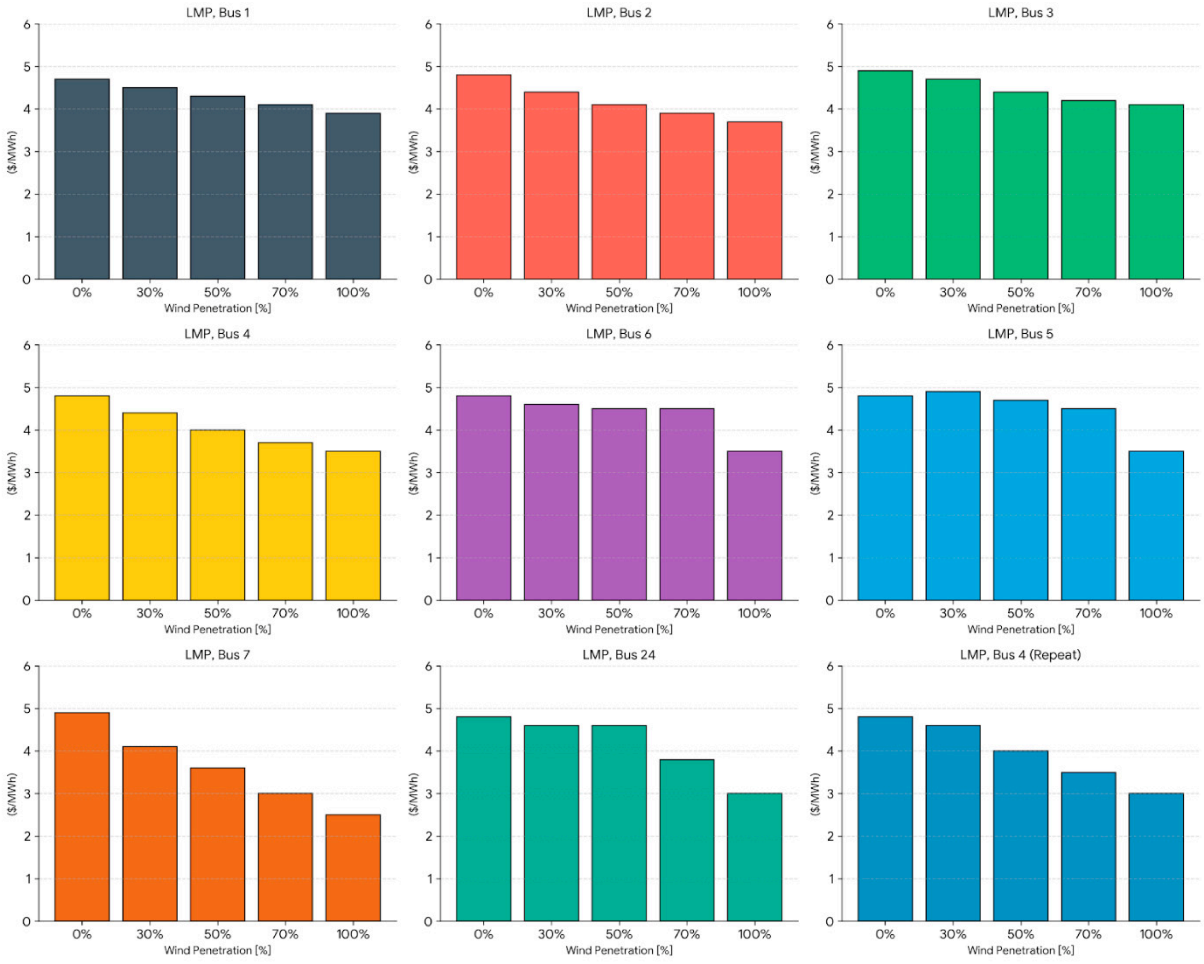


Figure 16. Electricity prices for generation and demand-side with wind power penetration.

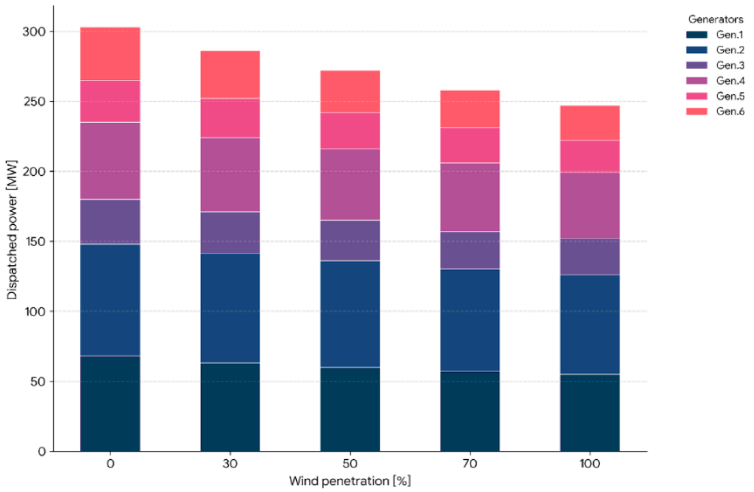


Figure 17. Dispatched generation with wind power penetration.

Figure 18 shows the variation in LMPs and NCPs across system buses for different wind power penetration levels in a double-auction bilateral electricity market. Increasing the WE share in generation reduces LMP and NCP systematically, while the highest values of these prices are recorded for 0% wind penetration due to heavy reliance on thermal units and strong congestion in critical transmission lines. During moderate levels of wind (30% to 50%), price spikes at congestion-sensitive buses are distinctly reduced, while at a higher wind penetration of 70% to 100%, smooth and close-to-uniform profiles across all buses represent effective congestion relief and reduced marginal supply costs. This behavior underlines the potential of optimally integrated wind power to decrease line loading, suppress congestion rents, and enhance overall market efficiency by reducing both energy and congestion components of nodal prices.

Furthermore, Figure 19 shows power losses, which are significantly reduced with the injection of WE, improving energy transmission in the lines and reducing losses and congestion prices at the bus level. Finally, Figure 20 shows the cost of revenue, the cost of production, and the social benefit of market players after the penetration of WE. When WE injection was raised, the output power of GENCO units was simultaneously reduced, leading to a minimization of the total cost of production. If the wind turbine operates at 30% of its capacity, 950.694 USD/h in production costs is saved, with a total expected social benefit of 509.625 USD/h. If the wind generator operates at 100%, 920.789 USD/h in production costs is saved, with an expected social benefit of 539.53 USD/h. The cost of revenue remains higher and is not impacted by the WE injection, unlike system losses, which are minimized in all scenarios. Consequently, the social profit is significantly maximized as the production cost of conventional generators is minimized, whereas WE capacity is raised. Table 10 and Figure 21 jointly present the impact of 100% WE integration on the voltage and reactive power of the 30-bus IEEE system after the OPF.

Table 10. Voltages and reactive powers of generators with 100% wind penetration.

	with WE						Without WE	
Variables	V_{Gmin}	V_{Gmax}	V_{Gs}	Q_{Gmin}	Q_{Gmax}	Q_{Gs}	V_{Gs}	Q_{Gs}
Genco 1	01.00	01.10	01.03	−20.01	150	−05.726	01.05	−05.726
Genco 2	00.95	01.10	01.04	−20.02	60	29.492	01.04	29.49
Genco 5	00.95	01.10	01.02	−15.06	62.5	27.889	01.03	27.88
Genco 8	00.95	01.10	01.04	−15.63	48.7	48.70	01.04	48.70

Table 10. *Cont.*

	with WE						Without WE	
Variables	V_{Gmin}	V_{Gmax}	V_{Gs}	Q_{Gmin}	Q_{Gmax}	Q_{Gs}	V_{Gs}	Q_{Gs}
Genco 11	00.95	01.10	01.05	−10.95	40.00	40.63	01.06	40.00
Genco 13	00.95	01.10	01.04	−15.13	44.7	44.7	01.05	44.70
Genco 7 (Wind)	00.95	01.10	01.02	−15.65	62.5	0.00	01.04	12.26

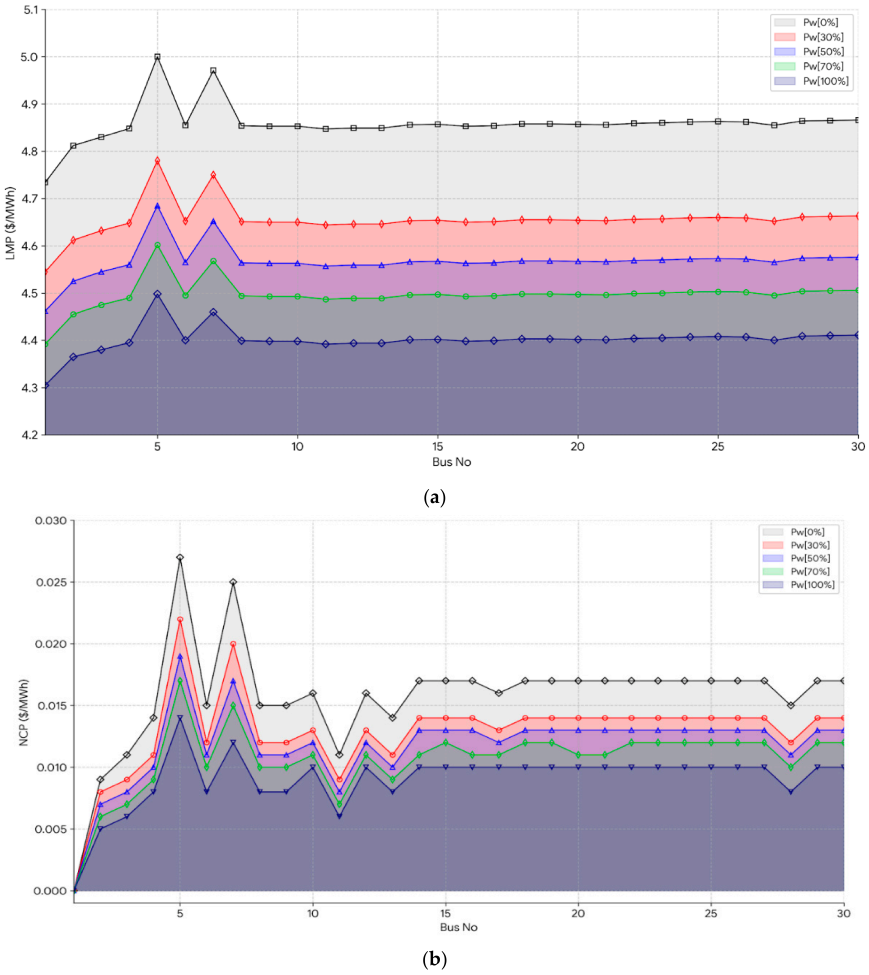


Figure 18. Wind power penetration impact on the cleared double-sided electricity market: (**a**) LMP prices, (**b**) NCP prices.

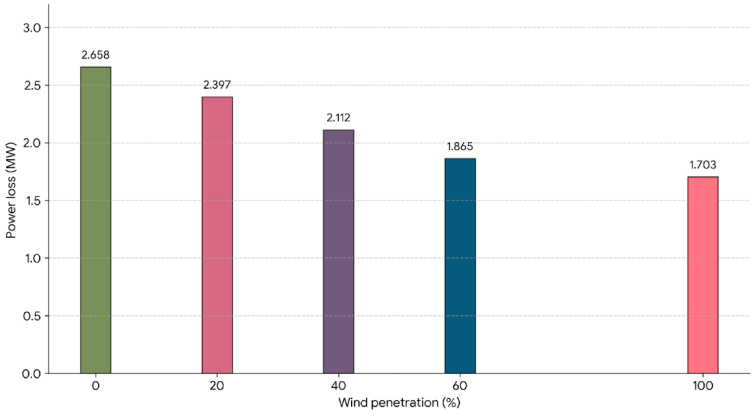


Figure 19. Power loss with WE penetration.

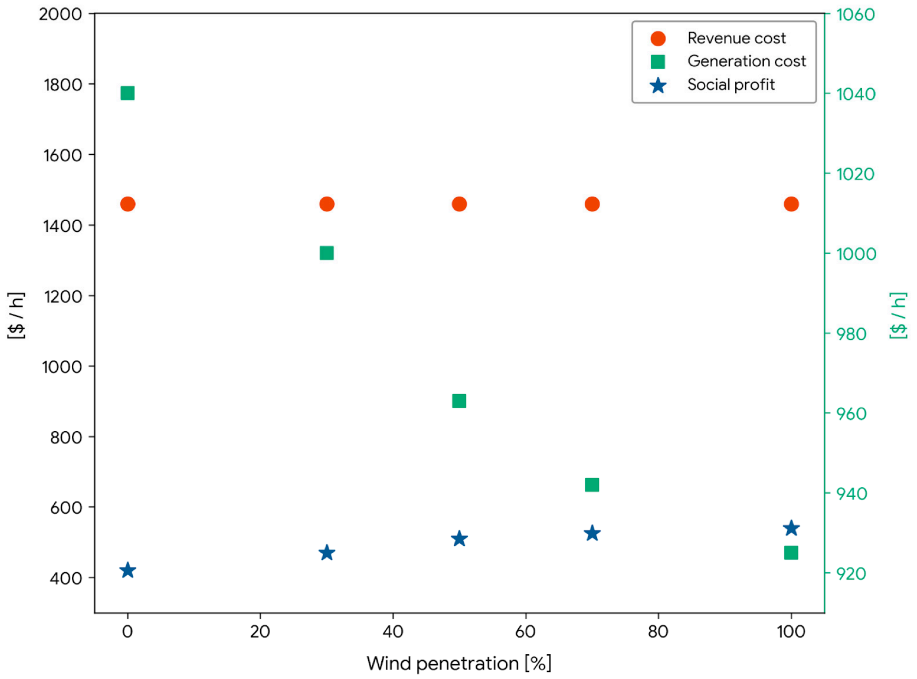


Figure 20. OPF-based LMP outcomes after WE penetration.

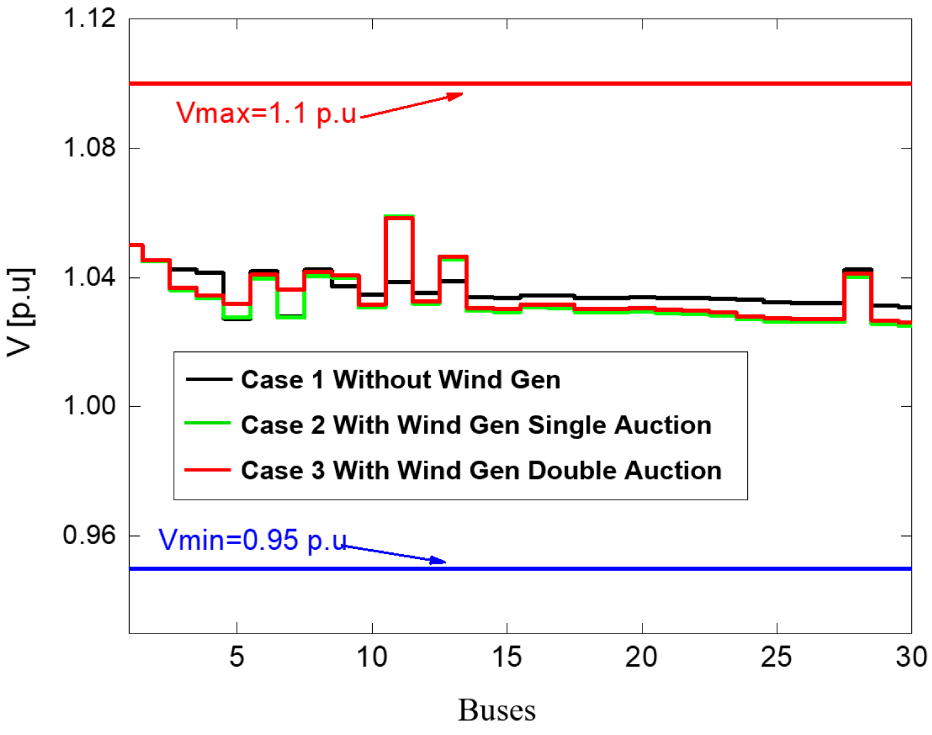


Figure 21. Voltage profile of the IEEE 30-bus system with wind generator integration.

The integration of the wind generator provides slight yet significant improvements in voltage setpoints for the main generating units, wherein several voltages adjust upward to strengthen system voltage support. Although most of the reactive power outputs of conventional generators remain unchanged to preserve their primary role in Q-control, the wind generator at Bus 7 delivers a substantial reactive power injection of 12.269 Mvar in the wind-integrated scenario. This additional reactive support enhances the voltage stability of the system on its own. Figure 21 also validates the same by depicting an improved voltage profile along the weaker buses of the network in the presence of a wind generator. In fact,

the reactive power contribution at Bus 7 effectively strengthens local voltages, reduces voltage sag, and alleviates stress on the vulnerable nodes. Overall, full wind penetration not only optimizes the reactive power sharing among generators but also delivers a substantial improvement in the voltage profile of the IEEE 30-bus system.

6.2. Algerian 114-Bus Test System

In this section, we conduct a study of the behavior of a virtual electricity market planned in Algeria in a real network using the OPF-LMP model under the PDIPM–GSF framework. The Algerian 114-node system is considered as the case, which represents a large-scale power system. Figure 22 shows the actual map of the Algerian electricity transmission network in 2015 with 220 kV, 90 kV, and 60 kV transmission lines (high voltage and extra-high voltage). Based on technical statistical data provided by SONELGAZ in 2011, this real electricity system consists of 15 generators, 175 lines, 99 load nodes, and 16 tap changers located on lines 160 to 175. The total scheduled power demand to be met is 3.79261 GW for real power and 2.070 GVAR for reactive power in 2007. The active and reactive power limits and the generator cost function coefficients [84,85], which represent the production bid price parameters, are shown in Table 11. The voltage and reactive power parameters of the 15 generator nodes and the parameters of 99 load nodes and transmission lines in the network are taken from the SONELGAZ company and presented in Tables A1 and A2 (Appendix A). For the test system, the basic MVA limit is set at 100 MVA with a frequency of 50 Hz, where node 1 (Mersat el Hadjadj 1) is used as a balance node. The voltage magnitude limits for PV and PQ buses are set between 0.9 and 1.1 p.u., except for the slack bus, whose minimum voltage magnitude is maintained at 1.00 p.u. The parameters adopted for the Algerian case study are based on available information describing the Algerian power sector and the corresponding network characteristics. The generator operating costs, generation limits, load demand, and network parameters are selected according to the available system data and the assumptions required for OPF and market-clearing analysis. The renewable-generation scenario and bidding parameters are specified in the corresponding tables, while the single-sided and double-sided market configurations define the participating generators and consumers. The deregulated market is considered as a virtual/analytical scenario applied to the Algerian power-system structure rather than as a representation of the current operational electricity market. These assumptions are introduced to provide a consistent framework for evaluating LMP calculation, congestion management, and renewable-energy integration.

Table 11. Generator parameters for the Algerian 114-bus grid.

Generation Companies	Bus No.	Generation Bid Price Parameters			Generator Limit			
		a_{gi} (USD/MWh^2)	b_{gi} (USD/MWh)	c_{gi} (USD)	P_{min} (MW)	P_{max} (MW)	Q_{min} (MW)	Q_{max} (MW)
SONELGAZ GENCO	Genco 1	0.0085	01.50	0	135.00	1350	20	400
	Genco 5	0.0085	1.50	0	135.00	1350	20	200
	Genco 11	0.0170	02.50	0	10.00	100	−50	100
	Genco 15	0.0170	02.50	0	30.00	300	0	100
	Genco 17	0.0085	01.50	0	135.00	1350	0	400
	Genco 52	0.0170	02.50	0	34.50	3450	0	50
	Genco 80	0.0170	02.50	0	34.50	3450	0	60
	Genco 83	0.0170	02.50	0	30.00	300	−50	200
	Genco 98	0.0170	02.50	0	30.00	300	0	50

Table 11. *Cont.*

Generation Companies	Bus No.	Generation Bid Price Parameters			Generator Limit			
		a_{gi} (USD/MWh^2)	b_{gi} (USD/MWh)	c_{gi} (USD)	P_{min} (MW)	P_{max} (MW)	Q_{min} (MW)	Q_{max} (MW)
SONATRACH GENCO	Genco 19	0.0170	02.50	0	34.50	3450	0	60
	Genco 22	0.0170	02.50	0	34.50	3450	0	50
GENERAL ELECTRIC GENCO	Genco 100	0.0030	02.00	0	60.00	600	0	270
	Genco 101	0.0030	02.00	0	20.00	200	−50	200
	Genco 109	0.0170	02.50	0	10.00	100	−50	100
	Genco 111	0.0170	02.50	0	10.00	100	−50	155

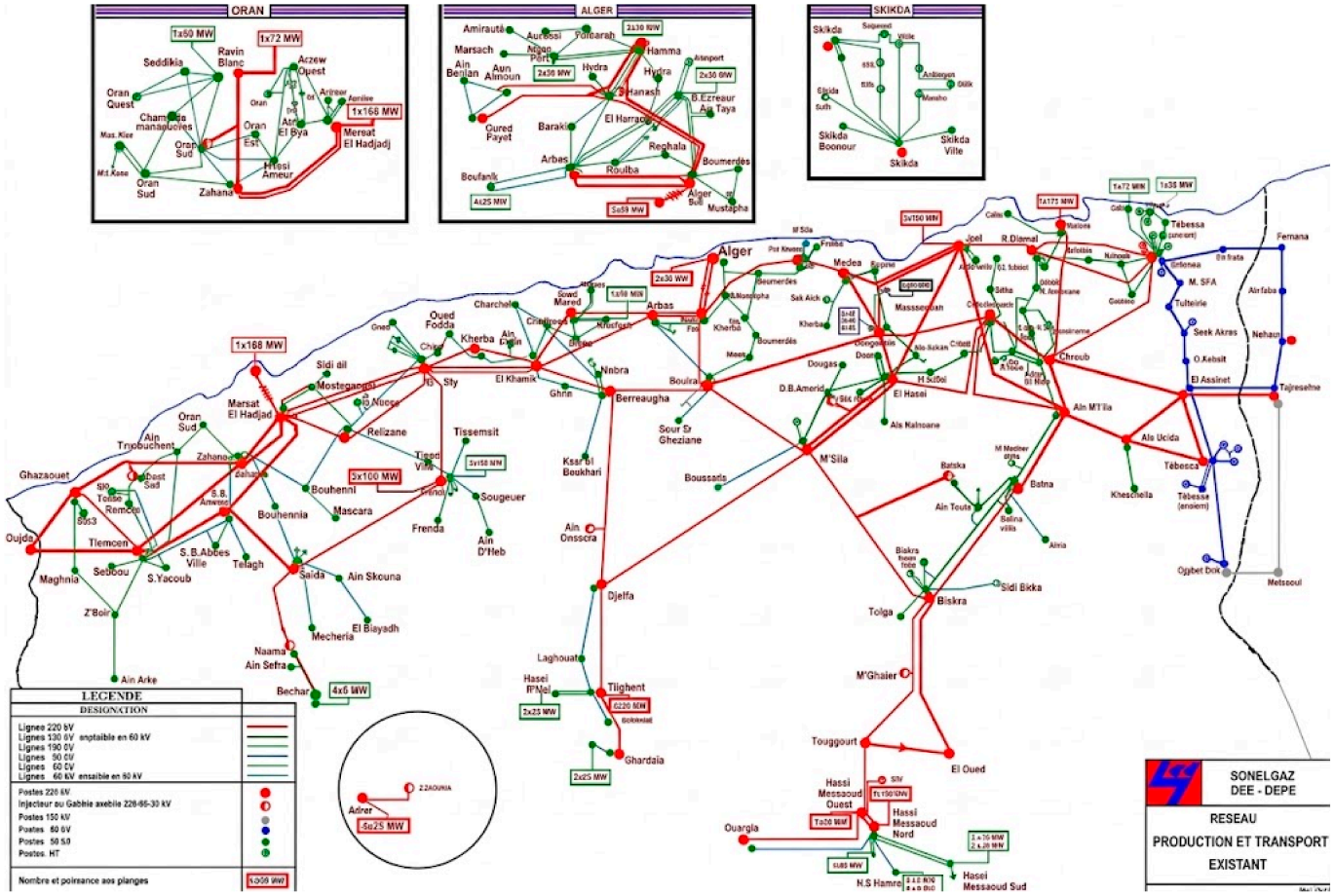


Figure 22. Algerian 114-bus power grid based on data from SONELGAZ [86].

With the strong growth in electricity demand in recent years and the long distances between electricity systems, ranging from 200 to 1000 km, supplying electricity to isolated regions in the south poses serious technical and economic challenges. New conventional and renewable energy power plants are being built to ensure that all load demands are met 24 h a day, all year round. To this end, we used the new, updated electricity consumption data to simulate the virtual electricity market in Algeria, where we assumed that three companies would participate in the electricity market after the deregulation of the electricity sector, two of which are national companies and the third is a private American company.

The main company, SONELGAZ, owns nine generators [Gen1, Gen5, Gen11, Gen15, Gen17, Gen52, Gen80, Gen83, and Gen98], which account for 60.2% of electricity production to meet the total load; followed by Sonatrach, which accounts for 34.76% of electricity production with two large generators [Gen19 and Gen22]; and finally General Electric, which accounts for 5.04% of electricity production with four small generators [Gen100, Gen101, Gen109, and Gen111]. In this study, we assumed that the electricity market is perfectly competitive under a centralized pool model where the price of electricity is determined after production and consumption bids have been submitted. The Algerian Electricity and Gas Regulatory Commission is responsible for determining prices and managing the market as an independent market operator, with each power plant bidding according to its production cost coefficient and marginal cost. Each load represents a DISCO or a large consumer. The auction is assumed to be unilateral for the production side only, and for the consumption side, the supply coefficients of demand are assumed to be zero.

Case Study 3: OPF-Based LMP in the Algerian 114-Bus Power System with Renewable Energy Integration

In this case study, electricity consumption data remain active in the Centre for Economic Information and Statistics (CEIC) [87] and are reported by SONELGAZ. The data are classified in Algeria's global database. Figure 23 shows Algeria's electricity consumption for the year 2019/2020, from February 2019 to January 2020. Algeria's consumption for the year 2019/2020 for April, when consumption was lowest at 5238.7 MW, and the month of July, when consumption was highest (the peak) at 8661.9 MW during that year, is used to model demand on the electricity market, taking into account that the bids submitted on the market are only those from the three participating GENCOs, SONELGAZ, Sonatrach, and General Electric. In this case, each GENCO has its own renewable power plants. Details of the power plants connected to the grid (24 PV plants, 01 wind farm) based on renewable energies are managed by the electricity and renewable energy company (SKTM), which concerns the installed capacity and energy produced from the date of commissioning until 2017/2018, are provided in Table 12 [88].

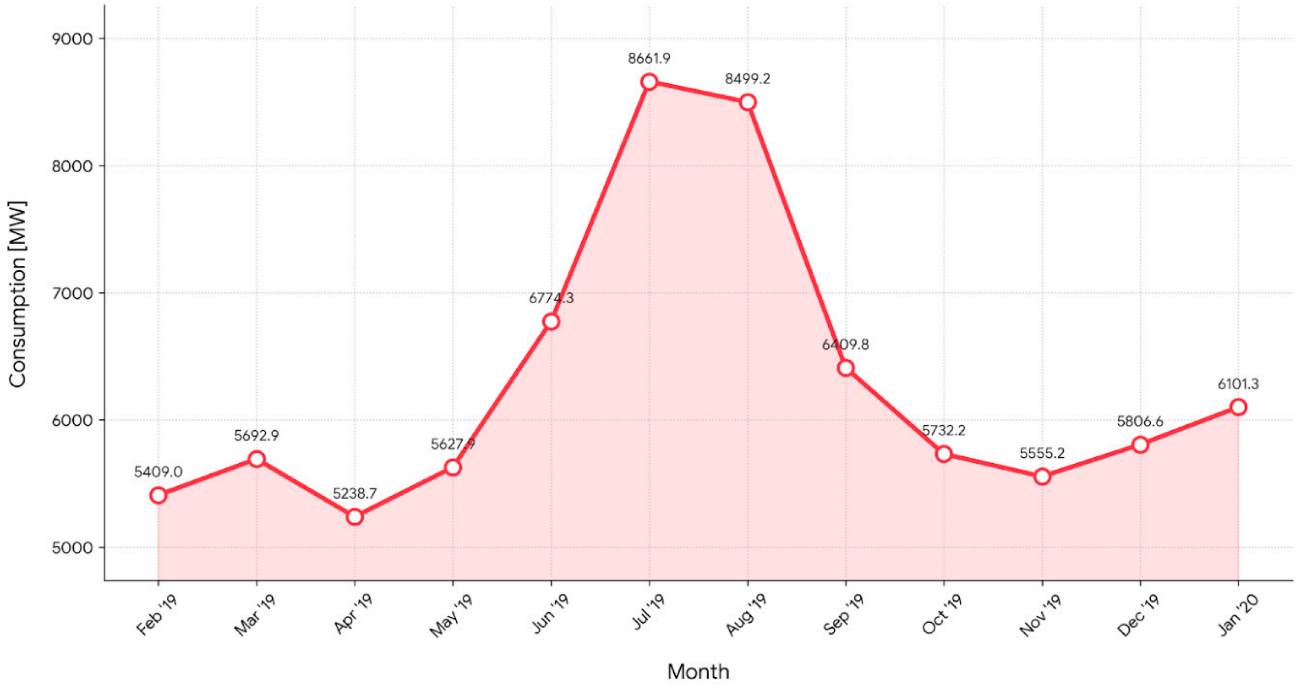


Figure 23. Algeria's electricity consumption for the year 2019/2020 [87].

Table 12. Installed capacity and energy produced from the date of commissioning to June 2017/2018.

Plant	Technology	Province	Commissioning Year	Area (Ha)	Installed Power (MW)	Energy Output 2017 (GWh)
Kabertene	Wind	Adrar	2014	33	10.2	51.579
Ain El Melh	PV	M'Sila	2017	40	20	16.473
Adrar City	PV	Adrar	2015	40	20	59.585
Telagh	PV	Sidi Bel Abbès	2016	30	12	7.417
In Salah	PV	Tamanrasset	2016	10	5	12.328
Oued El Kebrit	PV	Souk Ahras	2016	20	15	28.900
Tamanrasset	PV	Tamanrasset	2015	26	13	36.410
Ain Skhouna	PV	Saïda	2016	60	30	14.213
Timimoun	PV	Adrar	2016	18	9	23.822
Labioh Sidi Chikh	PV	El Bayadh	2016	40	23	19.146
Djanet	PV	Illizi	2015	6	3	10.729
Oued Nechou	PV	Ghardaïa	2014	5	1.1	4.593
Zaouiat Kounta	PV	Adrar	2016	12	6	15.213
Ain Leghzel	PV	Saïda	2016	60	30	14.213
Tindouf	PV	Tindouf	2015	18	9	6.376
Reggan	PV	Adrar	2016	10	5	12.221
El Hadjira	PV	Ouargla	2017	60	30	9.738
Kabertene	PV	Adrar	2015	6	3	9.584
Ain El Bel 1 and 2	PV	Djelfa	2016–2017	120	53	25.134
Serdret Leghzel	PV	Naâma	2016	32	20	40.715
Lekhneg 1 and 2	PV	Laghouat	2016–2017	120	60	53.576

The renewable power-plant data considered in the OPF-LMP formulation are incorporated as follows:

1. Generator limits: The installed active power of each solar PV and wind power plant shown in Table 12 is taken as the maximum power P_{max}, and the minimum power P_{min} is considered to be equal to 0.
2. Generation bid price parameters: In this study, for renewable generators, the direct cost coefficient is assumed to represent the operating and maintenance (O&M) cost, while the fuel cost is assumed to be zero. For solar PV generators, the coefficient is 1.655 USD/MWh, and for wind generators, the coefficient is 2.250 USD/MWh [89–91].

For the integration of 25 renewable energy generators, including wind and PV generators, so that they can participate in the electricity market alongside conventional generators, the best location for renewable energy generators is chosen to be at load nodes with the highest consumption that are far from the supply of conventional generators after several ACOPF simulations to obtain the lowest production cost and reduction in losses and congestion in the network's transmission lines, noting that in the sizing of renewable energy plants, the site and climatic conditions are the main factors when integrating renewable energy generators. Table 13 presents the data parameters of renewable generators and their location at network nodes [88].

Table 13. Characteristics and locations of the renewable energy generators.

Bus ID	Plant Name	Technology	Voltage Setpoint (p.u.)	Reactive Power Range (MVAr)
63	Tamanrasset	PV	1.08	0 to 25
4	Kabertene	Wind	1.05	−10 to 15
91	El Hadjira	PV	1.08	−5 to 25
6	Adrar City	PV	1.06	0 to 18
29	Oued El Ma	PV	1.02	−5 to 4
99	Lekhneg 1 and 2	PV	1.10	−25 to 40
8	In Salah	PV	1.02	−5 to 5

Table 13. *Cont.*

Bus ID	Plant Name	Technology	Voltage Setpoint (p.u.)	Reactive Power Range (MVAr)
10	Ain Skhouna	PV	1.07	0 to 20
32	Ain El Bel 1 and 2	PV	1.08	−10 to 25
85	Oued Nechou	PV	1.02	−10 to 5
73	Bir Rebaa	PV	1.07	−10 to 20
7	Kabertene	PV	1.00	0 to 2
88	Timimoun	PV	1.06	−7 to 18
21	Ain Leghzel	PV	1.09	−30 to 30
106	Oued El Kebrit	PV	1.05	−5 to 15
24	Oued El Kebrit	PV	1.05	0 to 15
94	Tindouf	PV	1.07	0 to 20
82	Djanet	PV	1.05	0 to 15
107	Labioh Sidi Chikh	PV	1.08	−10 to 25
84	Telagh	PV	1.08	−10 to 24
26	Zaouiat Kounta	PV	1.07	−5 to 20
97	Ain El Melh	PV	1.09	−10 to 30
103	Serdret Leghzel	PV	1.07	−5 to 20
41	Aoulef	PV	1.07	0 to 20
9	Reggan	PV	1.04	−10 to 10

The LMP-OPF model is performed using the Algerian power system with 114 buses simulated using the PDIPM–GSF algorithm, integrating renewable energy generators with 3792.61 MW and 2070 MVAR for an initial comparison. The results of the LMP, the total production cost of the GENCOs, the total revenue, and the total profit calculated from the two OPF model cases in perfect competition are presented in Tables 14 and 15, and Figure 24.

Table 14. The results of the OPF in the electricity market with the integration of renewable energies.

SONELGAZ GENCO	Outcomes	SONATRACH GENCO	Outcomes
Genco 1	410.15	Genco 19	158.60
Genco 5	410.19	Genco 22	155.16
Genco 11	100.00	LMP19	07.89
Genco 15	175.29	LMP22	07.77
Genco 17	376.86	Generation cost (USD/h)	1621.28
Genco 52	111.32	Revenue (USD/h)	3395.10
Genco 80	156.71	Profit (USD/h)	1773.82
Genco 83	154.99	GENERAL ELECTRIC GENCO	Outcomes
Genco 98	155.35	Genco 100	600.00
LMP1	08.47	Genco 101	200.00
LMP5	08.47	Genco 109	100.00
LMP11	08.68	Genco 111	100.00
LMP15	08.46	LMP100	07.67
LMP17	07.90	LMP101	08.04
LMP52	06.28	LMP109	08.17
LMP80	07.82	LMP111	08.68
LMP83	07.77	Generation cost (USD/h)	3640
LMP98	07.78	Revenue (USD/h)	9299.10
Generation cost (USD/h)	10,136.36	Profit (USD/h)	5659.10
Revenue (USD/h)	22,310.88		
Profit (USD/h)	12,174.52		

Table 15. The results of the OPF in the electricity market with the integration of renewable energies in the 114-bus Algerian power system.

Results	Electricity Market (Without Renewable Energy)	Electricity Market (With Renewable Energy)
Losses (MW)	62.378	46.903
Total Revenue (USD/h)	35,005.08	35,005.08
Total generation Cost (USD/h)	19,074.74	16,080.98
Total Profit (USD/h)	15,930.34	18,924.10
Convergence Time(s)	07.96	9.30

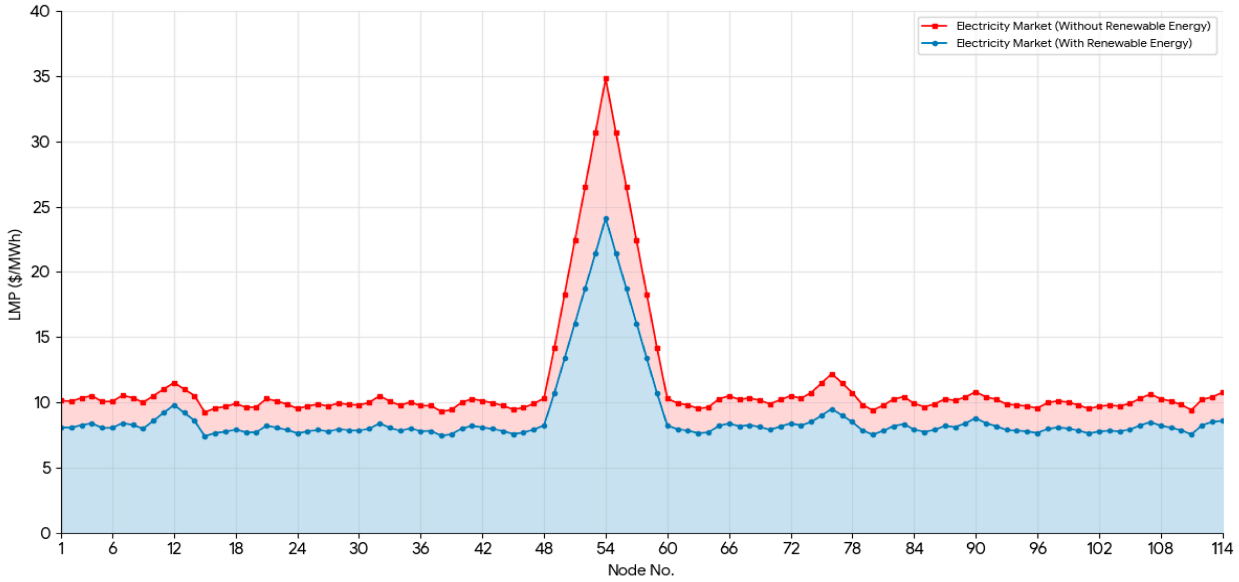


Figure 24. Comparison of LMP prices in the electricity market with and without renewable energy on the Algerian power system.

The integration of renewable energy generators into the Algerian power system reduced the optimal active and reactive production of conventional generators, which minimized production costs and maximized profits for GENCOs, except for General Electric, whose revenue remained fixed and was not affected by energy distribution during the trading period. For SONELGAZ GENCO, production costs were minimized from USD 13,262.92/h to USD 10,136.36/h, leading to a profit maximization of USD 9047.963/h to USD 12,174.52/h; for SONATRACH GENCO, production costs were minimized from USD 2171.82/h to USD 1621.28/h, leading to profit maximization from USD 1223.28/h to USD 1773.82/h and for General Electric, the production cost remained constant compared to the first case (without renewable energy) at USD 3640/h since its generators operate at their maximum limits, which also kept the profit constant at USD 5659.1/h. Algerian power system losses decreased from 62.378 MW to 46.903 MW after the integration of renewable energy generators. Figure 24 clearly shows that the integration of renewable energy generators has reduced LMP prices at all nodes in the Algerian grid, particularly those located for the integration of renewable generators. This decrease is due to the reduction in energy transmission losses and, at the same time, congestion in transmission lines, which has improved prices across the entire grid. Table 16 shows the optimal voltages and reactive powers of the generators in the 114-bus Algerian power system obtained in the OPF-LMP model.

Table 16. Voltage and reactive power of generators in the Algerian 114-bus power system, including RES.

Gencos	V_{Gmin}	V_{Gmax}	V_{Gs}	Q_{Gmin}	Q_{Gmax}	Q_{Gs}
Genco 1	01.00	01.10	01.10	20	400	217.68
Genco 5	00.90	01.10	01.096	20	200	200.00
Genco 11	00.90	01.10	01.10	−50	100	71.39
Genco 15	00.90	01.10	01.10	00.00	100	70.42
Genco 17	00.90	01.10	01.070	00.00	400	211.58
Genco 19	00.90	01.10	01.039	00.00	60	44.91
Genco 22	00.90	01.10	01.050	00.00	50	32.27
Genco 52	00.90	01.10	01.020	00.00	50	0.00
Genco 80	00.90	01.10	01.079	00.00	60	60.00
Genco 83	00.90	01.10	01.10	−50	200	109.49
Genco 98	00.90	01.10	01.10	00.00	50	41.34
Genco 100	00.90	01.10	01.10	00.00	270	0.00
Genco 101	00.90	01.10	01.10	−50	200	84.33
Genco 109	00.90	01.10	01.10	−50	100	20.26
Genco 111	00.90	01.10	01.069	−50	155	63.44

Figure 25 shows the voltage profile of the nodes for the solutions obtained by the OPF-LMP model with the integration of renewable energy generators. It can be seen that the voltage amplitudes are precisely within the defined range and that the reactive energy generated by the wind farm and solar PV generators integrated into the Algerian grid significantly improves the voltage profile of weak buses, particularly those located for the integration of renewable energy generators.

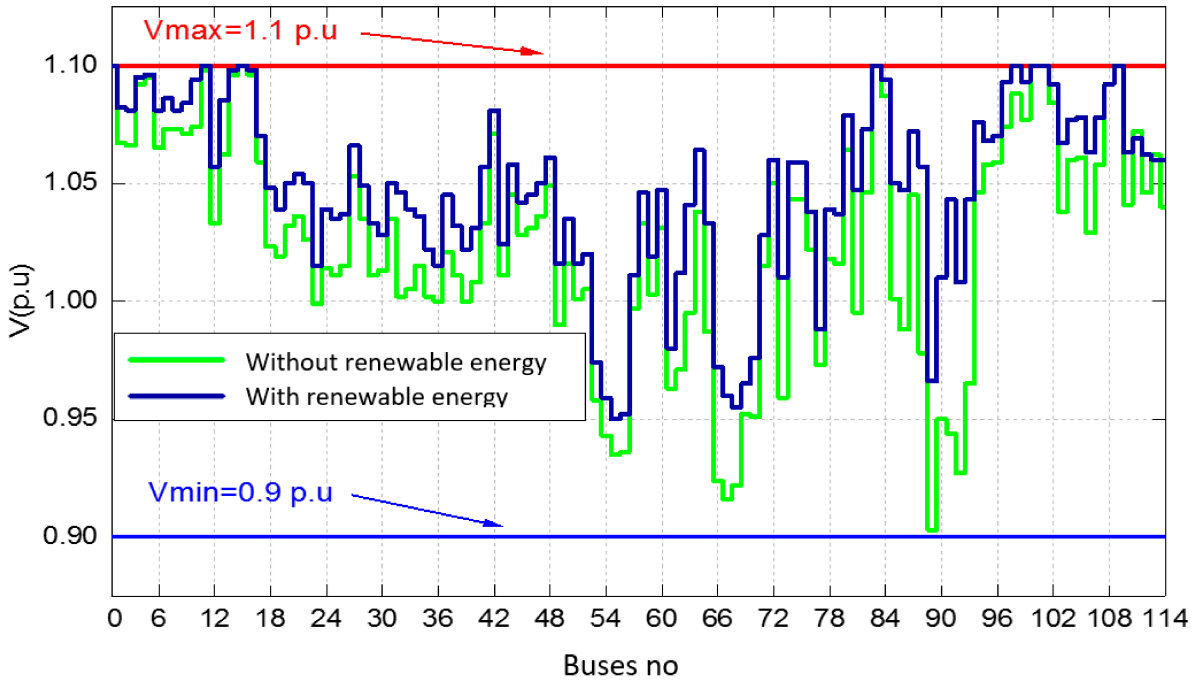


Figure 25. Voltage profile of OPF models for the Algerian 114-bus power system.

In addition to this study, the problem of OPF is solved for 12 months of load demand during the 2019/2020 year from February 2019 to January 2020 to show the impact of high load levels (peak) and low load levels on the behavior of the electricity market in Algeria, including the impact on (1) transmission losses, (2) LMP nodal prices, (3) production costs, (4) revenues, and (5) total profits of GENCOs. Figure 26 shows the active and reactive

transmission losses of the Algerian power system at 114 buses during power exchange between GENCOs and consumers over 12 periods.

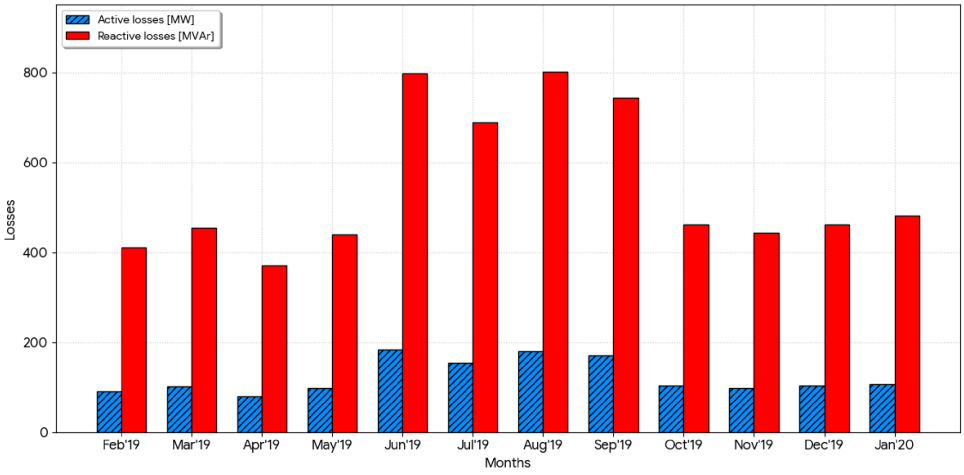


Figure 26. Active and reactive transmission losses in the Algerian 114-bus power system.

We can see that the high level of active and reactive power transmission losses was achieved during the summer months.

- For June, with 183.275 MW and 797.42 MVAr.
- For July, with 153.71 MW and 688.32 MVAr.
- For August, 178.94 MW and 800.45 MVAr.
- For September, 170.485 MW and 742.42 MVAr.

This is due to the high energy consumption recorded for these months in the Algerian grid, noting that the peak consumption month (June) recorded the highest losses. Figures 27 and 28 show the heatmap and distribution of the LMP prices of the Algerian electricity grid, with the variation in load demand during 12 electricity trading periods after market equilibrium with the OPF model in the virtual market compared to the actual price of electricity in Algeria, equivalent to 5.4796 DA/kWh, which is equal to USD0.04/kWh (USD40/MWh) [92].

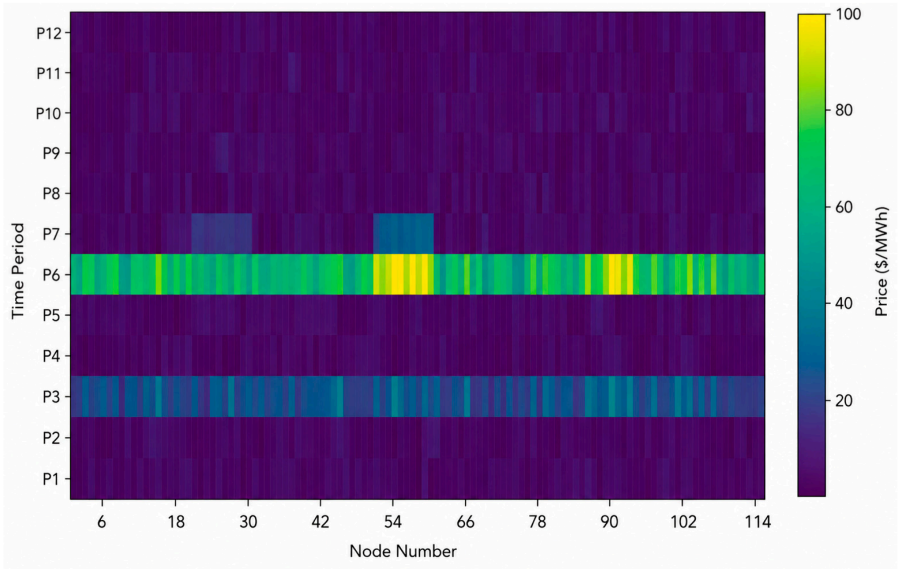


Figure 27. The heatmap of the LMP prices of the Algerian electricity grid with the variation in load demand during 12 electricity trading periods.

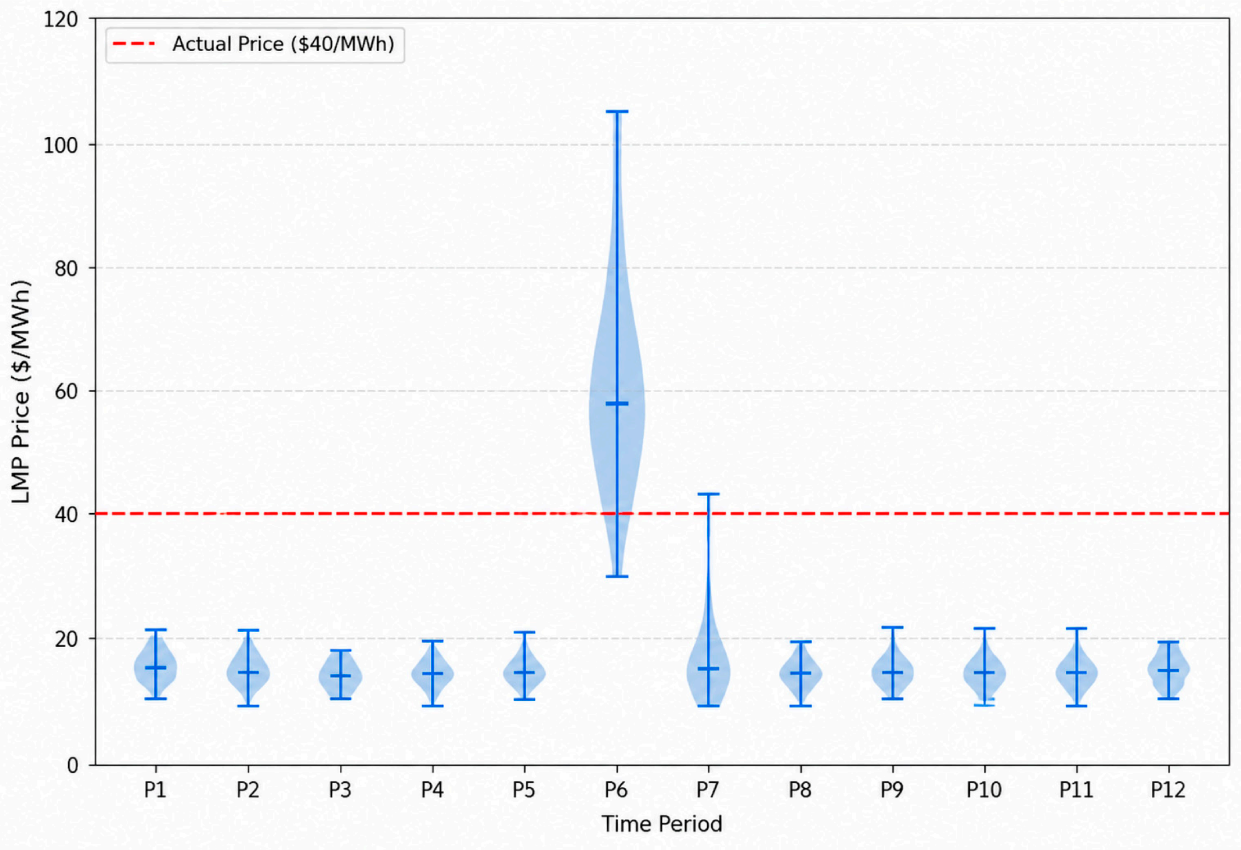


Figure 28. The distribution of the LMP prices of the Algerian electricity grid with the variation in load demand during 12 electricity trading periods.

The electricity price in Algeria for consumption above 1 MWh was approximately USD40/MWh during 2019/2020, according to Sonelgaz and the Electricity and Gas Regulatory Commission [92]. This value is considered in this study as a reference regulated electricity price for comparison and should not be interpreted as the nodal LMP obtained from the proposed virtual-market model. As shown in Figure 28, when the virtual electricity market is considered for the Algerian electricity network, with each GENCO submitting its bid during the 12 power-exchange periods, the calculated LMPs vary spatially across the network and temporally between periods rather than remaining constant. This variation results from changes in load demand, transmission-line congestion, and network losses, which are not explicitly reflected in the regulated pricing mechanism used by Sonelgaz and CREG. After solving the ACOPF model using the LMP-based pricing approach with PDIPM–GSF, the LMPs are observed to be highest during period 6 (June), corresponding to the peak-demand month, across several nodes and locations in the network. In particular, bus 53 reaches the highest LMP of approximately USD103/MWh in June, while the lowest observed LMP is approximately USD1.65/MWh in February. Conversely, relatively low LMP values are observed across the network during period 3 (April), which corresponds to the lowest electricity-consumption level. These results demonstrate that, unlike the regulated reference price, the proposed virtual-market LMPs reflect the spatial and temporal effects of network operating conditions, congestion, and losses. The overall results of the electricity market using the IPM-GSF model applied to the virtual Algerian power market for 12 periods of electricity exchange between GENCOs and consumers, including total production cost, total revenue, and total profit, are presented in Figure 29.

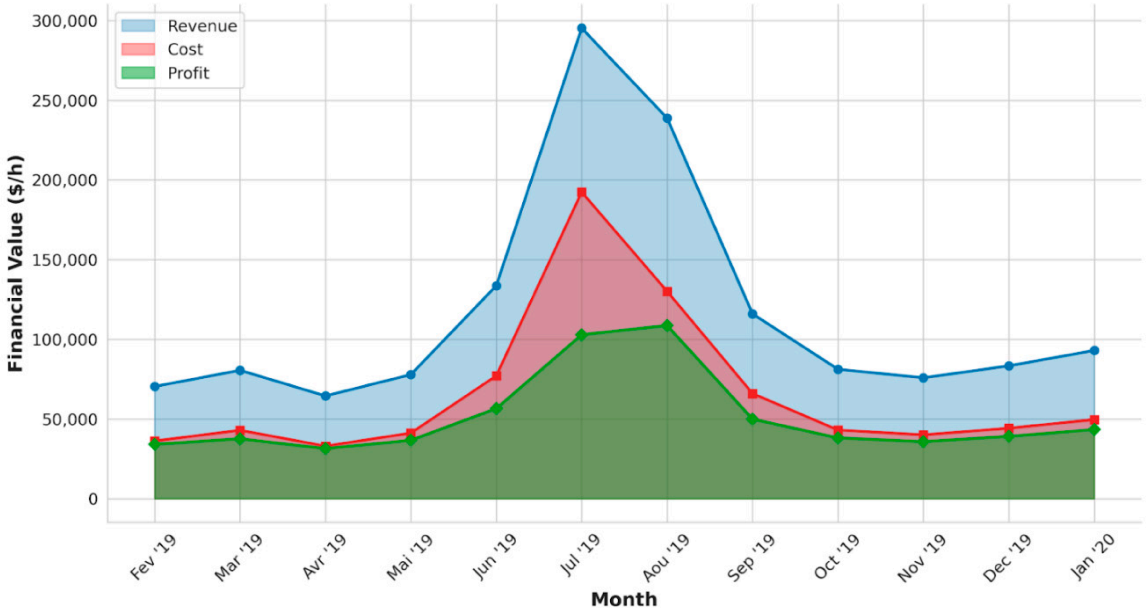


Figure 29. The total revenue, cost, and profit of the Algerian electricity grid with the variation in load demand during 12 electricity trading periods.

It can be clearly seen that, following the ACOPF resolution, the production costs, revenues, and profits of players in the Algerian electricity market change significantly in line with variations in load demand over the 12 trading periods. The highest production cost is reflected in the results for the month of July, which is the peak month for production costs, amounting to 108,703.81 USD/h. This is justified by the high electricity consumption level that occurs during the summer season in Algeria, which is largely attributed to the heavy use of air conditioners as well as the use of less efficient production units. From a technical point of view, partial saturation of the grid and transmission constraints can also lead to the activation of generators located in areas with higher marginal costs. Conversely, the lowest production cost is achieved in April at 31,481.95 USD/h, corresponding to a period of low demand, during which high-efficiency base units can cover the load without major constraints on the grid. In economic terms, GENCOs' total revenue peaks in July at 295,270.5794 USD/h, followed by August at 238,779.7897 USD/h, mainly due to high local marginal prices (LMP) set by the market operator (CREG) during periods of high load and stress on the electricity system. These high prices reflect both the increase in marginal production costs and the economic value of electricity in a context of critical demand. Conversely, the lowest total revenue is observed in April at 64,475.2686 USD/h, when demand is moderate, technical constraints are reduced, and LMP prices are lower. As a direct result of the joint evolution of costs and revenues, the total cumulative profit of the three GENCOs (SONELGAZ, SONATRACH, and General Electric) shows a strong correlation with the load level, reaching a maximum in July with 192,368.4494 USD/h. This high level of profit can be explained economically by the possibility for producers to submit bids close to their maximum capacity at high LMP prices, and technically by the need for the system to use all available production capacity to meet peak demand. In contrast, the minimum profit is recorded in April at 32,993.31861 USD/h, a period characterized by low demand on the system, improved overall efficiency of the generation mix, and reduced economic margins for producers. The successful application of the proposed framework to the Algerian 114-bus network provides an additional assessment of its scalability beyond the IEEE 30-bus benchmark. This system comprises more power components and data, thereby providing a substantially larger and more realistic test case. The results demonstrate that the PDIPM–GSF framework remains capable of obtaining

feasible OPF solutions while managing congestion and renewable-energy integration in a larger network. Although the 114-bus system does not represent the full scale of modern interconnected networks, it provides an intermediate validation of the proposed approach before application to very large systems.

7. Conclusions

In this study, the OPF-based LMP problem was solved using the PDIPM–GSF algorithm under single- and double-sided market auctions with wind-power integration. By integrating the GSF into the PDIPM framework, the proposed approach improved congestion handling while maintaining stable convergence and satisfying the system constraints. Tests on the modified IEEE 30-bus system demonstrated clear improvements in generation-cost performance, social profit, congestion management, and LMP determination under both market structures. The integration of wind power also provided considerable economic and operational benefits, including reductions in generation cost, transmission losses, and nodal LMPs, together with improvements in social profit. Moreover, the placement analysis showed that the proper placement of the wind generator can be found in order to reduce LMP and relieve congestion. The obtained results clearly show the effectiveness and robustness of the PDIPM–GSF approach in solving the OPF-LMP problem with variable renewable generation in electricity markets. However, some drawbacks of the proposed methodology have been found. First, the model of the uncertainty associated with the generation of wind is not developed taking into account the forecast errors and their correlations. Second, the generation of PV energy is modeled deterministically and also disregards the impact of irradiation forecast errors. Future work will include the introduction of sophisticated models for the forecast errors, time series, and correlation of the models of wind and PV generation uncertainties and their impact on reserve requirements, congestion management, and LMPs. The presented technique will be applied to real-time LMP mechanisms using machine learning techniques to enhance the speed of computations, accuracy of forecasts, and responsiveness of the market. Future research will involve the application of the presented framework to large-scale systems comprising several hundred or thousands of buses.

Author Contributions: R.B.: conceptualization; methodology; data curation; project administration; resources; writing—original draft preparation. A.B.: conceptualization; methodology; data curation; project administration; resources; writing—original draft preparation. N.B.: methodology; formal analysis; modeling support; technical validation; writing—review and editing. B.A.: data curation; investigation; software implementation; simulation support; writing—review and editing. F.B.: data curation; investigation; software implementation; simulation support; writing—review and editing. E.A.-E.: writing—review and editing, formal analysis, supervision, investigation, validation. M.I.M.: writing—review and editing, formal analysis, supervision, investigation, validation. All authors have read and agreed to the published version of the manuscript.

Funding: This research received no external funding.

Data Availability Statement: Data will be made available upon request from the corresponding author.

Conflicts of Interest: The authors declare no conflicts of interest.

Abbreviations

The following abbreviations are used in this manuscript:

CAISO	California Independent System Operator
ED	Economic Dispatch
ERCOT	Electric Reliability Council of Texas

GENCOs	Generating Companies
GHI	Global Horizontal Irradiation
GSF	Generating Scaling Factor
GWEC	Global Wind Energy Council
IPM	Interior Point Method
ISO	Independent System Operator
MISO	Midcontinent Independent System Operator
NYSO	New York Independent System Operator
OPF	Optimal Power Flow
PDF	Probability Density Function
PDIPM–GSF	Primal–Dual Interior Point Method Combined with a Generation Scaling Factor
RES	Renewable Energy Sources
SCOPF	Security-Constrained Optimal Power Flow
SP	Stochastic Programming
SQP	Sequential Quadratic Programming
TRV	The Total Revenue
UPFC	Unified Power Flow Controller
TCULs	Tap-Changing Under Load Transformer

List of Symbols

The following symbols are used in this manuscript:

P_{Di}, Q_{Di}	Demand active/reactive power
N_{dn}	The number of demand buses
N_{g_n}	The number of conventional generators
$C_{g,i}$, and $C_{\omega,j}$, $C_{pv,j}$	cost functions of conventional, wind, and solar PV generators, respectively
N_{pv}	The number of solar PV units
N_w	The number of wind power units
$P_{d,j}$	The active power demand at bus j
∂	The shape parameter of the PDF
$\emptyset$	The scale parameter of the PDF
μ	Shadow price for a binding constraint (USD/MW h)
a, b	Sending and receiving buses of transmission line k
a_{gi}, b_{gi}, c_{gi}	Generator bid cost coefficients
B^{-1}	The susceptance inverse matrix (B)
$B_{a,i}^{(-1)}$	Element (a, i) of the inverse reduced bus susceptance matrix
$B_{b,i}^{(-1)}$	Element (b, i) of the inverse reduced bus susceptance matrix
B_{ij}	The susceptance
$C_{g,i}(P_{g,i})$	The cost function of the thermal unit i
c_i	Weibull scale parameter (m/s)
C_P	Power aerodynamic coefficient
$c_{pv,s}$	Marginal cost coefficient of PV units (USD/MWh)
$C_{pv,s}(P_{pv,s})$	Operating cost of PV units (USD/h)
$C_{Rw,i}$	Reserve cost of wind power unit i (USD)
$C_w(P_w)$	The cost function of the wind unit
DF_i	The delivery factor of the power unit supplied to the customer on this load bus
D_j	Demand at bus j
e	Vector of ones
$f(x)$	Objective function
$f_{w,i}$	Probability density function of wind power for unit i
$\overline{g}$	Upper bound of inequality constraints
$\underline{g}$	Lower bound of inequality constraints

$g(x)$	Vector of inequality constraint functions
G_{ij}	The conductance
GSF_{k-i}	Generation scaling factor between bus i and line k
$h(x)$	Vector of equality constraint functions
H'	Hessian of the Lagrangian
i	Index of conventional generators
k	Transmission line index
ki	Weibull shape parameter (–)
l	Lower-bound slack variable vector
LMP^{cong}	Congestion component of the LMP
LMP_j	Locational marginal price at bus j (USD/MWh)
LMP^{loss}	Loss component of the LMP
LMP^{ref}	Reference (energy) component of the LMP
M	Number of lines
M_{Rewi}	The coefficient of reserve cost
M_{Rewi}	The coefficient of reserve cost
$M_{Rw,i}$	Reserve cost coefficient of wind unit i (USD/MW)
N	Hellman coefficient (0.143)
N_d	Number of demand buses
N_{gn}	Number of generators
P_{dj}	Demanded active power
PF	Social profit objective function (USD/h)
$P_{g,i}$	Active bid quantity of generator i
$Q_{g,i}$	Reactive bid quantity of generator i
P_{Gimin}, P_{Gimax}	Generator active power limits
P_i, Q_i	Net injected active/reactive power at bus i
P_L	Transmission losses
$P_{pv,s}$	Active power output of PV units (MW)
$P_{pv,smax}$	Maximum available power of PV units (MW)
P_{ri}	The rated power of the plan
$P_w(v)$	Wind turbine output power
P_{wavi}	The real power generated from the plant
$P_{ws,i}$	Scheduled wind power of unit i (MW)
Qc_{imin}, Qc_{imax}	Capacitive reactive power limits
Q_{Gimin}, Q_{Gimax}	Generator reactive power limits
r	Number of inequality constraints
R_P	Rotor radius (m)
RV	Total revenue of demand-side bidders (USD/h)
s	PV unit index
TC	The total cost
TGC	Total generation cost (USD/h)
u	Upper-bound slack variable vector
v	Wind speed (m/s)
V_i	Voltage magnitude at bus i (p.u.)
V_{imin}, V_{imax}	Bus voltage limits
v_{in}, v_r, v_{out}	Cut-in, rated, cut-out speeds
V_W	Wind speed (m/s)
w	Dual variables for upper inequality bounds
W_{s10}	Standard wind speed at a height of 10 (m)
W_{sh}	Wind speed at a specific height (h)
x	Vector of primal decision variables
x_k	The reactance of the k-line
xk	Reactance of transmission line k (p.u.)
y	Dual variables for equality constraints

Y_{ij}	Bus admittance matrix element
z	Dual variables for lower inequality bounds
α_p, α_d	Primal and dual step sizes
δ_{ij}	Angle difference between buses i and j
Δx, Δy, ...	Newton search directions
θi	Voltage angle at bus i (rad)
θ_{ij}	The voltage angle of the bus phase
θ_{imin}, θ_{imax}	Voltage angle limits
λ	Lambda (the marginal cost of supplying energy)
μ	Barrier parameter
π	Mathematical constant ($\approx$3.1416)
ρ	The air density (1.225 kg/m^3)
$\rho(v)$	Weibull PDF
σ	Centering parameter
τ	Fraction-to-boundary parameter
$\mathcal{L}$	Lagrangian function

Appendix A

Table A1. Algerian 114-bus power system bus parameters data.

Bus Number	Bis Name	Voltage (kV)	Voltage (p.u.)	Angle (Deg)	Gen (MW)	Gen (MVar)	Active Load (MW)	Reactive (MVar)
1 (Slack)	MERSAT EL HADJADJ 1	220	1.07	0	750	400	125	94
2	OUJDA	220	1.0	0	0	0	0	0
3	GHAZAOUET	220	1.0	0	0	0	36	17
4	ZAHANA	220	1.0	0	0	0	64	31
5	MERSAT EL HADJADJ 2	220	1.0	0	300	160	335	250
6	TLEMCEN	220	1.0	0	0	0	78	37
7	SIDI BELABES	220	1.0	0	0	0	55	26
8	RELIZANE	220	1.0	0	0	0	50	24
9	BENI SAF	220	1.0	0	0	0	40	19
10	SAIDA	220	1.0	0	0	0	42	21
11	TIARET	220	1.0	0	160	30	96	47
12	BECHAR	220	1.0	0	0	0	31	15
13	AIN-SEFRA	220	1.0	0	0	0	13	6
14	PETIT LAC 1	220	1.0	0	0	0	0	0
15	RAVIN BLANC	220	1.0	0	60	30	136	65
16	PETIT LAC 2	220	1.0	0	0	0	0	0
17	ALGER EST 1	220	1.0	0	640	400	0	0
18	ALGER EST 2	60	1.0	0	0	0	0	0
19	ALGER PORT	60	1.0	0	100	60	11	5
20	LARBAA 1	60	1.0	0	0	0	14	9
21	LARBAA 2	220	1.0	0	0	0	70	52
22	BAB EZZOUAR	60	1.0	0	60	40	42	25
23	BEN AKNOUN	60	1.0	0	0	0	23	11
24	EL HARRACH	60	1.0	0	0	0	60	36
25	GLACIERE	60	1.0	0	0	0	17	8
26	EL HAMMA 1	60	1.0	0	0	0	55	26
27	EL HAMMA 2	220	1.0	0	0	0	0	0
28	EL HAMMA 3	220	1.0	0	0	0	0	0
29	EL KOUBA	60	1.0	0	0	0	37	18
30	OULED FAYET 1	60	1.0	0	0	0	30	15
31	OULED FAYET 2	220	1.0	0	0	0	0	0
32	ROUIBA 1	60	1.0	0	0	0	40	24
33	ROUIBA 2	60	1.0	0	0	0	29	14
34	TAFOURA	60	1.0	0	0	0	29	14

Table A1. *Cont.*

Bus Number	Bis Name	Voltage (kV)	Voltage (p.u.)	Angle (Deg)	Gen (MW)	Gen (MVar)	Active Load (MW)	Reactive (MVar)
35	BARAKI	60	1.0	0	0	0	33	16
36	AIN BENIANE	60	1.0	0	0	0	17	8
37	AIN TAYA	60	1.0	0	0	0	11	5
38	AURASSI	60	1.0	0	0	0	20	10
39	EL GOLF	60	1.0	0	0	0	20	10
40	CHLEF	60	1.0	0	0	0	21	10
41	OUED SLY 1	60	1.0	0	0	0	53	32
42	OUED SLY 2	220	1.0	0	0	0	0	0
43	EL KHEMIS 1	60	1.0	0	0	0	31	18
44	EL KHEMIS 2	220	1.0	0	0	0	0	0
45	AIN DEFLA 1	60	1.0	0	0	0	12	6
46	AIN DEFLA 2	60	1.0	0	0	0	0	0
47	KHERBA 1	60	1.0	0	0	0	21	10
48	KHERBA 2	220	1.0	0	0	0	0	0
49	TENES	60	1.0	0	0	0	13	6
50	OUED ELFODA	60	1.0	0	0	0	4	2
51	GHRIB	60	1.0	0	0	0	1	1
52	BOUFARIK	60	1.0	0	80	50	56	27
53	BLIDA	60	1.0	0	0	0	16	8
54	EL AFFROUN	60	1.0	0	0	0	21	10
55	CHERCHEL	60	1.0	0	0	0	18	9
56	MEDEA	60	1.0	0	0	0	33	20
57	BERROUAGH 1	60	1.0	0	0	0	35	21
58	BERROUAGH 2	220	1.0	0	0	0	0	0
59	BENI MERAD 1	60	1.0	0	0	0	36	17
60	BENI MERAD 2	220	1.0	0	0	0	0	0
61	EL KOLEA	60	1.0	0	0	0	27	13
62	BOUMERDES	60	1.0	0	0	0	22	11
63	TIZI OUZOU 1	60	1.0	0	0	0	49	29
64	TIZI OUZOU 2	220	1.0	0	0	0	0	0
65	FREHA	60	1.0	0	0	0	11	5
66	DRÄA BEN KHEDDA	60	1.0	0	0	0	35	21
67	TIZI MEDDEN	60	1.0	0	0	0	10	5
68	S. E. DJEMÄA	60	1.0	0	0	0	11	5
69	SOR ELGHOZLANE	60	1.0	0	0	0	20	10
70	ILLITEN	60	1.0	0	0	0	7	3
71	BOUIRA 1	60	1.0	0	0	0	36	22
72	BOUIRA 2	220	1.0	0	0	0	0	0
73	SI MUSTAPHA	60	1.0	0	0	0	36	22
74	AIN OUSSARA 1	220	1.0	0	0	0	0	0
75	AIN OUSSARA 2	220	1.0	0	0	0	0	0
76	AIN OUSSARA 3	30	1.0	0	0	0	12	6
77	BOUFARIK	60	1.0	0	0	0	7	3
78	MUSTAPHA BACHA	60	1.0	0	0	0	13	7
79	EL AMIRALIA	60	1.0	0	0	0	14	7
80	EL HADJAR 1	220	1.0	0	100	56	157	107
81	EL AOUINET 1	220	1.0	0	0	0	0	0
82	EL KHROUB	220	1.0	0	0	0	75	36
83	SKIKDA	220	1.0	0	230	120	70	51
84	R. DJAMEL	220	1.0	0	0	0	46	34
85	AIN BEIDA	220	1.0	0	0	0	45	22
86	TEBESSA 1	220	1.0	0	0	0	0	0
87	AIN MLILA	220	1.0	0	0	0	32	15
88	EL HADJAR 2	90	1.0	0	0	0	46	22
89	SOUK AHRAS	90	1.0	0	0	0	34	17
90	EL AOUINET 2	90	1.0	0	0	0	18	9

Table A1. *Cont.*

Bus Number	Bis Name	Voltage (kV)	Voltage (p.u.)	Angle (Deg)	Gen (MW)	Gen (MVar)	Active Load (MW)	Reactive (MVar)
91	TEBESSA 2	90	1.0	0	0	0	44	21
92	DJEBEL ONK	90	1.0	0	0	0	10	5
93	TEBESSA 3	90	1.0	0	0	0	0	0
94	OUED ATHMANIA	220	1.0	0	0	0	48	23
95	AKBOU 1	220	1.0	0	0	0	35	17
96	AKBOU 2	220	1.0	0	0	0	0	0
97	EL KSEUR	220	1.0	0	0	0	42	20
98	DARGUINA	220	1.0	0	100	30	13	6
99	ELHASSI	220	1.0	0	0	0	105	50
100	JIJEL	220	1.0	0	550	50	33	16
101	M'SILA	220	1.0	0	360	50	50	24
102	BORDJ BOU-ARRERIDJ	220	1.0	0	0	0	34	16
103	BISKRA	220	1.0	0	0	0	66	32
104	BARIKA 1	220	1.0	0	0	0	18	9
105	BARIKA 2	220	1.0	0	0	0	0	0
106	BATNA	220	1.0	0	0	0	64	31
107	DJELFA	220	1.0	0	0	0	65	37
108	GHARDAIA	220	1.0	0	0	0	22	11
109	TILGHEMT	220	1.0	0	180	85	37	18
110	M'GHAIER	220	1.0	0	0	0	13	6
111	H. MESSAOUD NORD	220	1.0	0	200	85	94	56
112	TOUGGOURT	220	1.0	0	0	0	24	12
113	OUARGLA	220	1.0	0	0	0	23	11
114	EL OUED	220	1.0	0	0	0	24	12

Table A2. Parameters of the transmission lines in the Algerian 114-bus power system.

Branches	Resistance (p.u.)	Reactance (p.u.)	Susceptance (p.u.)
16-4	0.0041	0.0144	0.0103
16-14	0.0013	0.0045	0.0032
8-42	0.0171	0.0629	0.0454
8-1	0.0184	0.0870	0.0657
10-7	0.0150	0.0709	0.0535
10-11	0.0228	0.1076	0.0811
7-6	0.0157	0.0740	0.0558
11-42	0.0170	0.0806	0.0608
6-4	0.0288	0.1012	0.0730
9-3	0.0042	0.0284	0.0442
3-2	0.0085	0.0403	0.0303
6-2	0.0122	0.0578	0.0436
3-6	0.0140	0.0498	0.0355
1-42	0.0274	0.1295	0.0976
1-42	0.0139	0.0121	0.1474
1-4	0.0033	0.0158	0.0482
5-4	0.0028	0.0189	0.0294
5-1	0.0018	0.0126	0.0197
1-7	0.0144	0.0678	0.0512
15-16	0.0038	0.0135	0.0097
9-4	0.0088	0.0600	0.0933
13-12	0.0501	0.2365	0.1784

Table A2. *Cont.*

Branches	Resistance (p.u.)	Reactance (p.u.)	Susceptance (p.u.)
10-13	0.0464	0.2190	0.1652
17-20	0.0065	0.0244	0.0176
17-21	0.0073	0.0278	0.0202
17-72	0.0197	0.0732	0.0530
72-58	0.0183	0.0863	0.0651
58-75	0.0148	0.0701	0.0528
75-107	0.0185	0.0876	0.0660
75-74	0.0006	0.0026	0.0026
44-42	0.0248	0.0903	0.0649
60-31	0.0037	0.0253	0.0393
21-60	0.0056	0.0263	0.0198
60-44	0.0122	0.0578	0.0436
58-44	0.0121	0.0569	0.0429
72-101	0.0213	0.1007	0.0760
17-27	0.0046	0.0237	0.1003
17-31	0.0061	0.0311	0.0617
31-28	0.0017	0.0088	0.0746
17-64	0.0198	0.0727	0.0525
21-44	0.0240	0.0861	0.0615
44-42	0.0183	0.0864	0.0651
42-48	0.0074	0.0506	0.0786
48-44	0.0025	0.0158	0.0245
107-101	0.0334	0.1577	0.1189
64-97	0.0178	0.0654	0.0470
72-96	0.0152	0.0540	0.0386
96-98	0.0203	0.0720	0.0515
96-95	0.0015	0.0070	0.0053
18-22	0.0290	0.1397	0.0017
18-37	0.0256	0.1233	0.0015
37-22	0.0171	0.0822	0.0010
19-26	0.0058	0.0077	0.0017
19-26	0.0058	0.0077	0.0017
19-34	0.0019	0.0126	0.0001
20-18	0.1348	0.2944	0.0013
20-24	0.0376	0.1390	0.0006
20-24	0.0368	0.1361	0.0006
20-29	0.0319	0.1178	0.0005
20-35	0.0428	0.1528	0.0006
35-29	0.0458	0.1639	0.0007
20-32	0.0708	0.2365	0.0010
22-32	0.0342	0.1142	0.0005
22-24	0.0239	0.0799	0.0003
22-24	0.0239	0.0799	0.0003
23-30	0.0239	0.0799	0.0003
23-36	0.0136	0.0457	0.0002
36-30	0.0273	0.0913	0.0004
33-18	0.0205	0.0685	0.0003
32-33	0.0239	0.0799	0.0003
26-25	0.0139	0.0517	0.0002
24-25	0.0164	0.0608	0.0003
26-34	0.0049	0.0318	0.0002
29-26	0.0119	0.0158	0.0034
29-39	0.0126	0.0820	0.0004

Table A2. *Cont.*

Branches	Resistance (p.u.)	Reactance (p.u.)	Susceptance (p.u.)
38-34	0.0047	0.0307	0.0002
18-73	0.1557	0.3427	0.0015
18-73	0.0854	0.3028	0.0012
62-18	0.0508	0.1941	0.0008
20-52	0.0873	0.2162	0.0011
20-52	0.0875	0.2167	0.0011
54-59	0.1188	0.3063	0.0015
70-68	0.1204	0.2180	0.0009
44-45	0.1025	0.3425	0.0015
51-43	0.2067	0.3556	0.0015
54-55	0.1196	0.3996	0.0018
55-43	0.1708	0.5708	0.0025
52-30	0.0722	0.1789	0.0009
71-70	0.1599	0.3148	0.0013
40-41	0.0586	0.1623	0.0008
40-50	0.1343	0.3645	0.0016
71-69	0.1093	0.3653	0.0016
52-59	0.0360	0.1014	0.0005
57-51	0.1227	0.4098	0.0018
57-77	0.1366	0.4566	0.0020
52-53	0.0937	0.1788	0.0007
53-54	0.0937	0.1788	0.0007
73-62	0.0410	0.1370	0.0006
73-67	0.3347	0.7007	0.0031
68-67	0.1648	0.3569	0.0015
29-26	0.0119	0.0158	0.0034
73-66	0.1623	0.5752	0.0023
63-66	0.0683	0.2283	0.0010
63-65	0.0557	0.1861	0.0008
63-65	0.0557	0.1861	0.0008
56-54	0.1025	0.3425	0.0015
57-56	0.1196	0.3996	0.0018
57-56	0.1196	0.3996	0.0018
47-50	0.1196	0.3996	0.0018
47-46	0.0342	0.1142	0.0005
67-66	0.1128	0.2794	0.0014
49-41	0.1265	0.4225	0.0019
19-78	0.0042	0.0055	0.0012
19-79	0.0105	0.0139	0.0030
59-61	0.0513	0.1816	0.0007
45-46	0.0171	0.0605	0.0002
85-87	0.0158	0.0745	0.0562
85-86	0.0139	0.0657	0.0495
85-81	0.0099	0.0467	0.0352
87-106	0.0105	0.0495	0.0373
87-82	0.0056	0.0266	0.0200
87-99	0.0322	0.1249	0.0909
103-105	0.0130	0.0613	0.0462
105-101	0.0171	0.0806	0.0608
105-104	0.0015	0.0070	0.0053
103-106	0.0208	0.0983	0.0741
81-82	0.0303	0.1075	0.0768
80-82	0.0319	0.1129	0.0807

Table A2. *Cont.*

Branches	Resistance (p.u.)	Reactance (p.u.)	Susceptance (p.u.)
80-84	0.0191	0.0676	0.0483
84-83	0.0051	0.0180	0.0129
82-83	0.0191	0.0676	0.0483
100-98	0.0102	0.0598	0.0754
100-97	0.0111	0.0759	0.1179
98-97	0.0121	0.0448	0.0325
99-100	0.0231	0.1089	0.0821
87-100	0.0102	0.0694	0.0105
100-84	0.0065	0.0442	0.0687
84-80	0.0074	0.0506	0.0786
86-81	0.0055	0.0379	0.0589
98-99	0.0163	0.0580	0.0414
101-102	0.0116	0.0547	0.0413
99-102	0.0116	0.0547	0.0413
99-101	0.0111	0.0759	0.1179
98-94	0.0357	0.1275	0.0918
94-82	0.0056	0.0263	0.0198
92-93	0.1624	0.4088	0.0099
93-91	0.0304	0.1074	0.0021
93-91	0.0379	0.1342	0.0027
90-89	0.0776	0.2400	0.0052
90-89	0.1354	0.4100	0.0089
90-93	0.1852	0.3189	0.0068
103-110	0.0185	0.0876	0.0660
110-112	0.0185	0.0876	0.0660
103-114	0.0419	0.1979	0.1493
109-108	0.0148	0.0701	0.0528
109-107	0.0388	0.1833	0.1382
112-114	0.0190	0.0896	0.0675
112-111	0.0297	0.1402	0.1057
113-111	0.0167	0.0787	0.0608
80-88	0.0123	0.3140	0.0
81-90	0.0062	0.1452	0.0
86-93	0.0012	0.0742	0.0
42-41	0.0012	0.0742	0.0
58-57	0.0012	0.0742	0.0
44-43	0.0029	0.1053	0.0
60-59	0.0014	0.0516	0.0
64-63	0.0019	0.0700	0.0
72-71	0.0012	0.0742	0.0
18-17	0.0014	0.0516	0.0
21-20	0.0016	0.0525	0.0
27-26	0.0024	0.1484	0.0
28-26	0.0024	0.1484	0.0
31-30	0.0007	0.0495	0.0
48-47	0.0012	0.0742	0.0
74-76	0.1197	4.4904	0.0

References

1. Ragosa, G. The Political Economy of Wholesale Power Market Reform and Renewable Energy Integration: A Comparison of Britain, Italy, and California. Doctoral Dissertation, University College London (UCL), London, UK, 2024.
2. Baker, L.H.; Cao, U.; Chipango, E.F.; Fathoni, H.S.; Munro, P.G.; Samarakoon, S. *Electricity Capital and Energy Poverty: Perspectives from Developmental States and Decentralised Markets*; Springer Nature: Berlin/Heidelberg, Germany, 2025.

3. Bouddou, R.; Benhamida, F.; Ziane, I.; Zeggai, A.; Belgacem, M. Solving Bid-Based Dynamic Economic Dispatch in Competitive Electricity Market Using Improved Simulated Annealing Algorithm. *Math. Model. Eng. Probl.* **2020**, *7*, 621–630. [CrossRef]
4. Mandić, M.; Modrić, T.; Sutlović, E. A Method for Calculating the Optimal Size of Energy Storage for a GENCO. *Sustainability* **2025**, *17*, 2278. [CrossRef]
5. Algarvio, H.; Sousa, V. Strategies to Incentivize the Participation of Variable Renewable Energy Generators in Balancing Markets. *Energies* **2025**, *18*, 2800. [CrossRef]
6. Nascimento, P.S.C.; Deotti, L.M.P.; Marcato, A.L.M.; Farias, W.C.M. Wind Power Forecasting for Independent System Operators: Modeling Approaches, Practical Applications, and Operational Challenges in the Brazilian Context. *IEEE Access* **2026**, *14*, 27895–27914. [CrossRef]
7. Das, S.S.; Singh, P.; Kumar, J.; Dawn, S.; Ghosh, A. A machine learning-based approach for maximizing system profit in a power system by imbalance price curtailment. *Comput. Electr. Eng.* **2025**, *121*, 109874. [CrossRef]
8. DeLosa, J., III; Pfeifenberger, J.P.; Joskow, P.L. Regulation of access, pricing, and planning of high-voltage transmission in the US. In *Handbook on Electricity Regulation*; Edward Elgar Publishing: Cheltenham, UK, 2025; pp. 121–153.
9. Shen, Z.; Wei, W.; Wu, L.; Shafie-khah, M.; Catalão, J.P. Economic dispatch of power systems with LMP-dependent demands: A non-iterative MILP model. *Energy* **2021**, *233*, 121015. [CrossRef]
10. Li, Z.; Xie, A.; Liu, J.; Zhang, Y.; Lu, Y.; Zu, W.; Wang, Y.; Zhang, X. An Electricity Market Pricing Method with the Optimality Limitation of Power System Dispatch Instructions. *Processes* **2025**, *13*, 2235. [CrossRef]
11. Norouzi, M.; Uzzaman, M.A.; Mohammadi-Ivatloo, B.; Aghaei, J. Market-Driven Optimization of Energy Storage Technologies: A Comparative Study of MISO and NYISO. In *Proceedings of the 2025 IEEE PES Conference on Innovative Smart Grid Technologies-Middle East (ISGT Middle East)*; IEEE: New York, NY, USA, 2025; pp. 1–5.
12. Wang, X.; Li, F.; Bai, L.; Fang, X. DLMP of competitive markets in active distribution networks: Models, solutions, applications, and visions. *Proc. IEEE* **2022**, *111*, 725–743. [CrossRef]
13. Lin, X.; Wang, B.; Xiang, Z.; Zheng, Y. A review of market power-mitigation mechanisms in electricity markets. *Energy Convers. Econ.* **2022**, *3*, 304–318. [CrossRef]
14. Hogan, W.W. Electricity market design and zero-marginal cost generation. *Curr. Sustain. Energy Rep.* **2022**, *9*, 15–26. [CrossRef]
15. Haba, M.; Benhamida, F.; Souag, S.; Bouddou, R.; Graa, A. Post-contingency assessment by sensitivity factors for power system congestion. *Eng. Rev.* **2024**, *44*, 103–115. [CrossRef]
16. Daealhaq, H.; Falah Hassan, Y.; Ghanimi, H.; Azimian, M. Bidding strategy of a wind-thermal GENCO considering piecewise linear AC power flow and correlated uncertainties. *Int. Trans. Electr. Energy Syst.* **2022**, *2022*, 6301902. [CrossRef]
17. Meng, Q.; Jin, X.; Luo, F.; Wang, Z.; Hussain, S. Distributionally robust scheduling for benefit allocation in regional integrated energy system with multiple stakeholders. *J. Mod. Power Syst. Clean Energy* **2024**, *12*, 1631–1642. [CrossRef]
18. Gautam, D.; Nadarajah, M. Influence of distributed generation on congestion and LMP in competitive electricity market. *Int. J. Electr. Power Eng.* **2010**, *3*, 228–235.
19. Di Foggia, G.; Beccarello, M. Designing new energy markets to promote renewables. *Heliyon* **2024**, *10*, e31427. [CrossRef] [PubMed]
20. Xiao, D.; Chen, H.; Cai, W.; Wei, C.; Zhao, Z. Integrated risk measurement and control for stochastic energy trading of a wind storage system in electricity markets. *Prot. Control Mod. Power Syst.* **2023**, *8*, 60. [CrossRef]
21. Zheng, K.; Sun, Z.; Song, Y.; Zhang, C.; Zhang, C.; Chang, F.; Yang, D.; Fu, X. Stochastic scenario generation methods for uncertainty in wind and photovoltaic power outputs: A comprehensive review. *Energies* **2025**, *18*, 503. [CrossRef]
22. Patil, G.S.; Mulla, A.; Ustun, T.S. Impact of wind farm integration on LMP in deregulated energy markets. *Sustainability* **2022**, *14*, 4354. [CrossRef]
23. Sieraszewsk, D.; Olsen, O.K.; Ivanko, D.; Oleinikova, I.; Farahmand, H. Multi-Period Hybrid AC/DC-OPF Model for Flexibility Market Clearing with Seamless TSO-DSO Coordination. *IEEE Access* **2023**, *11*, 40093–40106. [CrossRef]
24. Sumarsono, N.; Wahyuni, S.; Sudhartio, L. A paradigm shift of energy sources: Critical review on competitive dynamics of solar PV industry in Indonesia. *Renew. Energy Focus* **2022**, *41*, 236–245. [CrossRef]
25. Al-Dahidi, S.; Madhiarasan, M.; Al-Ghussain, L.; Abubaker, A.M.; Ahmad, A.D.; Alrbai, M.; Aghaei, M.; Alahmer, H.; Alahmer, A.; Baraldi, P.; et al. Forecasting solar photovoltaic power production: A comprehensive review and innovative data-driven modeling framework. *Energies* **2024**, *17*, 4145. [CrossRef]
26. Sweeney, S.; Shorten, R.; O'Malley, M. A Fair, Flexible, Zero-Waste Digital Electricity Market: A First-Principles Approach Combining Automatic Market Making, Holarchic Architectures and Shapley Theory. *arXiv* **2025**, arXiv:2512.13871.
27. Wu, H.; Qiu, D.; Zhang, L.; Sun, M. Adaptive multi-agent reinforcement learning for flexible resource management in a virtual power plant with dynamic participating multi-energy buildings. *Appl. Energy* **2024**, *374*, 123998. [CrossRef]
28. Mehmood, K.K.; Moura, R.A.A.; van der Molen, A.; Tonkoski, R.; Tzscheutschler, P.; van der Wielen, P.; Nguyen, P.H. A review of congestion management methods for power distribution networks: Current practices and future challenges. *Appl. Energy* **2026**, *407*, 127342. [CrossRef]

29. Ersoy, S.R.; Terrapon-Pfaff, J. *Sustainable Transformation of Algeria's Energy System*; Friedrich-Ebert-Stiftung, Algeria Office: Algiers, Algeria, 2021.
30. Abderrahmane, S.; Dalila, M. SONELGAZ in Algeria: Diversification into Industrial Energy Efficiency Services and Value Creation Potential in a Changing Sector. *Roa Iktissadia Rev.* **2024**, *14*, 123–140. [CrossRef]
31. Stambouli, A.B.; Khiat, Z.; Flazi, S.; Kitamura, Y. A review on the renewable energy development in Algeria: Current perspective, energy scenario and sustainability issues. *Renew. Sustain. Energy Rev.* **2012**, *16*, 4445–4460. [CrossRef]
32. Zahraoui, Y.; Khan, M.R.B.; AlHamrouni, I.; Mekhilef, S.; Ahmed, M. Current status, scenario, and prospective of renewable energy in Algeria: A review. *Energies* **2021**, *14*, 2354. [CrossRef]
33. Boukhatem, I.; Oei, P.Y. Fossil gas lock-in risks: Analysis of Algeria's electricity sector and implications for a renewable energy transition. In *Sustainability Nexus Forum*; Springer: Berlin/Heidelberg, Germany, 2023; Volume 31, pp. 25–40.
34. Hasni, T.; Malek, R.; Zouioueche, N. *Algeria 100% Renewable Energy*; Friedrich-Ebert-Stiftung, Algeria Office: Algiers, Algeria, 2021.
35. Omar, K.; Nadir, B.; Djamila, K.; Abdeladim, K. Algeria's Energy Transition: A Critical Assessment for a Sustainable Future. *Int. J. Environ. Sci.* **2025**, *11*, 582–592. [CrossRef]
36. Li, M.S.; Wu, Q.H.; Ji, T.Y.; Rao, H. Stochastic multi-objective optimization for economic-emission dispatch with uncertain wind power and distributed loads. *Electr. Power Syst. Res.* **2014**, *116*, 367–373. [CrossRef]
37. Akbari, E.; Hooshmand, R.A.; Gholipour, M.; Parastegari, M. Stochastic programming-based optimal bidding of compressed air energy storage with wind and thermal generation units in energy and reserve markets. *Energy* **2019**, *171*, 535–546. [CrossRef]
38. De la Nieta, A.A.S.; Contreras, J.; Muñoz, J.I.; O'Malley, M. Modeling the impact of a wind power producer as a price-maker. *IEEE Trans. Power Syst.* **2014**, *29*, 2723–2732. [CrossRef]
39. Bitar, E.Y.; Rajagopal, R.; Khargonekar, P.P.; Poolla, K.; Varaiya, P. Bringing wind energy to market. *IEEE Trans. Power Syst.* **2012**, *27*, 1225–1235. [CrossRef]
40. Geetha, K.; Deve, V.S.; Keerthivasan, K. Design of economic dispatch model for GENCOs with thermal and wind powered generators. *Int. J. Electr. Power Energy Syst.* **2015**, *68*, 222–232. [CrossRef]
41. Sita, H.; Reddy, P.U.; Kiranmayi, R. Optimal location and sizing of UPFC for optimal power flow in a deregulated power system using a hybrid algorithm. *Int. J. Ambient Energy* **2020**, *43*, 1413–1419. [CrossRef]
42. Rubin, O.D.; Babcock, B.A. The impact of expansion of wind power capacity and pricing methods on the efficiency of deregulated electricity markets. *Energy* **2013**, *59*, 676–688. [CrossRef]
43. Dawn, S.; Tiwari, P.K.; Goswami, A.K. An approach for efficient assessment of the performance of double auction competitive power market under variable imbalance cost due to high uncertain wind penetration. *Renew. Energy* **2017**, *108*, 230–243. [CrossRef]
44. Mansouri, F.; Chaouche, N.S. Transitioning to Renewable Energy: A pathway for Achieving Net-Zero Power Generation in Algeria by 2050. *Rev. D'écono. Stat. Appliquée* **2024**, *21*, 07–26.
45. SolarGIS. Solar Resource Maps & GIS Data for Algeria. Available online: https://solargis.com/resources/free-maps-and-gis-data?locality=algeria (accessed on 19 January 2026).
46. Riyadh, B. Optimisation du Profit dans un Marché D'électricité Concurrentiel. Doctoral Dissertation, Djillali Liabès University of Sidi Bel Abbès, Sidi Bel Abbès, Algeria, 2022.
47. Benkhaled, M.; Benmessaoud, M.T.; Boudghene Stambouli, A. High Penetration of Solar Energy to the Algerian Electricity System in the Context of an Energy Roadmap Toward a Sustainable Energy Paradigm by 2030. In *Alternative Energy Resources in the MENA Region*; Springer International Publishing: Cham, Switzerland, 2023; pp. 27–45.
48. Groupe Sonelgaz. *"Programme Des Energies Renouvelables Et De L'efficacité Energétique" Rapport*; Groupe Sonelgaz: Algiers, Algeria, 2011.
49. Boukaabache, R. Essai D'analyse de L'impact de L'évaluation D'une Entreprise sur sa Performance Financière cas de la Société de Distribution du gaz et de L'électricité de L'est. Doctoral Dissertation, University of Belgrade, Belgrade, Serbia, 2016.
50. Le Texier, Y.; Gliz, A. Intégration Progressive des Marchés de L'électricité de L'ALGÉRIE, du Maroc et de la Tunisie Dans le Marché Intérieur de L'électricité de L'UNION Européenne. 2009. Available online: https://www.developmentaid.org/organizations/awards/view/74908/integration-progressive-des-marches-de-lelectricite-de-lalgerie-du-maroc-et-de-la-tunisie-dans-le-ma (accessed on 2 January 2025).
51. Bouddou, R.; Benhamida, F.; Zeggai, A.; Ziane, I.; Belgacem, M. The dynamic economic dispatch in an integrated wind-thermal electricity market using simulated annealing algorithm. *Prz. Elektrotechniczny* **2020**, *96*, 55–60. [CrossRef]
52. Jiang, K.; Liu, N.; Yan, X.; Xue, Y.; Huang, J. Modeling strategic behaviors for GenCo with joint consideration on electricity and carbon markets. *IEEE Trans. Power Syst.* **2022**, *38*, 4724–4738. [CrossRef]
53. Rezvanfar, R.; Taghizad-Tavana, K.; Hagh, M.T. A Comprehensive Review and Simulation-Based Analysis of Power Market Pricing Mechanisms in Energy Systems with High Penetration of Distributed Energy Resources: An Analysis of Distribution Locational Marginal Pricing, Dynamic Tariff, and Machine Learning-Based Approaches. *e-Prime-Adv. Electr. Eng. Electron. Energy* **2025**, *13*, 101083. [CrossRef]

54. Knörr, J. Electricity Market Design: Clearing and Pricing in Non-Convex Markets. Doctoral Dissertation, Universitätsbibliothek der TU München, Munich, Germany, 2024.
55. Abaza, A.; El-Sehiemy, R.A.; Elbarabry, Z.; Barakat, A.F. Generic optimal power flow solution associated with technical improvements and emission reduction by multi-objective ARO algorithm. *Sci. Rep.* **2025**, *15*, 26524. [CrossRef] [PubMed]
56. Benhamida, F.; Salhi, Y.; Ziane, I.; Souag, S.; Belhachem, R.; Bendaoud, A. A PSO algorithm for the economic load dispatch including a renewable wind energy. In *Proceedings of the 3rd International Conference on Systems and Control*; IEEE: New York, NY, USA, 2013; pp. 1104–1109.
57. Hasan, M.S.; Chowdhury, M.M.U.T.; Kamalasadan, S. Optimal Power Flow in Electric Transmission System: Comparative Study and Analysis of Modeling Methods. *IEEE Trans. Ind. Appl.* **2025**, *61*, 4328–4341. [CrossRef]
58. Mohamed, S.A.; Anwer, N.; Mahmoud, M.M. Solving optimal power flow problem for IEEE-30 bus system using a developed particle swarm optimization method: Towards fuel cost minimization. *Int. J. Model. Simul.* **2025**, *45*, 307–320. [CrossRef]
59. Yang, C.; Sun, Y.; Zou, Y.; Zheng, F.; Liu, S.; Zhao, B.; Wu, M.; Cui, H. Optimal power flow in distribution network: A review on problem formulation and optimization methods. *Energies* **2023**, *16*, 5974. [CrossRef]
60. Zhang, C.; Wang, D.; Zhang, W.; He, L.; Zhou, K.; Li, J. A novel optimal power flow method considering interval uncertainties under high renewable penetration based on security limits definition. *IEEE Trans. Sustain. Energy* **2025**, *17*, 926–938. [CrossRef]
61. Nasreddine, B.; Fethi, B.; Yassine, H.; Imane, H.; Riyadh, B. Optimal sizing and placement of distributed generation with short-circuit analysis using a combined technique based on modified PSO and ETAP. In *Proceedings of the 2024 2nd International Conference on Electrical Engineering and Automatic Control (ICEEAC)*; IEEE: New York, NY, USA, 2024; pp. 1–6.
62. Bouchikhi, N.; Boussadia, F.; Bouddou, R.; Zaidi, S.; Adiche, S.; Belabbes, A. A Modified Genetic Algorithm for optimizing the placement and sizing of distributed generators in radial distribution systems including security analysis. *J. Renew. Energ.* **2024**, *1*, 131–149. [CrossRef]
63. Dashtdar, M.; Najafi, M.; Esmaeilbeig, M. Calculating the locational marginal price and solving optimal power flow problem based on congestion management using GA-GSF algorithm. *Electr. Eng.* **2020**, *102*, 1549–1566. [CrossRef]
64. Dashtdar, M.; Najafi, M.; Esmaeilbeig, M. Reducing LMP and resolving the congestion of the lines based on placement and optimal size of DG in the power network using the GA-GSF algorithm. *Electr. Eng.* **2021**, *103*, 1279–1306. [CrossRef]
65. Murali, M.; Kumari, M.S.; Sydulu, M. A Genetic Algorithm Based Security Constrained Economic Dispatch Approach for LMP Calculation. *Int. J. Energy Sci.* **2013**, *3*, 116–126.
66. Meng, F. *A generalized Optimal Power Flow Program for Distribution System Analysis and Operation with Distributed Energy Resources and Solid State Transformers*; Missouri University of Science and Technology: Rolla, Missouri, 2014.
67. Simão, H.P.; Powell, W.B.; Archer, C.L.; Kempton, W. The challenge of integrating offshore wind power in the US electric grid. Part II: Simulation of electricity market operations. *Renew. Energy* **2017**, *103*, 418–431. [CrossRef]
68. Aslan, A.; Tasci, M.; Kosunalp, S. Comprehensive Assessment of Wind Energy Potential with a Hybrid GRU–Weibull Prediction Model. *Electronics* **2025**, *14*, 4000. [CrossRef]
69. Mohamed, A.A.; Kamel, S.; Hassan, M.H.; Mosaad, M.I.; Aljohani, M. Optimal power flow analysis based on hybrid gradient-based optimizer with moth–flame optimization algorithm considering optimal placement and sizing of FACTS/wind power. *Mathematics* **2022**, *10*, 361. [CrossRef]
70. Biswas, P.P.; Suganthan, P.N.; Qu, B.Y.; Amaratunga, G.A. Multiobjective economic-environmental power dispatch with stochastic wind-solar-small hydro power. *Energy* **2018**, *150*, 1039–1057. [CrossRef]
71. Biswas, P.P.; Suganthan, P.N.; Amaratunga, G.A. Optimal power flow solutions incorporating stochastic wind and solar power. *Energy Convers. Manag.* **2017**, *148*, 1194–1207. [CrossRef]
72. Eager, D.; Hobbs, B.F.; Bialek, J.W. Dynamic modeling of thermal generation capacity investment: Application to markets with high wind penetration. *IEEE Trans. Power Syst.* **2012**, *27*, 2127–2137. [CrossRef]
73. Salhi, Y.; Benhamida, F.; Ziane, I.; Graa, A. The dynamic economic load dispatch in electricity market using genetic algorithm. *Electroteh. Electron. Autom.* **2017**, *65*, 54.
74. Bouddou, R.; Benhamida, F.; Zeggai, A.; Belgacem, M.; Khatir, M. Integration of wind power generation into a double-sided competitive electricity market for profit and social welfare maximization. In *Proceedings of the 2020 International Conference on Electrical and Information Technologies (ICEIT)*; IEEE: New York, NY, USA, 2020; pp. 1–6.
75. Zorkal'tsev, V.I. Interior point method: History and prospects. *Comput. Math. Math. Phys.* **2019**, *59*, 1597–1612. [CrossRef]
76. Jabr, R.A.; Coonick, A.H.; Cory, B.J. A primal-dual interior point method for optimal power flow dispatching. *IEEE Trans. Power Syst.* **2002**, *17*, 654–662. [CrossRef]
77. Xia, Y.; Chan, K.W.; Liu, M. Direct nonlinear primal–dual interior-point method for transient stability constrained optimal power flow. *IEE Proc.-Gener. Transm. Distrib.* **2005**, *152*, 11–16. [CrossRef]
78. Quintana, V.H.; Torres, G.L. *Introduction to Interior-Point Method Applications to Power Systems*; IEEE Pes: Piscataway, NJ, USA, 1997.
79. Capitanescu, F.; Glavic, M.; Wehenkel, L. An interior point method based optimal power flow. In Proceedings of the 3-rd ACOMEN Conference, Ghent, Belgium, 30 May–2 June 2005.

80. Granville, S. An Interior Point Method based Optimal Power Flow. *IEEE Trans. Power Syst.* **1994**, *9*, 136–146. [CrossRef]
81. Zimmerman, R.D.; Murillo-Sanchez, C.E.; Gan, D. MATPOWER: A MATLAB Power System Simulation Package. 2009. Available online: http://pserc.cornell.edu/matpower/ (accessed on 1 October 2024).
82. Makhloufi, S.; Mekhaldi, A.; Teguar, M. Three powerful nature-inspired algorithms to optimize power flow in Algeria's Adrar power system. *Energy* **2016**, *116*, 1117–1130. [CrossRef]
83. Souag, S.; Benhamida, F. A dynamic power system economic dispatch enhancement by wind integration considering ramping constraint—Application to Algerian power system. *Int. J. Renew. Energy Res.* **2015**, *5*, 794–805. [CrossRef]
84. Slimani, L.; Bouktir, A.T. Optimal Power Flow Solution of the Algerian Electrical Network Using Differential Evolution Algorithm. *Telkomnika* **2012**, *10*, 199. [CrossRef]
85. Arif, S. Différentes Techniques De Planification De L'énergie Réactive Dans Les Réseaux Electriques. Thèse De Doctorat, Ecole Nationale Polytechnique, El Harrach, Algeria, 2008.
86. Mahdad, B.; Kamel, S. New strategy based modified Salp swarm algorithm for optimal reactive power planning: A case study of the Algerian electrical system (114 bus). *IET Gener. Transm. Distrib.* **2019**, *13*, 4523–4540. [CrossRef]
87. CEIC. Algeria Electricity Consumption. Report. Available online: https://www.ceicdata.com/en/algeria/electricity-consumption (accessed on 19 January 2026).
88. Bouraiou, A.; Necaibia, A.; Boutasseta, E. Status of Renewable Energy Potential and Utilization in Algeria. *J. Clean. Prod.* **2020**, *246*, 119011. [CrossRef]
89. Doyle, C.; Truitt, A.; Inda, D.; Lawrence, R.; Lockhart, R.; Golden, M. *Solar Access to Public Capital (Sapc) Working Group: Best Practices in Commercial and Industrial (C&I) Solar Photovoltaic System Installation; Period of Performance: November 28, 2014-September 1, 2015*; National Renewable Energy Lab. (Nrel): Golden, CO, USA, 2015. [CrossRef]
90. Masebinu, S.; Akinlabi, E.; Et Muzenda, E. Renewable Energy: Deployment and the Roles of Energy Storage. In Proceedings of the World Congress on Engineering, London, UK, 29 June–1 July 2016; Volume 29.
91. Khaled, U.; Eltamaly, A.M.; Et Beroual, A. Optimal Power Flow Using Particle Swarm Optimization of Renewable Hybrid Distributed Generation. *Energies* **2017**, *10*, 1013. [CrossRef]
92. Electricity and Gas Regulatory Commission (CREG). Comment Lire Votre Facture. Available online: https://www.creg.dz/index.php/consommateurs/comment-lire-votre-facture (accessed on 19 January 2026).

Disclaimer/Publisher's Note: The statements, opinions and data contained in all publications are solely those of the individual author(s) and contributor(s) and not of MDPI and/or the editor(s). MDPI and/or the editor(s) disclaim responsibility for any injury to people or property resulting from any ideas, methods, instructions or products referred to in the content.